NUREG/CR–5408
ORNL/TM–11269

SEN Wide-Plate Crack-Arrest Tests Using A 533 Grade B Class 1 Material: WP-CE Test Series

Prepared by D. J. Naus, J. Keeney-Walker, B. R. Bass, S. K. Iskander/ORNL
R. J. Fields, R. deWit, S. R. Low III/NIST

Oak Ridge National Laboratory

National Institute of Standards and Technology

Prepared for
U.S. Nuclear Regulatory Commission

AVAILABILITY NOTICE

Availability of Reference Materials Cited in NRC Publications

Most documents cited in NRC publications will be available from one of the following sources:

1. The NRC Public Document Room, 2120 L Street, NW, Lower Level, Washington, DC 20555
2. The Superintendent of Documents, U.S. Government Printing Office, P.O. Box 37082, Washington, DC 20013-7082
3. The National Technical Information Service, Springfield, VA 22161

Although the listing that follows represents the majority of documents cited in NRC publications, it is not intended to be exhaustive.

Referenced documents available for inspection and copying for a fee from the NRC Public Document Room include NRC correspondence and internal NRC memoranda; NRC Office of Inspection and Enforcement bulletins, circulars, information notices, inspection and investigation notices; Licensee Event Reports; vendor reports and correspondence; Commission papers; and applicant and licensee documents and correspondence.

The following documents in the NUREG series are available for purchase from the GPO Sales Program: formal NRC staff and contractor reports, NRC-sponsored conference proceedings, and NRC booklets and brochures. Also available are Regulatory Guides, NRC regulations in the *Code of Federal Regulations*, and *Nuclear Regulatory Commission Issuances*.

Documents available from the National Technical Information Service include NUREG series reports and technical reports prepared by other federal agencies and reports prepared by the Atomic Energy Commission, forerunner agency to the Nuclear Regulatory Commission.

Documents available from public and special technical libraries include all open literature items, such as books, journal and periodical articles, and transactions. *Federal Register* notices, federal and state legislation, and congressional reports can usually be obtained from these libraries.

Documents such as theses, dissertations, foreign reports and translations, and non-NRC conference proceedings are available for purchase from the organization sponsoring the publication cited.

Single copies of NRC draft reports are available free, to the extent of supply, upon written request to the Office of Information Resources Management, Distribution Section, U.S. Nuclear Regulatory Commission, Washington, DC 20555.

Copies of industry codes and standards used in a substantive manner in the NRC regulatory process are maintained at the NRC Library, 7920 Norfolk Avenue, Bethesda, Maryland, and are available there for reference use by the public. Codes and standards are usually copyrighted and may be purchased from the originating organization or, if they are American National Standards, from the American National Standards Institute, 1430 Broadway, New York, NY 10018.

DISCLAIMER NOTICE

This report was prepared as an account of work sponsored by an agency of the United States Government. Neither the United States Government nor any agency thereof, or any of their employees, makes any warranty, expressed or implied, or assumes any legal liability of responsibility for any third party's use, or the results of such use, of any information, apparatus, product or process disclosed in this report, or represents that its use by such third party would not infringe privately owned rights.

NUREG/CR-5408
ORNL/TM-11269
RF

SEN Wide-Plate Crack-Arrest Tests Using A 533 Grade B Class 1 Material: WP-CE Test Series

Manuscript Completed: October 1989
Date Published: November 1989

Prepared by
D. J. Naus, J. Keeney-Walker, B. R. Bass, S. K. Iskander, Oak Ridge National Laboratory
R. J. Fields, R. deWit, S. R. Low III, National Institute of Standards and Technology

Oak Ridge National Laboratory
Operated by Martin Marietta Energy Systems, Inc.

Oak Ridge National Laboratory
Oak Ridge, TN 37831

Subcontractor:
National Institute of Standards and Technology
Gaithersburg, MD 20899

Prepared for
Division of Engineering
Office of Nuclear Regulatory Research
U.S. Nuclear Regulatory Commission
Washington, DC 20555
NRC FIN B0119
Under Contract No. DE-AC05-84OR21400

ABSTRACT

Current pressure vessel safety assessment methods are based largely on Sects. III and XI of the *American Society of Mechanical Engineers Boiler and Pressure Vessel Code (ASME B&PVC)*. These documents take the position that the fracture toughness correlations cannot be assumed for a crack-arrest toughness value >220 MPa·$\sqrt{m}$ for light-water-reactor (LWR) pressure vessel steels. This limit is imposed largely because, until recently, essentially no crack-arrest toughness (K_{Ia}) data existed at or above this level and because Charpy tests show that impact energy levels exhibit an upper-shelf behavior. In making assessments for LWR pressure vessels undergoing thermal transients with low accompanying pressure levels, the limit on crack-arrest toughness does not present difficulties. However, certain pressurized-thermal-shock scenarios could lead to conditions under which the driving force (K_I) on a propagating crack increases to levels higher than the ASME limit.

The Heavy-Section Steel Technology (HSST) Program at the Oak Ridge National Laboratory, under the sponsorship of the U.S. Nuclear Regulatory Commission, is conducting analytical and experimental studies aimed at understanding the circumstances that would initiate the growth of an existing crack in a reactor pressure vessel and the conditions that would lead to the arrest of a propagating crack. Objectives of these studies are to determine (1) whether the material will exhibit crack-arrest behavior when the driving force on a crack exceeds the ASME limit, (2) the relationship between K_{Ia} and temperature, and (3) the interaction of fracture modes (arrest, stable crack growth, unstable crack growth, and tensile instability) when arrest occurs at high temperatures. In meeting these objectives, crack-arrest data are being developed over an expanded temperature range through tests involving large thermally shocked cylinders, pressurized thermally shocked vessels, stub-panel specimens, and wide-plate specimens. The thick-vessel tests have very high crack-tip restraint and produce indisputably valid fracture data. The wide-plate specimens provide the opportunity to obtain a significant number of data points at reasonable costs. These tests are designed to measure fracture toughness near or above the onset of the Charpy upper-shelf regime in a rising toughness region and with an increasing driving force.

The HSST wide-plate crack-arrest tests are being performed at the National Institute of Standards and Technology, Gaithersburg, Maryland, in a 27-MN-capacity testing machine. This report contains results for two tests that used A 533 grade B class 1 material supplied by Combustion Engineering, Inc. Each test used a 1 × 1 × 0.1 m thick single-edge notched plate (a/w = 0.2) that was subjected to a linear thermal gradient along the plane of crack propagation. The thermal gradient was applied to the specimen by cooling the notched edge and heating the other edge. By varying the crack-tip temperature and transverse temperature profile, the initiation load and depth of crack propagation were changed from test to test. During each test, strain and temperature measurements were obtained as functions of position and time. Load, crack-opening displacement, and accelerometer data were also obtained as functions of time.

These tests have shown crack-arrest toughness values well above the limit recognized by the current *ASME B&PVC* guidelines, with arrests occurring at 58 to 95°C above the material's reference nil-ductility temperature (RT_{NDT} = -35°C) and up to 10°C higher than that for the material's onset of Charpy V-notch upper-shelf energy (USE) (onset USE = 50°C). Crack propagation has been by cleavage until arrest occurred, and, even for very high driving forces, ductile tearing occurred only after arrest. The fracture data support (1) the use of fracture-mechanics concepts to analyze cleavage run-arrest events, (2) the treatment of cleavage run/arrest and ductile fracture modes as separate events, and (3) the fact that cleavage arrest occurs above the ASME limit.

CONTENTS

LIST OF FIGURES

LIST OF TABLES

FOREWORD

The work reported here was performed at Oak Ridge National Laboratory under the Heavy-Section Steel Technology (HSST) Program, W. R. Corwin, Program Manager. The program is sponsored by the Office of Nuclear Regulatory Research of the U.S. Nuclear Regulatory Commission (NRC). The technical monitor for the NRC is M. E. Mayfield.

This report is designated HSST Report 100. Prior and future reports in this series are listed below.

1. S. Yukawa, *Evaluation of Periodic Proof Testing and Warm Prestressing Procedures for Nuclear Reactor Vessels*, HSSTP-TR-1, General Electric Company, Schenectady, N.Y. (July 1, 1969).

2. L. W. Loechel, *The Effect of Testing Variables on the Transition Temperature in Steel*, MCR-69-189, Martin Marietta Corporation, Denver, Colo. (November 20, 1969).

3. P. N. Randall, *Gross Strain Measure of Fracture Toughness of Steels*, HSSTP-TR-3, TRW Systems Group, Redondo Beach, Calif. (November 1, 1969).

4. C. Visser, S. E. Gabrielse, and W. VanBuren, *A Two-Dimensional Elastic-Plastic Analysis of Fracture Test Specimens*, WCAP-7368, Westinghouse Electric Corporation, PWR Systems Division, Pittsburgh, Pa. (October 1969).

5. T. R. Mager and F. O. Thomas, *Evaluation by Linear Elastic Fracture Mechanics of Radiation Damage to Pressure Vessel Steels*, WCAP-7328 (Rev.), Westinghouse Electric Corporation, PWR Systems Division, Pittsburgh, Pa. (October 1969).

6. W. O. Shabbits, W. H. Pryle, and E. T. Wessel, *Heavy-Section Fracture Toughness Properties of A533 Grade B Class 1 Steel Plate and Submerged Arc Weldment*, WCAP-7414, Westinghouse Electric Corporation, PWR Systems Division, Pittsburgh, Pa. (December 1969).

7. F. J. Loss, *Dynamic Tear Test Investigations of the Fracture Toughness of Thick-Section Steel*, NRL-7056, Naval Research Laboratory, Washington, D.C. (May 14, 1970).

8. P. B. Crosley and E. J. Ripling, *Crack Arrest Fracture Toughness of A533 Grade B Class 1 Pressure Vessel Steel*, HSSTP-TR-8, Materials Research Laboratory, Inc., Glenwood, Ill. (March 1970).

9. T. R. Mager, *Post-Irradiation Testing of 2T Compact Tension Specimens*, WCAP-7561, Westinghouse Electric Corporation, PWR Systems Division, Pittsburgh, Pa. (August 1970).

10. T. R. Mager, *Fracture Toughness Characterization Study of A533, Grade B, Class 1 Steel*, WCAP-7578, Westinghouse Electric Corporation, PWR Systems Division, Pittsburgh, Pa. (October 1970).

11. T. R. Mager, *Notch Preparation in Compact Tension Specimens*, WCAP-7579, Westinghouse Electric Corporation, PWR Systems Division, Pittsburgh, Pa. (November 1970).

12. N. Levy and P. V. Marcal, *Three-Dimensional Elastic-Plastic Stress and Strain Analysis for Fracture Mechanics, Phase I: Simple Flawed Specimens*, HSSTP-TR-12, Brown University, Providence, R.I. (December 1970).

13. W. O. Shabbits, *Dynamic Fracture Toughness Properties of Heavy Section A533 Grade B Class 1 Steel Plate*, WCAP-7623, Westinghouse Electric Corporation, PWR Systems Division, Pittsburgh, Pa. (December 1970).

14. P. N. Randall, *Gross Strain Crack Tolerance of A 533-B Steel*, HSSTP-TR-14, TRW Systems Group, Redondo Beach, Calif. (May 1, 1971).

15. H. T. Corten and R. H. Sailors, *Relationship Between Material Fracture Toughness Using Fracture Mechanics and Transition Temperature Tests*, T&AM Report 346, University of Illinois, Urbana, Ill. (August 1, 1971).

16. T. R. Mager and V. J. McLaughlin, *The Effect of an Environment of High Temperature Primary Grade Nuclear Reactor Water on the Fatigue Crack Growth Characteristics of A533 Grade B Class 1 Plate and Weldment Material*, WCAP-7776, Westinghouse Electric Corporation, PWR Systems Division, Pittsburgh, Pa. (October 1971).

17. N. Levy and P. V. Marcal, *Three-Dimensional Elastic-Plastic Stress and Strain Analysis for Fracture Mechanics, Phase II: Improved Modelling*, HSSTP-TR-17, Brown University, Providence, R.I. (November 1971).

18. S. C. Grigory, *Tests of 6-in.-Thick Flawed Tensile Specimens, First Technical Summary Report, Longitudinal Specimens Numbers 1 Through 7*, HSSTP-TR-18, Southwest Research Institute, San Antonio, Tex. (June 1972).

19. P. N. Randall, *Effects of Strain Gradients on the Gross Strain Crack Tolerance of A533-B Steel*, HSSTP-TR-19, TRW Systems Group, Redondo Beach, Calif. (June 15, 1972).

20. S. C. Grigory, *Tests of 6-Inch-Thick Flawed Tensile Specimens, Second Technical Summary Report, Transverse Specimens Numbers 8 Through 10, Welded Specimens Numbers 11 Through 13*, HSSTP-TR-20, Southwest Research Institute, San Antonio, Tex. (June 1972).

21. L. A. James and J. A. Williams, *Heavy Section Steel Technology Program Technical Report No. 21, The Effect of Temperature and Neutron Irradiation Upon the Fatigue-Crack Propagation Behavior of ASTM A533 Grade B, Class 1 Steel*, HEDL-TME 72-132, Hanford Engineering Development Laboratory, Richland, Wash. (September 1972).

22. S. C. Grigory, *Tests of 6-Inch-Thick Flawed Tensile Specimens, Third Technical Summary Report, Longitudinal Specimens Numbers 14 Through 16, Unflawed Specimen Number 17*, HSSTP-TR-22, Southwest Research Institute, San Antonio, Tex. (October 1972).

23. S. C. Grigory, *Tests of 6-Inch-Thick Tensile Specimens, Fourth Technical Summary Report, Tests of 1-Inch-Thick Flawed Tensile Specimens for Size Effect Evaluation*, HSSTP-TR-23, Southwest Research Institute, San Antonio, Tex. (June 1973).

24. S. P. Ying and S. C. Grigory, *Tests of 6-Inch-Thick Tensile Specimens, Fifth Technical Summary Report, Acoustic Emission Monitoring of One-Inch and Six-Inch-Thick Tensile Specimens*, HSSTP-TR-24, Southwest Research Institute, San Antonio, Tex. (November 1972).

25. R. W. Derby, J. C. Merkle, C. C. Robinson, C. D. Whitman, and F. J. Witt, *Test of 6-Inch-Thick Pressure Vessels. Series 1: Intermediate Test Vessels V-1 and V-2*, ORNL-4895, Oak Ridge Natl. Lab., Oak Ridge, Tenn. (February 1974).

26. W. J. Stelzman and R. C. Berggren, *Radiation Strengthening and Embrittlement in Heavy Section Steel Plates and Welds*, ORNL-4871, Oak Ridge Natl. Lab., Oak Ridge, Tenn. (June 1973).

27. P. B. Crosley and E. J. Ripling, *Crack Arrest in an Increasing K-Field*, HSSTP-TR-27, Materials Research Laboratory, Inc., Glenwood, Ill. (January 1973).

28. P. V. Marcal, P. M. Stuart, and R. S. Bettes, *Elastic-Plastic Behavior of a Longitudinal Semi-Elliptic Crack in a Thick Pressure Vessel*, HSSTP-TR-28, Brown University, Providence, R.I. (June 1973).

29. W. J. Stelzman, R. C. Berggren, and T. N. Jones, *ORNL Characterization of Heavy-Section Steel Technology Program Plates 01, 02 and 03*, NUREG/CR-4092 (ORNL/TM-9491), Oak Ridge Natl. Lab., Oak Ridge, Tenn. (April 1985).

30. Canceled.

31. J. A. Williams, *The Irradiation and Temperature Dependence of Tensile and Fracture Properties of ASTM A533, Grade B, Class 1 Steel Plate and Weldment*, HEDL-TME 73-75, Hanford Engineering Development Laboratory, Richland, Wash. (August 1973).

32. J. M. Steichen and J. A. Williams, *High Strain Rate Tensile Properties of Irradiated ASTM A533 Grade B Class 1 Pressure Vessel Steel*, Hanford Engineering Development Laboratory, Richland, Wash. (July 1973).

33. P. C. Riccardella and J. L. Swedlow, *A Combined Analytical-Experimental Fracture Study of the Two Leading Theories of Elastic-Plastic Fracture (J-Integral and Equivalent Energy)*, WCAP-8224, Westinghouse Electric Corporation, Pittsburgh, Pa. (October 1973).

34. R. J. Podlasek and R. J. Eiber, *Final Report on Investigation of Mode III Crack Extension in Reactor Piping*, Battelle Columbus Laboratories, Columbus, Ohio (December 14, 1973).

35. T. R. Mager, J. D. Landes, D. M. Moon, and V. J. McLaughlin, *Interim Report on the Effect of Low Frequencies on the Fatigue Crack Growth Characteristics of A533 Grade B Class 1 Plate in an Environment of High-Temperature Primary Grade Nuclear Reactor Water*, WCAP-8256, Westinghouse Electric Corporation, Pittsburgh, Pa. (December 1973).

36. J. A. Williams, *The Irradiated Fracture Toughness of ASTM A533, Grade B, Class 1 Steel Measured with a Four-Inch-Thick Compact Tension Specimen*, HEDL-TME 75-10, Hanford Engineering Development Laboratory, Richland, Wash. (January 1975).

37. R. H. Bryan, J. G. Merkle, M. N. Raftenberg, G. C. Robinson, and J. E. Smith, *Test of 6-Inch-Thick Pressure Vessels. Series 2: Intermediate Test Vessels V-3, V-4, and V-6*, ORNL-5059, Oak Ridge Natl. Lab., Oak Ridge, Tenn. (November 1975).

38. T. R. Mager, S. E. Yanichko, and L. R. Singer, *Fracture Toughness Characterization of HSST Intermediate Pressure Vessel Material*, WCAP-8456, Westinghouse Electric Corporation, Pittsburgh, Pa. (December 1974).

39. J. G. Merkle, G. D. Whitman, and R. H. Bryan, *An Evaluation of the HSST Program Intermediate Pressure Vessel Tests in Terms of Light-Water-Reactor Pressure Vessel Safety*, ORNL/TM-5090, Oak Ridge Natl. Lab., Oak Ridge, Tenn. (November 1975).

40. J. G. Merkle, G. C. Robinson, P. P. Holz, J. E. Smith, and R. H. Bryan, *Test of 6-In.-Thick Pressure Vessels. Series 3: Intermediate Test Vessel V-7*, ORNL/NUREG-1, Oak Ridge Natl. Lab., Oak Ridge, Tenn. (August 1976).

41. J. A. Davidson, L. J. Ceschini, R. P. Shogan, and G. V. Rao, *The Irradiated Dynamic Fracture Toughness of ASTM A533, Grade B, Class 1 Steel Plate and Submerged Arc Weldment*, WCAP-8775, Westinghouse Electric Corporation, Pittsburgh, Pa. (October 1976).

42. R. D. Cheverton, *Pressure Vessel Fracture Studies Pertaining to a PWR LOCA-ECC Thermal Shock: Experiments TSE-1 and TSE-2*, ORNL/NUREG/TM-31, Oak Ridge Natl. Lab., Oak Ridge, Tenn. (September 1976).

43. J. G. Merkle, G. C. Robinson, P. P. Holz, and J. E. Smith, *Test of 6-In.-Thick Pressure Vessels. Series 4: Intermediate Test Vessels V-5 and V-9 with Inside Nozzle Corner Cracks*, ORNL/NUREG-7, Oak Ridge Natl. Lab., Oak Ridge, Tenn. (August 1977).

44. J. A. Williams, *The Ductile Fracture Toughness of Heavy Section Steel Plate*, NUREG/CR-0859, Hanford Engineering Development Laboratory, Richland, Wash. (September 1979).

45. R. H. Bryan, T. M. Cate, P. P. Holz, T. A. King, J. G. Merkle, G. C. Robinson, C. C. Smith, J. E. Smith, and G. D. Whitman, *Test of 6-in.-Thick Pressure Vessels. Series 3: Intermediate Test Vessel V-7A Under Sustained Loading*, ORNL/NUREG-9, Oak Ridge Natl. Lab., Oak Ridge, Tenn. (February 1978).

46. R. D. Cheverton and S. E. Bolt, *Pressure Vessel Fracture Studies Pertaining to a PWR LOCA-ECC Thermal Shock: Experiments TSE-3 and TSE-4 and Update of TSE-1 and TSE-2 Analysis*, ORNL/NUREG-22, Oak Ridge Natl. Lab., Oak Ridge, Tenn. (December 1977).

47. D. A. Canonico, *Significance of Reheat Cracks to the Integrity of Pressure Vessels for Light-Water Reactors*, ORNL/NUREG-15, Oak Ridge Natl. Lab., Oak Ridge, Tenn. (July 1977).

48. C. C. Smith and P. P. Holz, *Repair Weld Induced Residual Stresses in Thick-Walled Steel Pressure Vessels*, NUREG/CR-0093 (ORNL/NUREG/TM-153), Oak Ridge Natl. Lab., Oak Ridge, Tenn. (June 1978).

49. P. P. Holz and S. W. Wismer, *Half-Bead (Temper) Repair Welding for HSST Vessels*, NUREG/CR-0113 (ORNL/NUREG/TM-177), Oak Ridge Natl. Lab., Oak Ridge, Tenn. (June 1978).

50. G. C. Smith, P. P. Holz, and W. J. Stelzman, *Crack Extension and Arrest Tests of Axially Flawed Steel Model Pressure Vessels*, NUREG/CR-0126 (ORNL/NUREG/TM-196), Oak Ridge Natl. Lab., Oak Ridge, Tenn. (October 1978).

51. R. H. Bryan, P. P. Holz, J. G. Merkle, G. C. Smith, J. E. Smith, and W. J. Stelzman, *Test of 6-in.-Thick Pressure Vessels. Series 3: Intermediate Test Vessel V-7B*, NUREG/CR-0309 (ORNL/NUREG-38), Oak Ridge Natl. Lab., Oak Ridge, Tenn. (October 1978).

52. R. D. Cheverton, S. K. Iskander, and S. E. Bolt, *Applicability of LEFM to the Analysis of PWR Vessels Under LOCA-ECC Thermal Shock Conditions*, NUREG/CR-0107 (ORNL/NUREG-40), Oak Ridge Natl. Lab., Oak Ridge, Tenn. (October 1978).

53. R. H. Bryan, D. A. Canonico, P. P. Holz, S. K. Iskander, J. G. Merkle, J. E. Smith, and W. J. Stelzman, *Test of 6-in.-Thick Pressure Vessels, Series 3: Intermediate Test Vessel V-8*, NUREG/CR-0675 (ORNL/NUREG-58), Oak Ridge Natl. Lab., Oak Ridge, Tenn. (December 1979).

54. R. D. Cheverton and S. K. Iskander, *Application of Static and Dynamic Crack Arrest Theory to TSE-4*, NUREG/CR-0767 (ORNL/NUREG-57), Oak Ridge Natl. Lab., Oak Ridge, Tenn. (June 1979).

55. J. A. Williams, *Tensile Properties of Irradiated and Unirradiated Welds of A533 Steel Plate and A508 Forgings*, NUREG/CR-1[illegible] (ORNL/Sub-79/50917/2), Hanford Engineering Development Laboratory, Richland, Wash. (February 1980).

56. K. W. Carlson and J. A. Williams, *The Effect of Crack Length and Side Grooves on the Ductile Fracture Toughness Properties of ASTM A533 Steel*, NUREG/CR-1171 (ORNL/Sub-79/50917/3), Hanford Engineering Development Laboratory, Richland, Wash. (October 1979).

57. P. P. Holz, *Flaw Preparations for HSST Program Vessel Fracture Mechanics Testing; Mechanical-Cyclic Pumping and Electron-Beam Weld-Hydrogen Charge Cracking Schemes*, NUREG/CR-1274 (ORNL/NUREG/TM-369), Oak Ridge Natl. Lab.. Oak Ridge, Tenn. (June 1980).

58. S. K. Iskander, *Two Finite Element Techniques for Computing Mode I Stress Intensity Factors in Two- or Three-Dimensional Problems*, NUREG/CR-1499 (ORNL/NUREG/CSD/TM-14), Computer Sciences Div., Union Carbide Corp. Nuclear Div., Oak Ridge, Tenn. (February 1981).

59. P. B. Crosley and E. J. Ripling, *Development of a Standard Test for Measuring K_{Ia} with a Modified Compact Specimen*, NUREG/CR-2294 (ORNL/Sub-81/7755/1), Materials Research Laboratory, Glenwood, Ill. (August 1981).

60. S. N. Atluri, B. R. Bass, J. W. Bryson, and K. Kathiresan, *NOZ-FLAW: A Finite Element Program for Direct Evaluation of Stress Intensity Factors for Pressure Vessel Nozzle-Corner Flaws*, NUREG/CR-1843 (ORNL/NUREG/CSD/TM-18), Computer Sciences Div., Oak Ridge Gaseous Diffusion Plant, Oak Ridge, Tenn. (March 1981).

61. A. Shukla, W. L. Fourney, and G. R. Irwin, *Study of Energy Loss and Its Mechanisms in Homalite 100 During Crack Propagation and Arrest*, NUREG/CR-2150 (ORNL/Sub-7778/1), University of Maryland, College Park, Md. (August 1981).

62. S. K. Iskander, R. D. Cheverton, and D. G. Ball, *OCA-I, A Code for Calculating the Behavior of Flaws on the Inner Surface of a Pressure Vessel Subjected to Temperature and Pressure Transients*, NUREG/CR-2113 (ORNL/NUREG-84), Oak Ridge Natl. Lab., Oak Ridge, Tenn. (August 1981).

63. R. J. Sanford, R. Chona, W. L. Fourney, and G. R. Irwin, *A Photoelastic Study of the Influence of Non-Singular Stresses in Fracture Test Specimens*, NUREG/CR-2179 (ORNL/Sub-7778/2), University of Maryland, College Park, Md. (August 1981).

64. B. R. Bass, S. N. Atluri, J. W. Bryson, and K. Kathiresan, *OR-FLAW: A Finite Element Program for Direct Evaluation of K-Factors for User-Defined Flaws in Plate, Cylinders, and Pressure-Vessel Nozzle Corners*, NUREG/CR-2494 (ORNL/CSD/TM-165), Oak Ridge Natl. Lab., Oak Ridge, Tenn. (April 1982).

65. B. R. Bass and J. W. Bryson, *Applications of Energy Release Rate Techniques to Part-Through Cracks in Plates and Cylinders*, Volume 1. *ORMGEN-3D: A Finite Element Mesh Generator for 3-Dimensional Crack Geometries*, NUREG/CR-2997, Vol. 1 (ORNL/TM-8527/V1), Oak Ridge Natl. Lab., Oak Ridge, Tenn. (December 1982).

66. B. R. Bass and J. W. Bryson, *Applications of Energy Release Rate Techniques to Part-Through Cracks in Plates and Cylinders*, Volume 2. *ORVIRT: A Finite Element Program for Energy Release Rate Calculations for 2-Dimensional and 3-Dimensional Crack Models*, NUREG/CR-2997, Vol. 2 (ORNL/TM-8527/V2), Oak Ridge Natl. Lab., Oak Ridge, Tenn. (February 1983).

67. R. D. Cheverton, S. K. Iskander, and D. G. Ball, *PWR Pressure Vessel Integrity During Overcooling Accidents: A Parametric Analysis*, NUREG/CR-2895 (ORNL/TM-7931), Oak Ridge Natl. Lab., Oak Ridge, Tenn. (February 1983).

68. D. G. Ball, R. D. Cheverton, J. B. Drake, and S. K. Iskander, *OCA-II, A Code for Calculating Behavior of 2-D and 3-D Surface Flaws in a Pressure Vessel Subjected to Temperature and Pressure Transients*, NUREG/CR-3491 (ORNL-5934), Oak Ridge Natl. Lab., Oak Ridge, Tenn. (February 1984).

69. A. Sauter, R. D. Cheverton, and S. K. Iskander, *Modification of OCA-I for Application to a Reactor Pressure Vessel with Cladding on the Inner Surface*, NUREG/CR-3155 (ORNL/TM-8649), Oak Ridge Natl. Lab., Oak Ridge, Tenn. (May 1983).

70. R. D. Cheverton and D. G. Ball, *OCA-P, A Deterministic and Probabilistic Fracture-Mechanics Code for Application to Pressure Vessels*, NUREG/CR-3618 (ORNL-5991), Oak Ridge Natl. Lab., Oak Ridge, Tenn. (May 1984).

71. J. G. Merkle, *An Examination of the Size Effects and Data Scatter Observed in Small Specimen Cleavage Fracture Toughness Testing*, NUREG/CR-3672 (ORNL/TM-9088), Oak Ridge Natl. Lab., Oak Ridge, Tenn. (April 1984).

72. C. R. Pugh et al., *Heavy-Section Steel Technology Program – Five-Year Plan FY 1983–1987*, NUREG/CR-3595 (ORNL/TM-9008), Oak Ridge Natl. Lab., Oak Ridge, Tenn. (April 1984).

73. D. G. Ball, B. R. Bass, J. W. Bryson, R. D. Cheverton, and J. B. Drake, *Stress Intensity Factor Influence Coefficients for Surface Flaws in Pressure Vessels*, NUREG/CR-3723 (ORNL/CSD/TM-216), Oak Ridge Natl. Lab., Oak Ridge, Tenn. (February 1985).

74. W. R. Corwin, R. G. Berggren, and R. K. Nanstad, *Charpy Toughness and Tensile Properties of Neutron Irradiated Stainless Steel Submerged-Arc Weld Cladding Overlay*, NUREG/CR-3927 (ORNL/TM-9309), Oak Ridge Natl. Lab., Oak Ridge, Tenn. (September 1984).

75. C. W. Schwartz, R. Chona, W. L. Fourney, and G. R. Irwin, *SAMCR: A Two-Dimensional Dynamic Finite Element Code for the Stress Analysis of Moving CRacks*, NUREG/CR-3891 (ORNL/Sub/79-7778/3), University of Maryland, College Park, Md. (November 1984).

76. W. R. Corwin, G. C. Robinson, R. K. Nanstad, J. G. Merkle, R. G. Berggren, G. M. Goodwin, R. L. Swain, and T. D. Owings, *Effects of Stainless Steel Weld Overlay Cladding on the Structural Integrity of Flawed Steel Plates in Bending, Series 1*, NUREG/CR-4015 (ORNL/TM-9390), Oak Ridge Natl. Lab., Oak Ridge, Tenn. (April 1985).

77. R. H. Bryan, B. R. Bass, S. E. Bolt, J. W. Bryson, D. P. Edmonds, R. W. McCulloch, J. G. Merkle, R. K. Nanstad, G. C. Robinson, K. R. Thoms, and G. D. Whitman, *Pressurized-Thermal-Shock Test of 6-in.-Thick Pressure Vessels. PTSE-1: Investigation of Warm Prestressing and Upper-Shelf Arrest*, NUREG/CR-4106 (ORNL-6135), Oak Ridge Natl. Lab., Oak Ridge, Tenn. (April 1985).

78. R. D. Cheverton, D. G. Ball, S. E. Bolt, S. K. Iskander, and R. K. Nanstad, *Pressure Vessel Fracture Studies Pertaining to the PWR Thermal-Shock Issue: Experiments TSE-5, TSE-5A, and TSE-6*, NUREG/CR-4249 (ORNL-6163), Martin Marietta Energy Systems, Inc., Oak Ridge Natl. Lab., Oak Ridge, Tenn. (June 1985).

79. R. D. Cheverton, D. G. Ball, S. E. Bolt, S. K. Iskander, and R. K. Nanstad, *Pressure Vessel Fracture Studies Pertaining to the PWR Thermal-Shock Issue: Experiment TSE-7*, NUREG/CR-4304 (ORNL-6177), Martin Marietta Energy Systems, Inc., Oak Ridge Natl. Lab., Oak Ridge, Tenn. (August 1985).

80. R. H. Bryan, B. R. Bass, S. E. Bolt, J. W. Bryson, J. G. Merkle, R. K. Nanstad, and G. C. Robinson, *Test of 6-in.-Thick Pressure Vessels. Series 3: Intermediate Test Vessel V-8A – Tearing Behavior of Low Upper-Shelf Material*, NUREG/CR-4760 (ORNL-6187),

Martin Marietta Energy Systems, Inc., Oak Ridge Natl. Lab., Oak Ridge, Tenn. (May 1987).

81. R. D. Cheverton and D. G. Ball, *A Parametric Study of PWR Pressure Vessel Integrity During Overcooling Accidents, Considering Both 2-D and 3-D Flaws*, NUREG/CR-4325 (ORNL/TM-9682), Martin Marietta Energy Systems, Inc., Oak Ridge Natl. Lab., Oak Ridge, Tenn. (August 1985).

82. E. C. Rodabaugh, *Comments on the Leak-Before-Break Concept for Nuclear Power Plant Piping Systems*, NUREG/CR-4305 (ORNL/Sub/82-22252/3), E. C. Rodabaugh Associates, Inc., Hilliard, Ohio (August 1985).

83. J. W. Bryson, *ORVIRT.PC: A 2-D Finite Element Fracture Analysis Program for a Microcomputer*, NUREG/CR-4367 (ORNL-6208), Martin Marietta Energy Systems, Inc., Oak Ridge Natl. Lab., Oak Ridge, Tenn. (October 1985).

84. D. G. Ball and R. D. Cheverton, *Adaptation of OCA-P, a Probabilistic Fracture-Mechanics Code, to a Personal Computer*, NUREG/CR-4468 (ORNL/CSD/TM-233), Martin Marietta Energy Systems, Inc., Oak Ridge Natl. Lab., Oak Ridge, Tenn. (January 1986).

85. J. W. Bryson and B. R. Bass, *ORMGEN.PC: A Microcomputer Program for Automatic Mesh Generation of 2-D Crack Geometries*, NUREG/CR-4475 (ORNL-6250), Martin Marietta Energy Systems, Inc., Oak Ridge Natl. Lab., Oak Ridge, Tenn. (March 1986).

86. G. D. Whitman, *Historical Summary of the Heavy-Section Steel Technology Program and Some Related Activities in Light-Water Reactor Pressure Vessel Safety Research*, NUREG/CR-4489 (ORNL-6259), Martin Marietta Energy Systems, Inc., Oak Ridge Natl. Lab., Oak Ridge, Tenn. (March 1986).

87. C. Inversini and J. W. Bryson, *ORPLOT.PC: A Graphic Utility for ORMGEN.PC and ORVIRT.PC*, NUREG/CR-4633 (ORNL-6291), Martin Marietta Energy Systems, Inc., Oak Ridge Natl. Lab., Oak Ridge, Tenn. (June 1986).

88. J. J. McGowan, R. K. Nanstad, and K. R. Thoms, *Characterization of Irradiated Current-Practice Welds and A533 Grade B Class 1 Plate for Nuclear Pressure Vessel Service*, NUREG/CR-4880 (ORNL/TM-10387), Martin Marietta Energy Systems, Inc., Oak Ridge Natl. Lab., Oak Ridge Tenn. (July 1988).

89. K. V. Cook and R. W. McClung, *Flaw Density Examinations of a Clad Boiling Water Reactor Pressure Vessel Segment*, NUREG/CR-4860 (ORNL/ TM-10364), Martin Marietta Energy Systems, Inc., Oak Ridge Natl. Lab., Oak Ridge, Tenn. (April 1987).

90. D. J. Naus et al., *Crack-Arrest Behavior in SEN Wide Plates of Quenched and Tempered A 533 Grade B Steel Tested Under Nonisothermal Conditions*, NUREG/CR-4930 (ORNL-6388), Martin Marietta Energy Systems, Inc., Oak Ridge Natl. Lab., Oak Ridge, Tenn. (August 1987).

91. D. B. Barker et al., *A Report on the Round Robin Program Conducted to Evaluate the Proposed ASTM Standard Test Method for Determining the Plane Strain Crack Arrest Fracture Toughness K_{Ia} of Ferritic Materials*, NUREG/CR-4996 (ORNL/Sub/79-7778/4), University of Maryland, College Park, Md. (January 1988).

92. W. H. Bamford, *A Summary of Environmentally Assisted Crack-Growth Studies Performed at Westinghouse Electric Corporation Under Funding from the Heavy-Section Steel Technology Program*, NUREG/CR-5020 (ORNL/Sub/82-21598/1), Westinghouse Electric Corp., Pittsburgh, Pa. (May 1988).

93. R. H. Bryan et al., *Pressurized-Thermal-Shock Test of 6-in.-Thick Pressure Vessels. PTSE-2: Investigation of Low Tearing Resistance and Warm Prestressing*, NUREG/CR-4888 (ORNL-6377), Martin Marietta Energy Systems, Inc., Oak Ridge Natl. Lab., Oak Ridge, Tenn. (December 1987).

94. J. H. Giovanola and R. W. Klopp, *Viscoplastic Stress-Strain Characterization of A533B Class 1 Steel*, NUREG/CR-5226 (ORNL/Sub/87-SA193/1), SRI International, Menlo Park, Calif. (September 1989).

95. L. F. Miller et al., *Neutron Exposure Parameters for the Metallurgical Test Specimens in the Fifth Heavy-Section Steel Technology Irradiation Series Capsules*, NUREG/CR-5019 (ORNL/TM-10582), Martin Marietta Energy Systems, Inc., Oak Ridge Natl. Lab., Oak Ridge, Tenn. (March 1988).

96. Canceled.

97. D. J. Naus, J. Keeney-Walker, B. R. Bass, S. E. Bolt, R. J. Fields, R. deWit, and S. R. Low III, *High-Temperature Crack-Arrest Behavior in 152-mm-Thick SEN Wide Plates of Quenched and Tempered A 533 Grade B Class 1 Steel*, NUREG/CR-5330 (ORNL/TM-11083), Martin Marietta Energy Systems, Inc., Oak Ridge Natl. Lab., Oak Ridge, Tenn. (April 1989).

98. K. V. Cook, R. A. Cunningham, Jr., and R. W. McClung, *Detection and Characterization of Indications in Segments of Reactor Pressure Vessels*, NUREG/CR-5322 (ORNL/TM-11072), Martin Marietta Energy Systems, Inc., Oak Ridge Natl. Lab., Oak Ridge, Tenn. (August 1989).

99. R. D. Cheverton, W. E. Pennell, G. C. Robinson, and R. K. Nanstad, *Impact of Radiation Embrittlement on Integrity of Pressure Vessel Supports for Two PWR Plants*, NUREG/CR-5320 (ORNL/TM-10966), Martin Marietta Energy Systems, Inc., Oak Ridge Natl. Lab., Oak Ridge, Tenn. (February 1989).

100. D. J. Naus, J. Keeney-Walker, B. R. Bass, S. K. Iskander, R. J. Fields, R. deWit, and S. R. Low III, *SEN Wide-Plate Crack-Arrest Tests Using A 533 Grade B Class 1 Material: WP-CE Test Series*, NUREG/CR-5408 (ORNL/TM-11269), Martin Marietta Energy Systems, Inc., Oak Ridge Natl. Lab., Oak Ridge, Tenn. (to be published).

ACKNOWLEDGMENTS

The authors wish to acknowledge the significant contributions made to this testing program by those who are not otherwise referred to in this report: D. E. Harne at the National Institute of Standards and Technology (performance of tests); C. R. Irwin, D. B. Barker, J. W. Dally, W. L. Fourney, and C. W. Schwartz at the University of Maryland (assistance in specimen design development, instrumentation and testing techniques, and analysis of test results); J. J. Henry and E. T. Manneschmidt of the Metals and Ceramics (M&C) Division at Oak Ridge National Laboratory (ORNL) (material characterization); R. K. Nanstad of the M&C Division at ORNL (guidance in material characterization); G. C. Robinson, Jr., S. E. Bolt, and W. F. Jackson of the Engineering Technology Division (ETD) at ORNL (specimen preparation, special test fixturing design, and fabrication); and C. E. Pugh and J. G. Merkle of the ETD at ORNL (developing the test program).

EXECUTIVE SUMMARY

The pressurized-thermal-shock (PTS) issue for pressurized-water reactors involves a broad range of fracture phenomena. In PTS scenarios, flaws in the inner surface of the reactor pressure vessel (RPV) have the greatest propensity to propagate because they are located in the region of highest thermal stress, lowest temperature, and greatest irradiation damage. If such flaws begin to propagate radially through the vessel wall, they will extend into regions of higher fracture toughness because of the higher temperatures and lesser irradiation damage. Although the thermal stresses may decrease with increasing propagation depth, the stress-intensity factor resulting from elevated-pressure loading will increase. In making assessments for light-water RPVs undergoing thermal transients with low accompanying pressure levels, the limit on crack-arrest toughness (220 MPa·$\sqrt{m}$) contained in the *American Society of Mechanical Engineers Boiler and Pressure Vessel Code (ASME B&PVC)* does not present difficulties. However, certain PTS scenarios could lead to conditions under which the driving force on a propagating crack increases to levels well over the ASME limit. Assessment of the integrity of an RPV under such a postulated crack run-arrest condition requires prediction of the arrest location, potential reinitiation, stable and unstable ductile crack growth, and structural instability of the remaining vessel wall ligament.

Work being conducted under Task H.5 of the Heavy-Section Steel Technology (HSST) Program at the Oak Ridge National Laboratory is concerned with the ability of RPV materials to arrest running cracks as they propagate into regions of higher toughness and conditions of increasing values for the stress-intensity factor. As a part of this task, the HSST Program in late FY 1984 initiated an investigation of the run-arrest behavior of cracks in large plates that possess steep toughness gradients. These tests use wide-plate (1 × 1 × 0.1 m or 1 × 1 × 0.15 m) specimens that possess a single-edge notch (crack) that initiates cleavage propagation at low temperature and arrests in a region of increased fracture toughness. The toughness gradient is achieved through a linear transverse temperature profile across the plate (edge-to-edge). The experiments, which require the application of large tensile loads, are being conducted at the National Institute of Standards and Technology in Gaithersburg, Maryland. The overall objectives of these tests are to determine (1) whether RPV materials will exhibit crack-arrest behavior when the driving force on a crack exceeds the ASME limit; (2) the relationship between crack-arrest toughness and temperature; and (3) the interaction of fracture modes (arrest, stable crack growth, unstable crack growth, and tensile instability) when arrest occurs at high temperatures. In meeting these objectives, tests have been conducted that use prototypic (A 533 grade B class 1 steel) as well as degraded (simulated) RPV materials.

This report contains results obtained from testing two 102-mm-thick wide plates that were fabricated from A 533 grade B material supplied by Combustion Engineering, Inc. Following are highlights of each chapter to aid readers who are interested only in certain parts of the report.

1. INTRODUCTION

Limitations imposed by the *ASME B&PVC*, as well as issues that must be addressed in making safety assessments for RPVs, are discussed. Objectives of the crack-arrest studies and program goals are presented.

2. BACKGROUND

Prior crack-arrest studies and their limitations are discussed. A summary of large-specimen, crack-arrest toughness data is presented in Fig. 2.1.

3. MATERIAL CHARACTERIZATION

A description of the A 533 grade B class 1 material used in the WP-CE test series is provided. Drop-weight (Table 3.1), Charpy V-notch (Table 3.2), and tensile (Table 3.5) properties are provided. Equations (3.1) and (3.2) present the relations for K_{Ic} and K_{Ia}, respectively, that were used for planning the tests.

4. SPECIMEN PREPARATION, INSTRUMENTATION, AND TESTING PROCEDURE

Procedures used for precracking and assembling the test articles are outlined. Instrumentation used to obtain pertinent data during a test (load, strain, temperature, crack-opening-displacement, dynamic displacement), as well as the data acquisition system, are described. The heating, cooling, and insulation systems used to produce the desired specimen transverse temperature profile are delineated. The technique used to conduct a wide-plate crack-arrest test (Fig. 4.9) is presented.

5. SUMMARY OF WIDE-PLATE CRACK-ARREST TESTS WP-CE-1 AND WP-CE-2

General test conditions (Table 5.1) for each wide-plate test are delineated, and transverse temperature profiles for each test are summarized (Fig. 5.1). The highlights for each test, as well as pertinent test data, are reiterated. Fracture surfaces for each specimen are provided (Fig. 5.2).

6. POSTTEST ANALYSES, CRACK-ARREST TOUGHNESS RESULTS, AND COMPARISON OF DATA WITH OTHER LARGE-SCALE TEST RESULTS

Posttest static and dynamic fracture analyses conducted for each wide-plate crack-arrest test are described. Crack-arrest toughness results determined by static and dynamic analyses, as well as by handbook techniques, are presented (Table 6.4). The relationship between fixed-load, generation-mode, crack-arrest toughness values for tests WP-CE-1 and -2, as well as for other tests that used A 533 grade B class 1 materials (WP-1 Series), and the K_{IR} curve of the *ASME B&PVC* is shown (Fig. 6.22). The wide-plate data are compared with other large-scale test results (Fig. 6.23).

7. CONCLUSIONS

Results of the investigation are summarized. Primary conclusions are that (1) crack arrest can and does occur at temperatures up to and above that which corresponds to the onset of Charpy upper-shelf behavior and (2) measured K_{Ia} values extend above the limit set in the *ASME B&PVC*.

SEN WIDE-PLATE CRACK-ARREST TESTS USING A 533 GRADE B CLASS 1 MATERIAL: WP-CE TEST SERIES

D. J. Naus
J. Keeney-Walker
B. R. Bass
S. K. Iskander
R. J. Fields
R. deWit
S. R. Low III

1. INTRODUCTION

Current light-water-reactor (LWR) pressure-vessel safety assessment methods are based largely on Sects. III and XI of the *American Society of Mechanical Engineers Boiler and Pressure Vessel Code (ASME B&PVC)*. In pressurized-thermal-shock (PTS) scenarios, flaws on the inner surface of a reactor pressure vessel (RPV) have the greatest propensity to propagate because they are in the region of highest thermal stress, lowest temperature, and greatest irradiation damage. If such a flaw begins to propagate radially through the vessel wall, it will extend into a region of higher fracture toughness because of the higher temperatures and lesser irradiation damage. Although the thermal stresses may decrease with increasing crack propagation depth, the stress-intensity factor caused by the elevated-pressure loading will increase. Assessment of the integrity of an RPV under such a postulated crack run-arrest scenario requires prediction of the arrest location, potential reinitiation, stable and unstable ductile crack growth, and structural instability of the remaining vessel wall ligament.

The fracture toughness correlations contained in the *ASME B&PVC* clearly show that one cannot assume a crack-arrest toughness value (K_{Ia}) >220 MPa·$\sqrt{m}$ for LWR pressure-vessel steels. The imposition of this limit is based primarily on the facts that (1) no K_{Ia} data existed at or above this level and (2) Charpy tests showed that impact energy levels exhibit an upper-shelf behavior. Therefore, the nature of crack-arrest behavior and K_{Ia} extrapolations to temperatures higher than that at which this limit occurred could not be presumed.

The ASME limit does not impose difficulties in making assessments for LWR pressure vessels undergoing thermal shock transients with low accompanying pressure levels. However, certain PTS scenarios could lead to conditions under which the driving force on a propagating crack increases to levels well over the current ASME limit. Thus, safety assessment methods for this type of condition would require an understanding of the following points.

1. If the driving force on a crack exceeds 220 MPa·$\sqrt{m}$ by a significant margin, can the material exhibit crack-arrest behavior?
2. If the material exhibits high K_{Ia} values with increasing temperature, what is the relationship between K_{Ia} and temperature? That is, does a temperature limit exist above which cleavage crack propagation cannot continue regardless of the magnitude of the driving force?

3. If crack arrest does occur at high temperatures, at which the material behavior is typically dominated by ductile behavior, then which interactions exist between the various fracture modes, including arrest, stable crack growth, unstable crack growth, and tensile instability?

Because wide-plate tests have the ability to provide a significant number of data points at reasonable cost, they were selected for use in the investigation.

The primary objective of the wide-plate crack-arrest studies under the Heavy-Section Steel Technology (HSST) Program is to generate data and associated analysis methods for understanding the crack-arrest behavior of prototypical RPV steels at temperatures near and above the onset of the Charpy upper-shelf region. Program goals include (1) extending the existing K_{Ia} data bases to include values above those associated with the upper limit in the *ASME B&PVC*; (2) clearly establishing that crack arrest occurs before fracture-mode conversion; and (3) validating the predictability of crack arrest, stable tearing, and/or unstable tearing sequences for ductile materials. The wide-plate tests and analyses provide bases for obtaining and interpreting dynamic-fracture data (with relatively long crack runs) and bases for validating viscoplastic fracture models and analysis methods. In the study discussed in this report, the program objectives and goals were investigated for one material, American Society for Testing and Materials (ASTM) A 533 grade B class 1 steel supplied by Combustion Engineering, Inc. (CE).

2. BACKGROUND

Under the HSST Program, crack-arrest data have been generated over an expanded temperature range in tests involving large thermally shocked cylinders[1,2] (TSCs), pressurized thermally shocked vessels (PTSVs),[3,4] and wide-plate specimens.[5,6] The TSCs and PTSVs also provide data under multiaxial transient and high restraint loadings for validation of fracture models and analysis methods. Although the thermal-shock experiments (TSEs) have generated a significant number of data points, the driving force in these experiments has been thermal stress only, and, consequently, crack-arrest data have not ranged above ~150 MPa·$\sqrt{m}$. An important conclusion of the TSEs is that the K_{Ia} data from these highly restrained propagations fall well within the range of K_{Ia} data from the small laboratory specimens and above the ASME reference toughness (K_{IR}) curve, which provides a lower bound of crack arrest (K_{Ia}) and dynamic fracture toughness (K_{Id}) as a function of the temperature relative to the nil-ductility temperature (NDT). The HSST pressurized-thermal-shock experiments (PTSEs) can provide higher K_{Ia} values under similar highly restrained conditions, as shown by the first two PTSEs, which produced K_{Ia} data as high as ~420 MPa·$\sqrt{m}$ at temperatures up to ~90°C above the drop-weight NDT for the vessel insert material (-75°C). Crack-arrest tests that used wide-plate specimens fabricated from A 533 grade B class 1 material (HSST Plate 13A) have produced K_{Ia} data >500 MPa·$\sqrt{m}$ (fixed-load, generation-mode analysis) at temperatures up to 115°C above the material RT_{NDT} (-23°C).

Large-specimen, high-temperature, crack-arrest data have also been developed by testing (1) moment-modified compact-tension (MMCT) specimens at CE under an Electric Power Research Institute (EPRI) program, Research Program RP-2180-3,[7] (2) wide-plate and ESSO specimens in Japan,[8-14] and (3) TSEs in France.[15] A summary of K_{Ia} data for the HSST Program TSEs, PTSEs, and wide-plate tests (A 533 grade B material); the CE/EPRI MMCT tests; the Japanese tests; and the French TSEs is presented in Fig. 2.1.

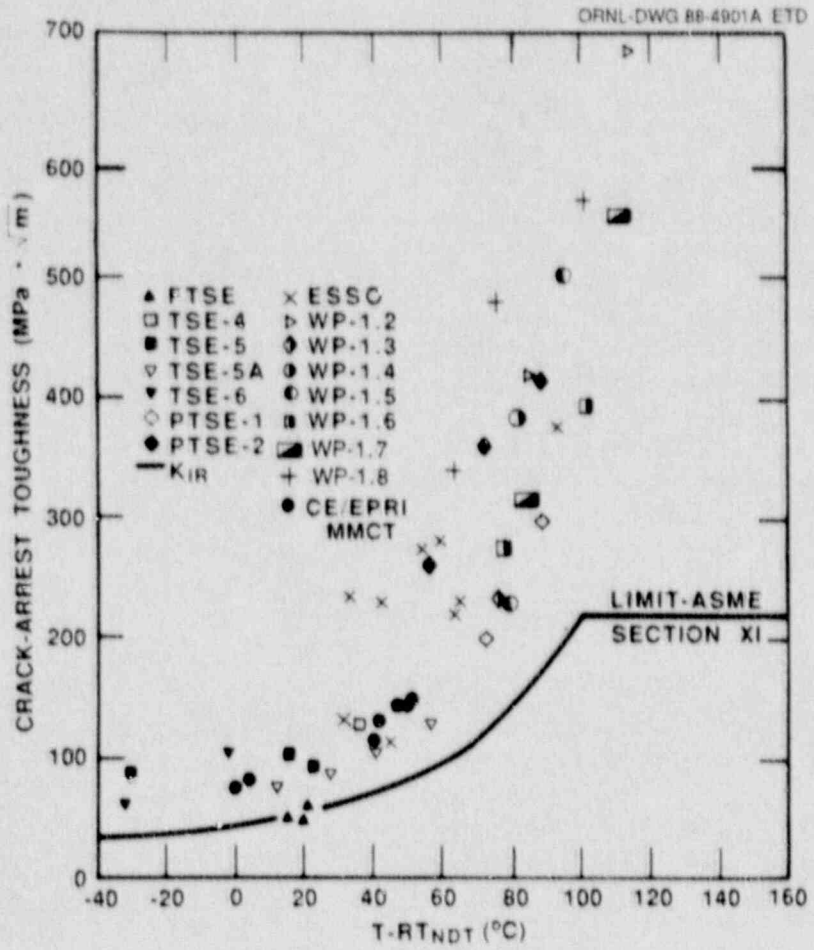

Fig. 2.1. Summary of large-specimen, high-temperature, crack-arrest data.

REFERENCES

1. R. D. Cheverton et al., Martin Marietta Energy Systems, Inc., Oak Ridge Natl. Lab., *Pressure Vessel Fracture Studies Pertaining to the PWR Thermal-Shock Issue: Experiments TSE-5, TSE-5A, and TSE-6*, USNRC Report NUREG/CR-4249 (ORNL-6163), June 1985.*

2. R. D. Cheverton et al., Martin Marietta Energy Systems, Inc., Oak Ridge Natl. Lab., *Pressure Vessel Fracture Studies Pertaining to the PWR Thermal-Shock Issue: Experiment TSE-7*, USNRC Report NUREG/CR-4304 (ORNL-6177), August 1985.*

3. R. H. Bryan et al., Martin Marietta Energy Systems, Inc., Oak Ridge Natl. Lab., *Pressurized-Thermal-Shock Test of 6-in.-Thick Pressure Vessels. PTSE-1: Investigation of Warm Prestressing and Upper-Shelf Arrest*, USNRC Report NUREG/CR-4106 (ORNL-6135), April 1985.*

4. R. H. Bryan et al., Martin Marietta Energy Systems, Inc., Oak Ridge Natl. Lab., *Pressurized-Thermal-Shock Test of 6-in.-Thick Pressure Vessels. PTSE-2: Investigation of Low Tearing Resistance and Warm Prestressing*, USNRC Report NUREG/CR-4888 (ORNL-6377), December 1987.*

5. D. J. Naus et al., Martin Marietta Energy Systems, Inc., Oak Ridge Natl. Lab., *Crack-Arrest Behavior in SEN Wide Plates of Quenched and Tempered A533 Grade B Steel Tested Under Nonisothermal Conditions*, USNRC Report NUREG/CR-4930 (ORNL-6388), August 1987.*

6. D. J. Naus et al., Martin Marietta Energy Systems, Inc., Oak Ridge Natl. Lab., *High-Temperature Crack-Arrest Behavior in 152-mm-Thick SEN Wide Plates of Quenched and Tempered A 533 Grade B Class 1 Steel*, USNRC Report NUREG/CR-5330 (ORNL/TM-11083), April 1989.*

7. R. Y. Schonenberg and D. M. Norris, "Moment Modified Compact Tension Specimen for Measuring Crack Arrest Toughness," *Nucl. Eng. Des.* 96, 277–86 (1986).†

8. Japan Welding Council, *Structural Integrity of Very Thick Steel Plate for Nuclear Reactor Pressure Vessels*, JWES-AE-7806, 1977 (in Japanese).

9. T. Kanazawa, S. Machida, and T. Teramoto, "Preliminary Approaches to Experimental and Numerical Study of Fast Crack Propagation and Crack Arrest," *Fast Fracture and Crack Arrest*, ASTM STP 627, 39–58 (1977).†

10. N. Ohashi et al., "Fracture Toughness of Heavy Section LWR Pressure Vessel Steel Plate Produced by Basic Oxygen Furnace and Ladle Refining Process," pp. 391–96 in *Proceedings of the Fourth International Conference on Pressure Vessel Technology*, Vol. 1, *I. Mech. E.*, 1980.*

11. T. Kanazawa et al., "Study on Fast Fracture and Crack Arrest," *Experimental Mechanics* 21(2), 77–88 (February 1981).†

12. S. Machida, Y. Kawaguchi, and M. Tsukamoto, "An Evaluation of the Crack Arrestability of 9% Ni Steel Plate to an Extremely Long Brittle Crack," *Journal of the Society of Naval Architects of Japan* 150, 511–17 (1981) (translation ORNL-tr-5052).†

13. T. Kanazawa, S. Machida, and H. Yajima, "Recent Studies on Brittle Crack Propagation and Arrest in Japan," in *Fracture Mechanics Technology Applied to Material and Structure Design*, G. C. Sih, N. E. Ryan, and R. Jones, Eds. (Martinua Nijhoff, The Hague, 1983), pp. 81–100.

14. Y. Nakano, "Stress Intensity Factor During Brittle Crack Propagation and Arrest in ESSO Specimens," pp. 204–9, in *Proceedings of*

the 18th National Symposium on X-Ray Study on Deformation and Fracture Solids, The Society of Materials Science, Japan, July 13-14, 1981. Translated from the Japanese *Zairyo* 31, N342, pp. 204–9 (1982), received Aug. 24, 1981, ORNL-tr-4874.

15. A. Pellissier-Tanon, P. Sollogoub, and B. Houssin, "Crack Initiation and Arrest in an SA 508 Class-3 Cylinder Under Liquid Nitrogen Thermal-Shock," paper G/F 1/8, Vol. G/H, pp. 137–42 in *Transactions of the 7th International Conference on Structural Mechanics in Reactor Technology*, Chicago, Aug. 22–26, 1983.†

---

*Available for purchase from National Technical Information Service, Springfield, Virginia 22161.

†Available in public technical libraries.

3. MATERIAL CHARACTERIZATION

3.1 INTRODUCTION

The steel plate used[1] to fabricate wide-plate specimens WP-CE-1 and -2 conforms to the specifications of ASME SA 533 grade B class 1. A limited amount of material characterization was performed at the Oak Ridge National Laboratory (ORNL) to determine various parameters required to analyze the wide-plate tests.* One of these parameters is reference temperature nil-ductility-transition (RT_{NDT}). In accordance with Subarticle NB-2330 of the *ASME Boiler and Pressure Vessel Code*, Sect. III, RT_{NDT} is the higher of the drop-weight NDT temperature and (T-33)°C, where T is defined as the temperature at which, for T-L orientation Charpy V-notch (CVN) specimens, both 68 J and a lateral expansion of 0.89 mm are attained. For this study, CVN impact tests in the L-T and T-L orientations have been performed. The wide-plate tests were performed such that the crack propagation orientation is L-T. The tests in the T-L orientation were performed to allow the tests reported in Ref. 1 to be compared and to determine the RT_{NDT}. For completeness, the tensile properties extracted from Ref. 1 have been included.

3.2 MATERIAL DESCRIPTION AND ALLOCATION

The two test sections used in the wide-plate tests were machined from an ~5600 × 2800 × 244 mm plate of SA 533 grade B class 1 steel. The location of the wide-plate test sections in the plate stock is shown shaded in Fig. 3.1. The plate stock was supplied by CE. The sections for the wide-plate tests were obtained by sawing the 244-mm-thick plate into two halves, each ~120 mm thick, as shown in Fig. 3.2.

Because some of the wide-plate test section material originated from near the surface of the plate stock, tests were performed to determine whether the material properties varied through the plate thickness. Posttest characterization was performed on material machined from a section flame cut from the broken halves of specimen WP-CE-2. The approximate location in the overall test section of the material used for posttest characterization is shown in Fig. 3.3. Specimens were obtained from each of 4 layers and are identified as "layer 1," "layer 2," "layer 3," etc. The layout of the specimens is shown in Figs. 3.4 and 3.5.

3.3 DETERMINATION OF RT_{NDT}

Drop-weight testing was performed according to the *ASTM Procedure for Conducting Drop-Weight Test to Determine Nil-Ductility Transition*

---

*Reference 1 presents more detailed information on characterization of the plate material.

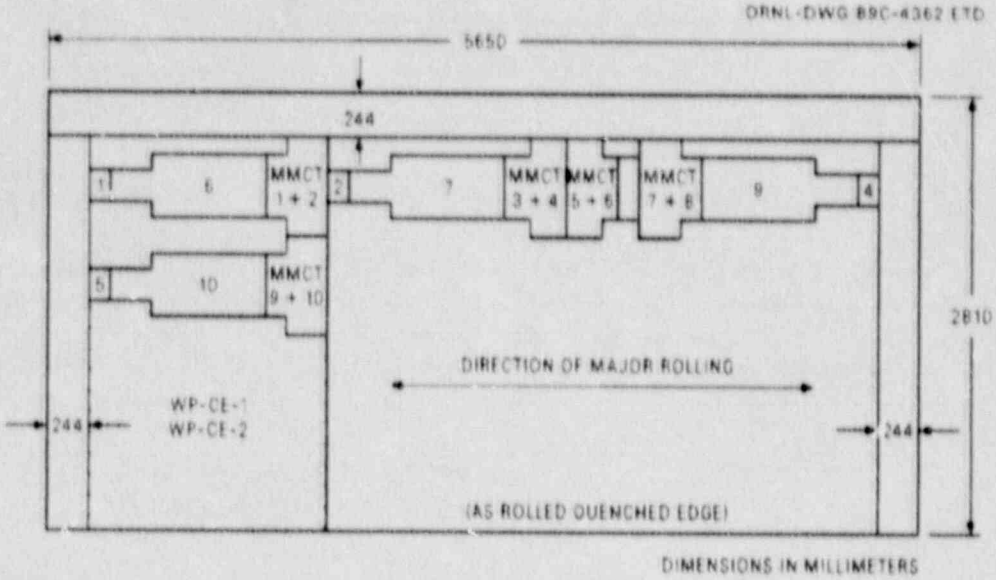

Fig. 3.1. Allocation of material in CE SA 533 grade B class 1 plate stock.

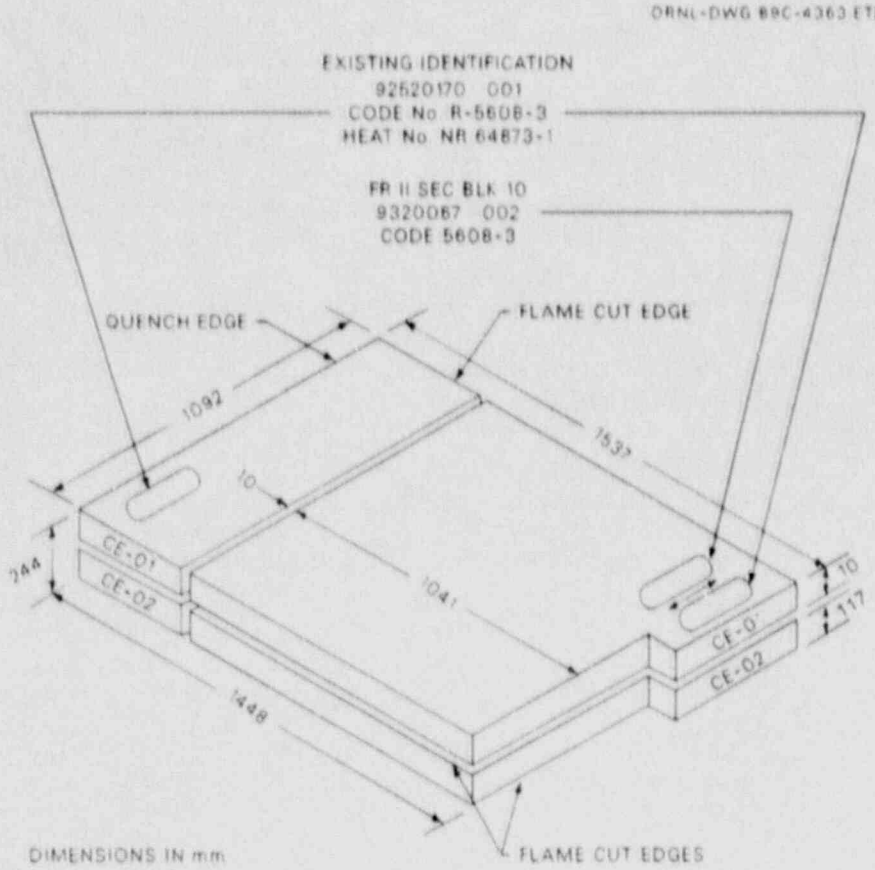

Fig. 3.2. Slabbing detail of SA 533 grade B class 1 material sent to ORNL by CE.

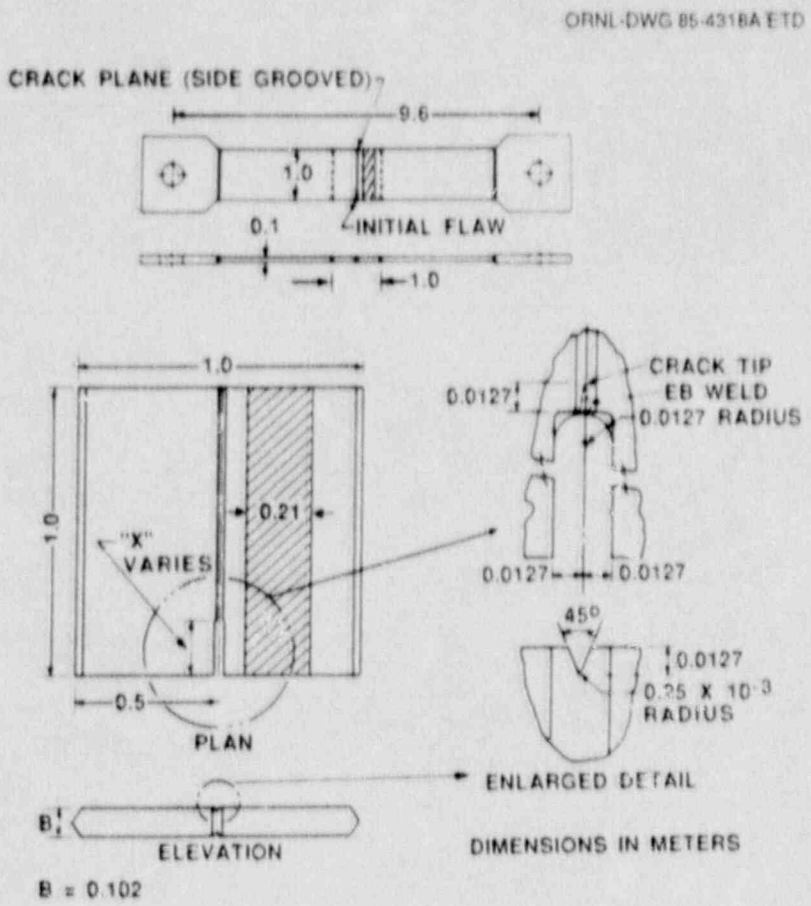

Fig. 3.3. Approximate location in specimen WP-CE-2 where material was obtained for posttest characterization.

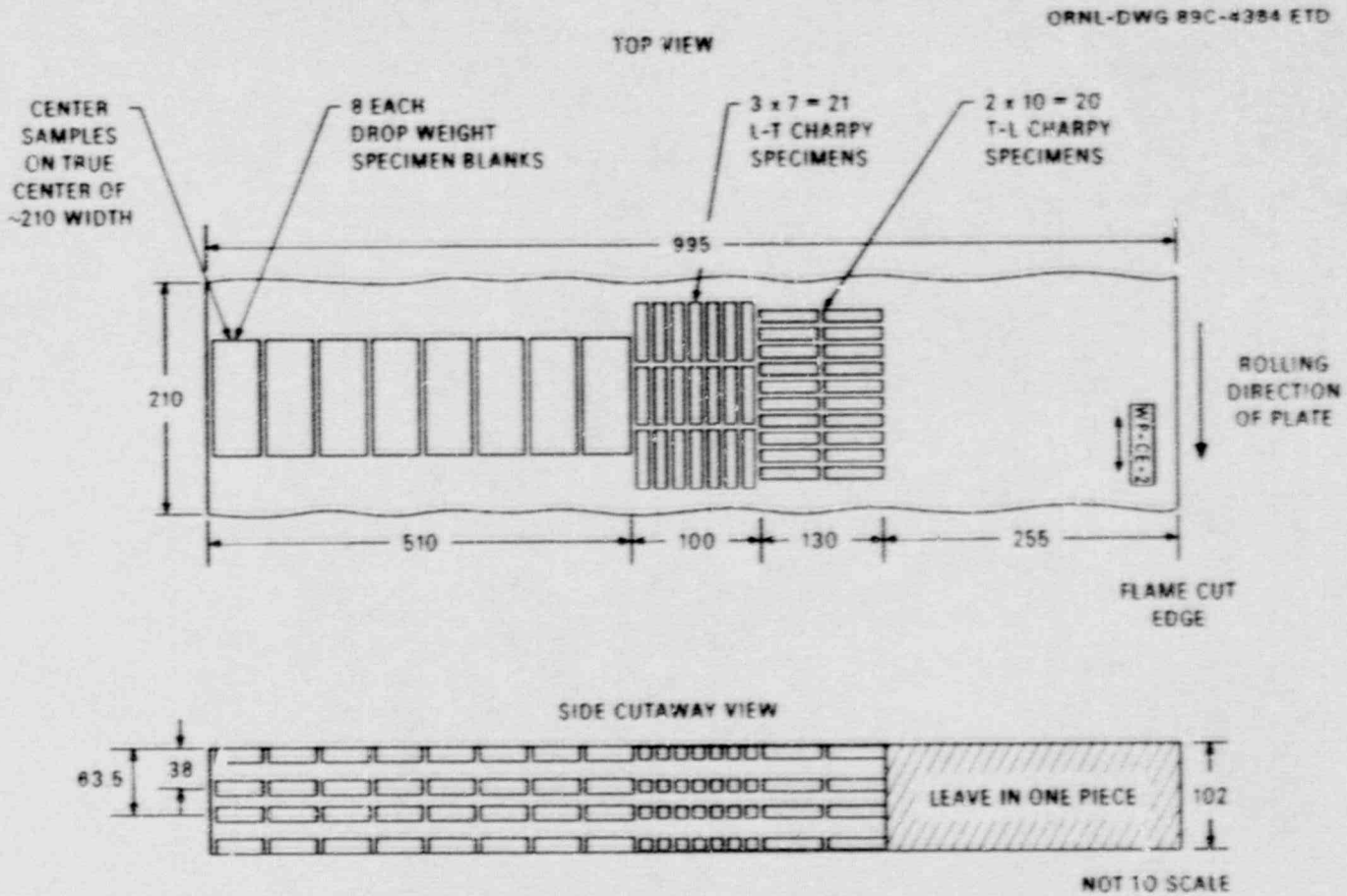

Fig. 3.6. Drop weight and CVN test specimen layout for posttest characterization studies.

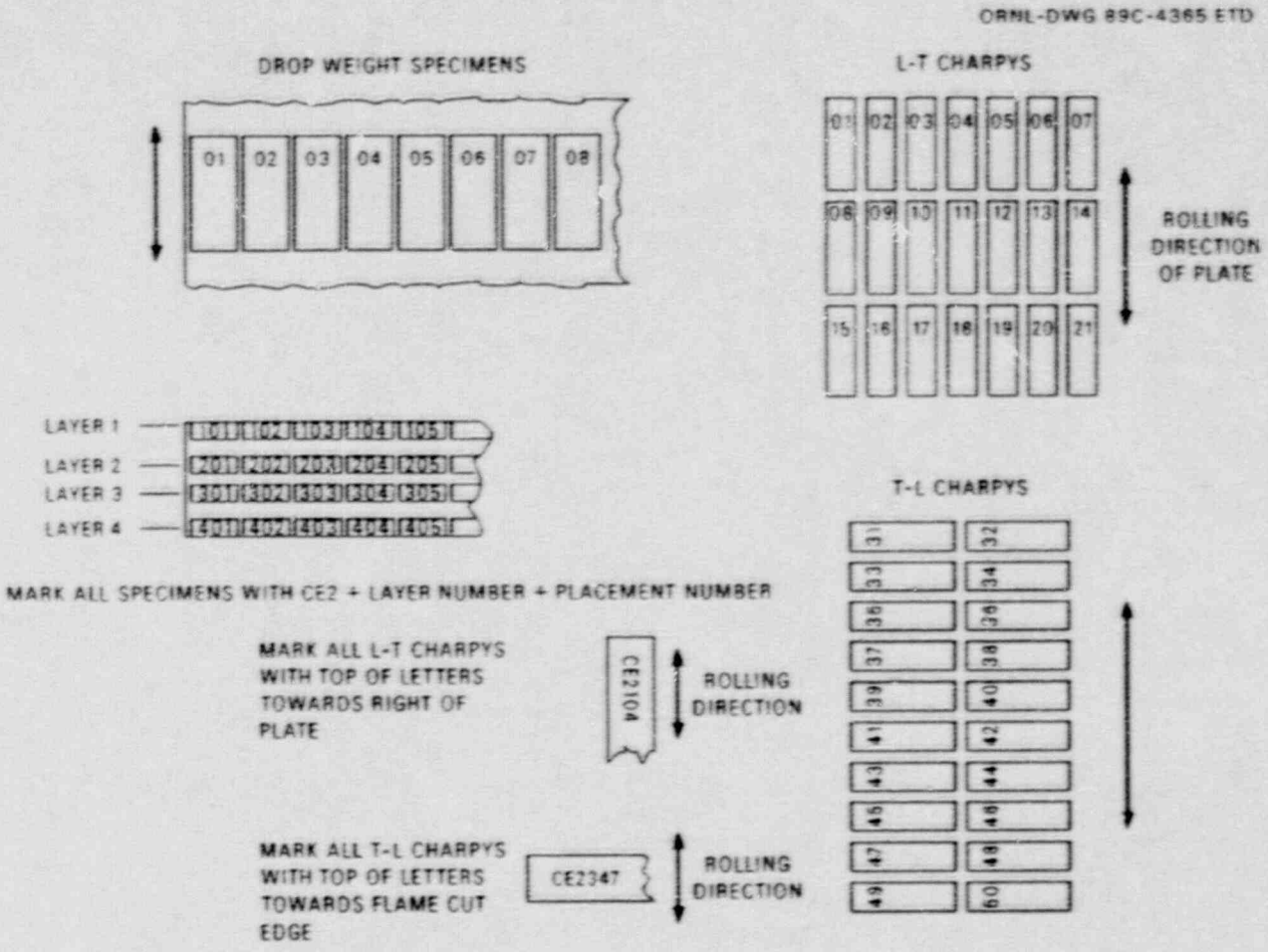

Fig. 3.5. Material characterization test specimen designation scheme.

Temperature of Ferritic Steels (E 208-87a). A specimen type P-3 with a single-pass crack starter weld bead was used, and the test results are shown in Table 3.1. The drop-weight NDT temperature can be considered to be -35°C because a 5 K difference found between layer 4 and the other three layers is not considered to be significant. This result also agrees with the -34.4°C (-30°F) drop-weight NDT value reported in Ref. 1 for material characterization blocks 6 and 10. (Characterization blocks 6 and 10, shown in Fig. 3.1, were obtained from a location in the plate stock that was in close proximity to the position where material was provided by CE for fabrication of specimens WP-CE-1 and -2. As noted in Ref. 1, some variation in material properties occurs along the 5600-mm length of the plate stock.)

CVN impact tests were performed using specimens with a T-L orientation obtained from each of the four layers at a temperature of -2°C (NDT + 33°C). The 68-J energy and 0.89-mm lateral expansion requirements of ASME Subarticle NB-2330 were both fulfilled. More details on the test results are given next in the section on CVN testing in the T-L orientation. Accordingly, the RT_{NDT} is -35°C.

3.4 CVN TESTING IN THE L-T AND T-L ORIENTATIONS

The results of the CVN impact testing in the L-T orientation are given in Table 3.2. The test results, together with a regression-fit hyperbolic tangent, have also been plotted in Figs. 3.6 to 3.9. The upper shelf energy (USE) for layer 1 is ~350 J. The onset of upper shelf, as indicated by 100% shear, is at 50°C, and if judged from the lateral expansion, it is at 25°C. The USEs for the other three layers are only slightly less, ranging from ~320 to 335 J.

The regression-fit hyperbolic tangent curves were used to compare the CVN impact energy results from all four layers (Fig. 3.10). The hyperbolic tangent curve fit parameters for the four layers tested in the L-T orientation are given in Table 3.3. These curves reflect the somewhat higher CVN toughness of layer 1 compared with the other three layers in the upper transition and upper-shelf regions. At some temperatures, such as the upper transition, there is about a 25% difference in CVN impact energy between the various layers. Layer 3 also indicated slightly elevated upper transition and upper-shelf CVN impact toughness when compared with layers 2 and 4. Assuming the NDT temperature to be -35°C, the energy level at the NDT temperature is at least 46 J. The CVN impact toughness at the NDT temperature increases from 46 J in layer 1 to 69 J in layer 4. As calculated from the regression fit, there is a consistent decrease in both the 41- and 68-J temperatures of 24 and 14 K, respectively, from layers 1 to 4. To analyze the results of the large wide-plate specimen tests, an average curve was derived by fitting the hyperbolic tangent curve to all the CVN-impact energy test data in the L-T orientation. The resultant regression parameters have been included in Table 3.3 and are labeled "average." Note that the parameters are almost the same as those for layer 3. This "average" curve is shown in Fig. 3.10(*b*).

The results of the CVN impact tests in the T-L orientation are given in Table 3.4. The curve fit parameters are given in Table 3.3.

Table 3.1 Results of drop-weight testing on A 533 grade B class 1 material for samples taken at various depths of specimen WP-CE-2

Specimen	Test temperature (°C)	Test results		NDT (°C)
		Break	No break	
	Layer 1			
CE2108	−50	✓		
CE2107	−40	✓		
CE2106	−30		✓	
CE2101	−35		✓	
CE2103	−35	✓		
CE2104	−30		✓	
				−35
	Layer 2			
CE2207	−35	✓		
CE2206	−30		✓	
CE2202	−30		✓	
				−35
	Layer 3			
CE2305	−35		✓	
CE2307	−40	✓		
CE2306	−35	✓		
CE2304	−30		✓	
CE2301	−30		✓	
				−35
	Layer 4			
CE2405	−20		✓	
CE2407	−30		✓	
CE2402	−50	✓		
CE2403	−35		✓	
CE2406	−35		✓	
CE2408	−40	✓		
				−40

Table 3.2 CVN impact test results in L-T orientation for material obtained from specimen WP-CE-2

Specimen No.	Test temperature (°C)	CVN energy (J)	Lateral expansion (mm)	Fracture appearance (%)
		Layer 1		
CE2116	-75	6	0.08	0
CE2104	-50	15	0.23	13
CE2108	-25	47	0.76	18
CE2112	-25	79	1.17	24
CE2107	-25	60	0.97	18
CE2110	0	121	1.60	47
CE2105	0	161	2.06	52
CE2115	0	153	1.88	48
CE2101	23	179	2.31	70
CE2102	23	166	2.01	60
CE2109	23	177	2.11	62
CE2113	50	284	2.11	100
CE2106	50	263	2.13	100
CE2114	75	353	2.13	100
CE2111	100	341	1.83	100
CE2120	150	343	2.06	100
CE2103	150	347	1.93	100
CE2118	200	340	1.80	100
CE2121	200	331	1.57	100
CE2119	250	339	1.70	100
CE2117	300	335	1.70	100
		Layer 2		
CE2114	-75	9	0.10	0
CE2208	-50	17	0.25	11
CE2215	-25	48	0.74	23
CE2216	-25	50	0.76	20
CE2203	-25	59	0.86	23
CE2211	0	123	1.63	25
CE2212	0	110	1.50	30
CE2204	0	110	1.42	18
CE2201	23	145	1.75	50
CE2202	23	179	2.08	70
CE2209	23	153	1.80	55
CE2206	50	229	2.29	100
CE2207	100	262	2.06	100
CE2218	150	303	1.80	100
CE2213	150	310	1.65	100
CE2219	200	321	1.52	100
CE2220	200	322	1.52	100
CE2221	250	346	1.63	100
CE2217	300	304	1.42	100

Table 3.2 (continued)

Specimen No.	Test temperature (°C)	CVN energy (J)	Lateral expansion (mm)	Fracture appearance (%)
		Layer 3		
CE2301	−75	8	0.00	0
CE2307	−50	19	0.30	10
CE2310	−25	67	0.94	28
CE2312	−25	82	1.17	25
CE2308	−25	64	0.97	21
CE2302	0	114	1.60	20
CE2316	0	146	1.80	46
CE2306	0	127	1.65	38
CE2305	23	170	2.01	65
CE2311	23	176	1.96	50
CE2314	23	180	2.24	77
CE2315	50	248	2.31	100
CE2303	100	315	2.01	100
CE2318	150	318	2.01	100
CE2317	150	323	1.70	100
CE2320	200	339	1.68	100
CE2321	200	340	1.50	100
CE2309	250	320	1.52	100
CE2319	300	323	1.65	100
		Layer 4		
CE2411	−75	10	0.13	0
CE2401	−50	36	0.48	18
CE2413	−50	45	0.71	13
CE2414	−25	105	1.42	30
CE2404	−25	91	1.30	27
CE2407	−25	72	1.04	21
CE2405	0	122	1.75	45
CE2406	0	111	1.50	52
CE2415	0	145	1.93	50
CE2416	23	163	2.03	40
CE2403	23	166	2.11	52
CE2412	23	162	2.18	75
CE2409	50	219	2.29	100
CE2402	150	285	1.96	100
CE2420	150	305	1.55	100
CE2421	200	342	1.63	100
CE2418	200	326	1.60	100
CE2417	250	337	1.68	100
CE2419	300	341	1.65	100

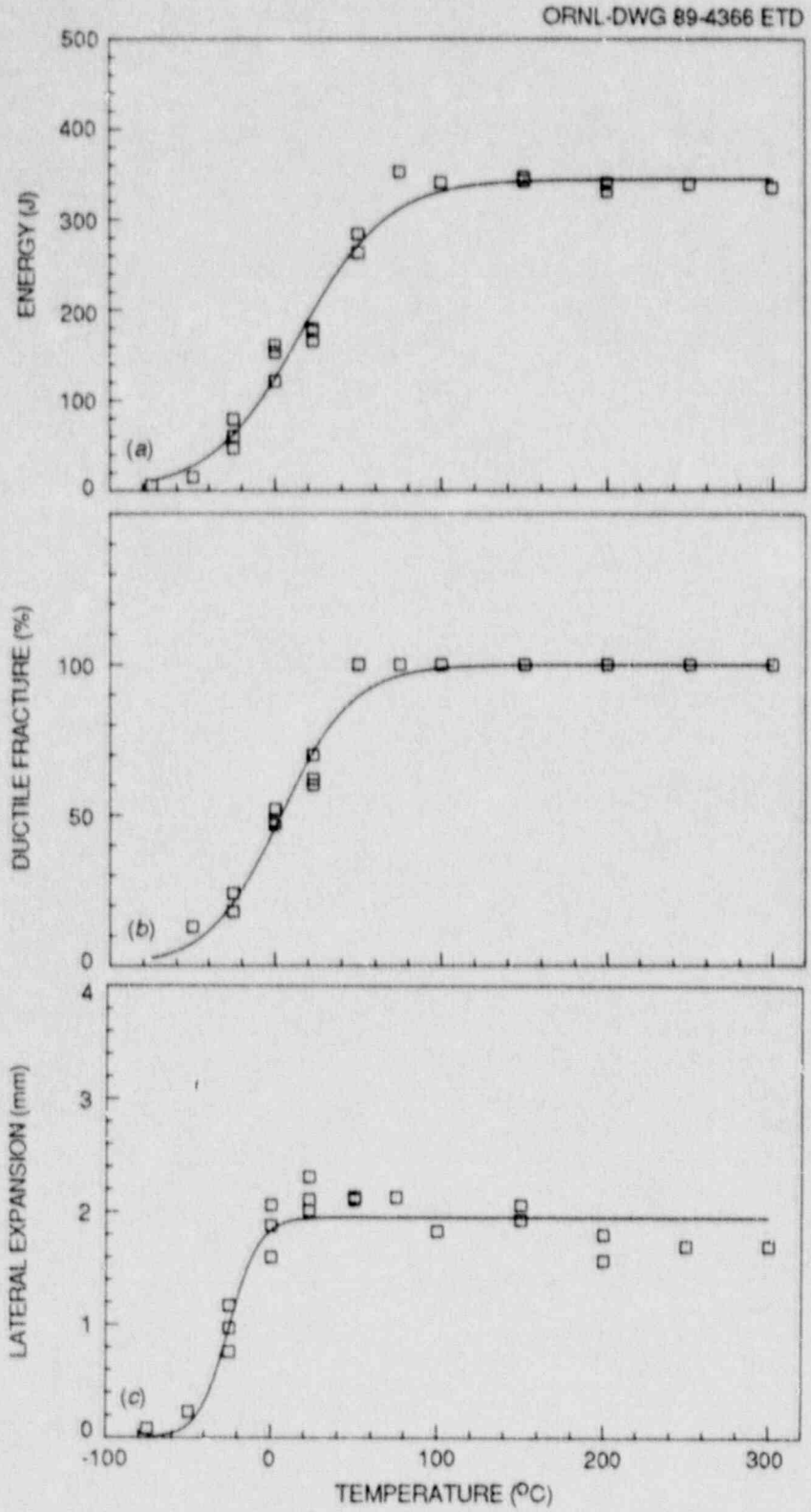

Fig. 3.6. CVN test results in L-T orientation for material obtained from layer 1 of specimen WP-CE-2: (a) CVN impact energy, (b) percent ductile fracture, and (c) lateral expansion.

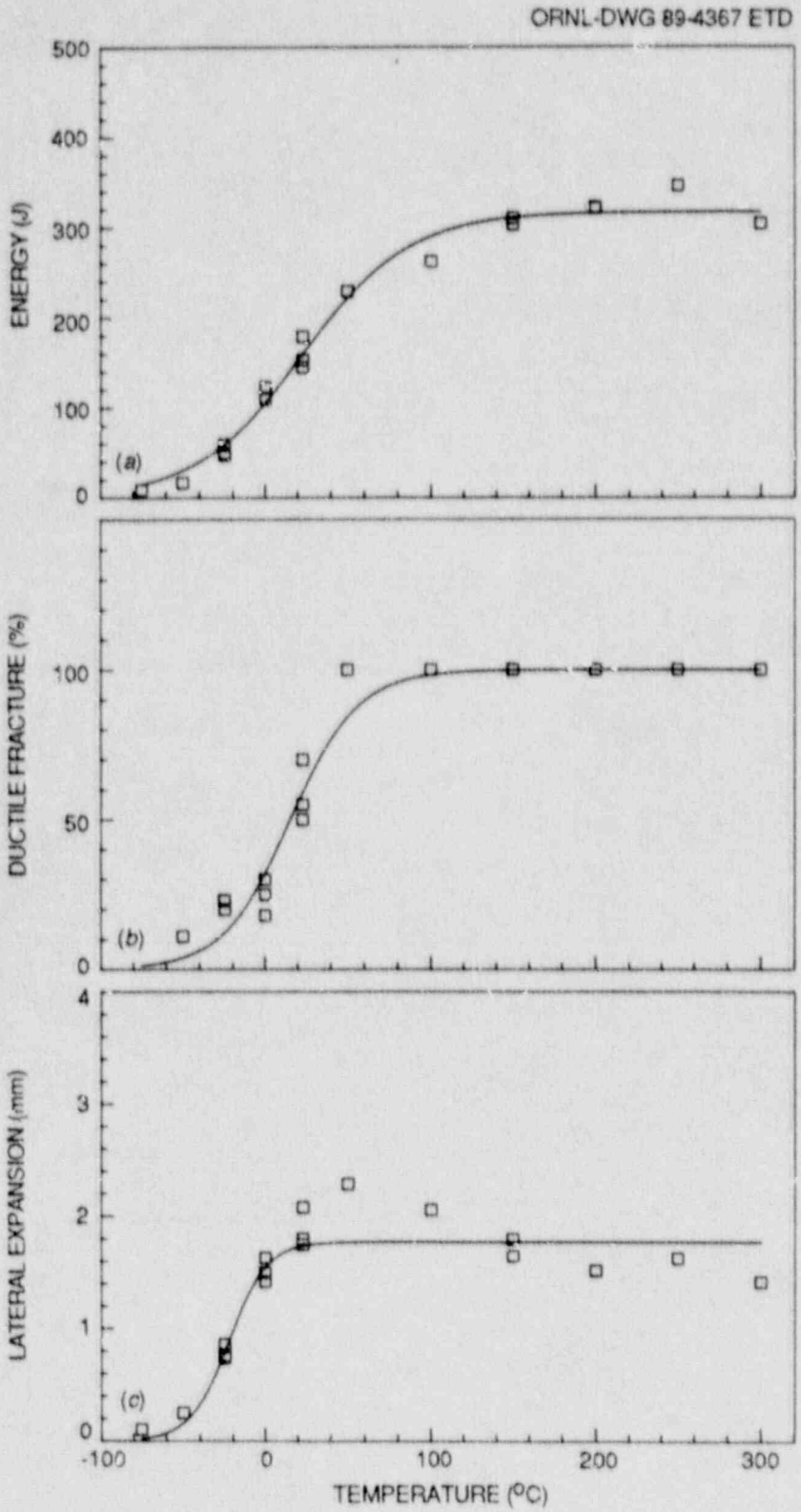

Fig. 3.7. CVN test results in L-T orientation for material obtained from layer 2 of specimen WP-CE-2: (*a*) CVN impact energy, (*b*) percent ductile fracture, and (*c*) lateral expansion.

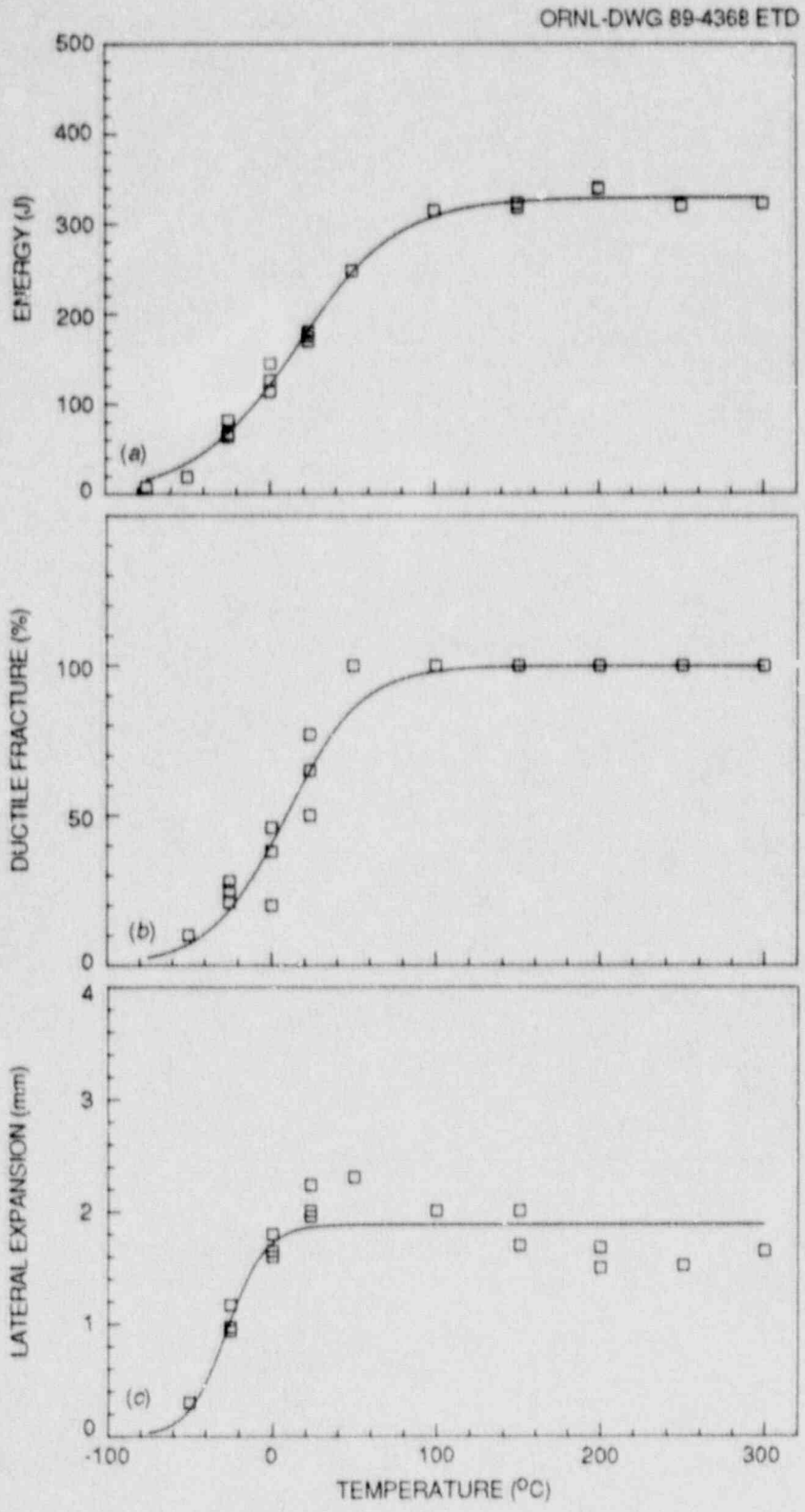

Fig. 3.8. CVN test results in L-T orientation for material obtained from layer 3 of specimen WP-CE-2: (*a*) CVN impact energy, (*b*) percent ductile fracture, and (*c*) lateral expansion.

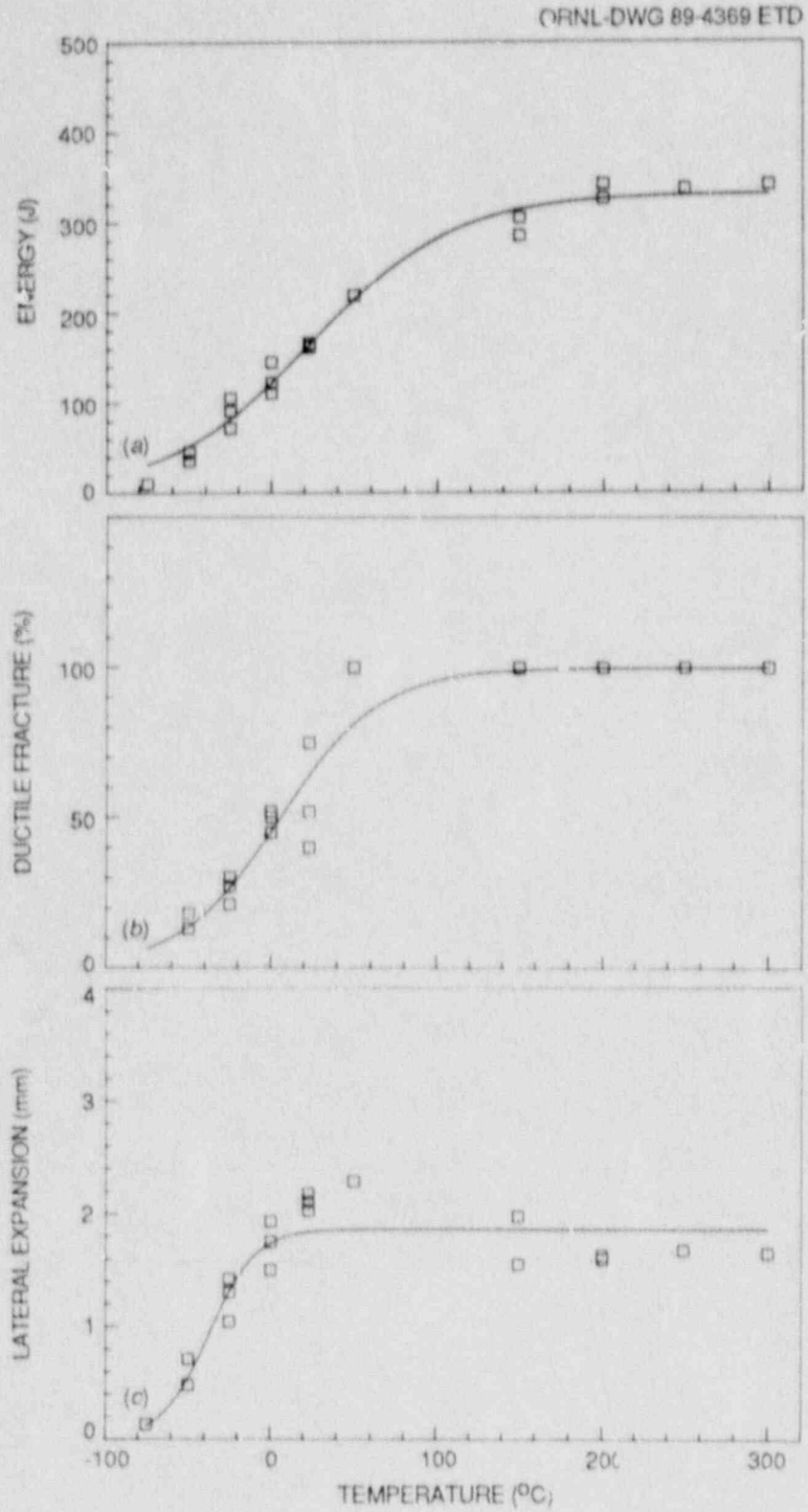

Fig. 3.9. CVN test results in L-T orientation for material obtained from layer 4 of specimen WP-CE-2: (*a*) CVN impact energy, (*b*) percent ductile fracture, and (*c*) lateral expansion.

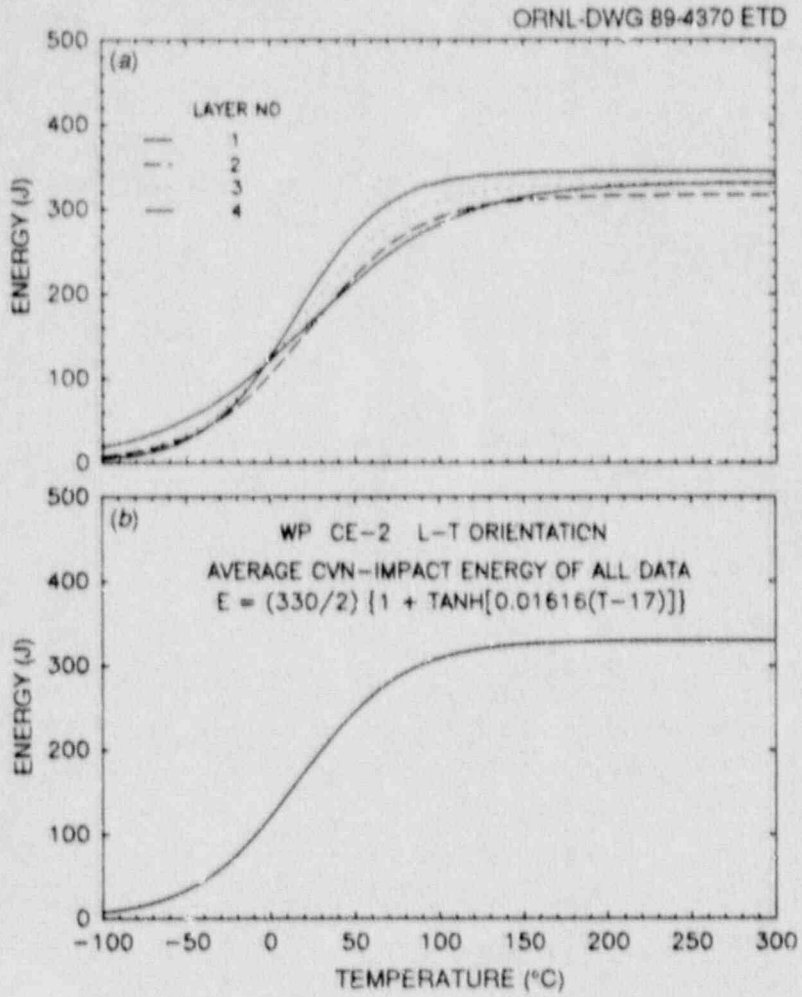

Fig. 3.10. Comparison of L-T orientation CVN regression curve fits to the impact energy: (*a*) for the four layers of material in specimen WP-CE-2 from which results were obtained and (*b*) average regression curve fit to all CVN-impact energy test data.

Table 3.3 Form of hyperbolic tangent equation used in the regression analysis and the resulting curve fit parameters for material obtained from four layers of specimen WP-CE-2 in the L-T and T-L orientations (NDT = -35°C)

Layer No.	$E = (A/2)\,[1+\tanh[B(T-C)]]^a$			E^a at NDT	Temperature (°C)	
	A (J)	B ($°C^{-1}$)	C (°C)		41 J	68 J
			L-T orientation			
1	345	0.01878	15	46	−38	−22
2	317	0.01537	23	46	−40	−20
3	330	0.01615	17	53	−44	−25
4	332	0.01143	24	69	−62	−36
Average	330	0.01616	17	52	−43	−25
			T-L orientation			
1	233	0.01783	8	42	−35	−17
2	240	0.01561	13	44	−38	−17
3	273	0.01197	18	60	−54	−28
4	228	0.01419	−2	64	−56	−32
Average	244	0.01453	9	53	−46	−24

[a] E = CVN energy at temperature T (°C)

A = USE

B = related to slope of curve in transition region

C = temperature corresponding to energy equal to one-half of USE

The CVN results for each of the four layers have been plotted in Figs. 3.11–3.14. Comparisons of the regression curve fits are shown in Fig. 3.15. The through-thickness variations between the various layers in the T-L orientation are consistent with those exhibited in the L-T orientation. The CVN-impact energy level at NDT increased from 42 J in layer 1 to 64 J in layer 4. Similarly, the 41- and 68-J temperatures decreased 21 and 15 K, respectively. An "average" regression curve was fitted to all the CVN-impact energy test data in the T-L orientation. The regression-fit parameters are included in Table 3.3, and the curve is shown in Fig. 3.15(*b*).

Testing in the T-L orientation was not performed at temperatures >200°C. Moreover, in view of the scatter at these higher temperatures in some of the layers, more testing is needed to provide a better statistical basis for judging the USE. Test results at 200°C imply that the upper-shelf CVN impact energy has not yet been reached. The CVN

Table 3.4 CVN impact test results in T-L orientation for material obtained from specimen WP-CE-2

Specimen No.	Test temperature (°C)	CVN energy (J)	Lateral expansion (mm)	Fracture appearance (%)
		Layer 1		
CE2134	−75	3	0.08	0
CE2131	−50	7	0.10	0
CE2143	−50	9	0.15	0
CE2132	−25	55	0.86	13
CE2149	−25	70	0.99	22
CE2135	−2	91	1.42	29
CE2144	−2	104	1.63	38
CE2147	−2	113	1.57	33
CE2138	0	88	1.24	26
CE2141	0	95	1.45	34
CE2140	23	154	2.03	59
CE2150	23	163	2.03	52
CE2145	50	176	2.16	92
CE2137	50	179	2.11	86
CE2146	75	208	2.24	100
CE2133	75	225	2.16	100
CE2136	100	198	2.11	100
CE2142	150	208	2.13	100
CE2148	150	222	1.83	100
CE2139	200	290	1.65	100
		Layer 2		
CE2233	−75	7	0.13	0
CE2242	−50	11	0.23	0
CE2243	−50	16	0.28	0
CE2247	−25	46	0.71	13
CE2248	−25	52	0.74	18
CE2244	−2	97	1.45	33
CE2237	−2	97	1.42	37
CE2238	−2	119	1.65	43
CE2234	0	89	1.30	33
CE2235	0	95	1.45	38
CE2236	23	146	1.93	62
CE2231	23	156	1.83	50
CE2249	50	176	1.96	79
CE2250	50	178	2.08	92
CE2241	75	197	2.21	100
CE2232	75	207	2.21	100
CE2246	100	194	2.18	100
CE2245	150	236	1.96	100
CE2240	150	241	1.91	100
CE2239	200	272	2.01	100

Table 3.4 (continued)

Specimen No.	Test temperature (°C)	CVN energy (J)	Lateral expansion (mm)	Fracture appearance (%)
		Layer 3		
CE2333	−75	10	0.18	0
CE2346	−50	17	0.28	0
CE2339	−50	39	0.61	11
CE2347	−25	36	0.66	11
CE2336	−25	80	1.12	27
CE2337	−2	116	1.60	42
CE2331	−2	119	1.68	45
CE2348	−2	128	1.52	43
CE2341	0	102	1.47	31
CE2349	0	112	1.60	40
CE2334	23	150	1.80	66
CE2350	23	155	1.91	53
CE2340	50	192	2.26	100
CE2332	50	201	2.39	100
CE2338	75	195	2.18	100
CE2344	75	212	2.21	100
CE2345	100	201	2.16	100
CE2343	150	206	2.03	100
CE2342	150	296	2.26	100
CE2335	200	320	1.57	100
		Layer 4		
CE2431	−100	5	0.03	0
CE2440	−75	12	0.25	0
CE2433	−50	40	0.64	3
CE2444	−50	44	0.66	13
CE2446	−25	79	1.17	23
CE2438	−25	88	1.24	16
CE2443	−7	107	1.52	43
CE2434	−7	109	1.68	45
CE2450	−7	114	1.60	42
CE2432	0	107	1.47	52
CE2442	0	111	1.55	43
CE2435	23	154	1.98	67
CE2447	23	172	2.11	76
CE2448	50	180	2.13	100
CE2449	50	206	2.31	100
CE2437	75	183	2.16	100
CE2439	75	189	2.21	100
CE2445	100	202	2.13	100
CE2441	150	204	2.11	100
CE2436	200	276	1.93	100

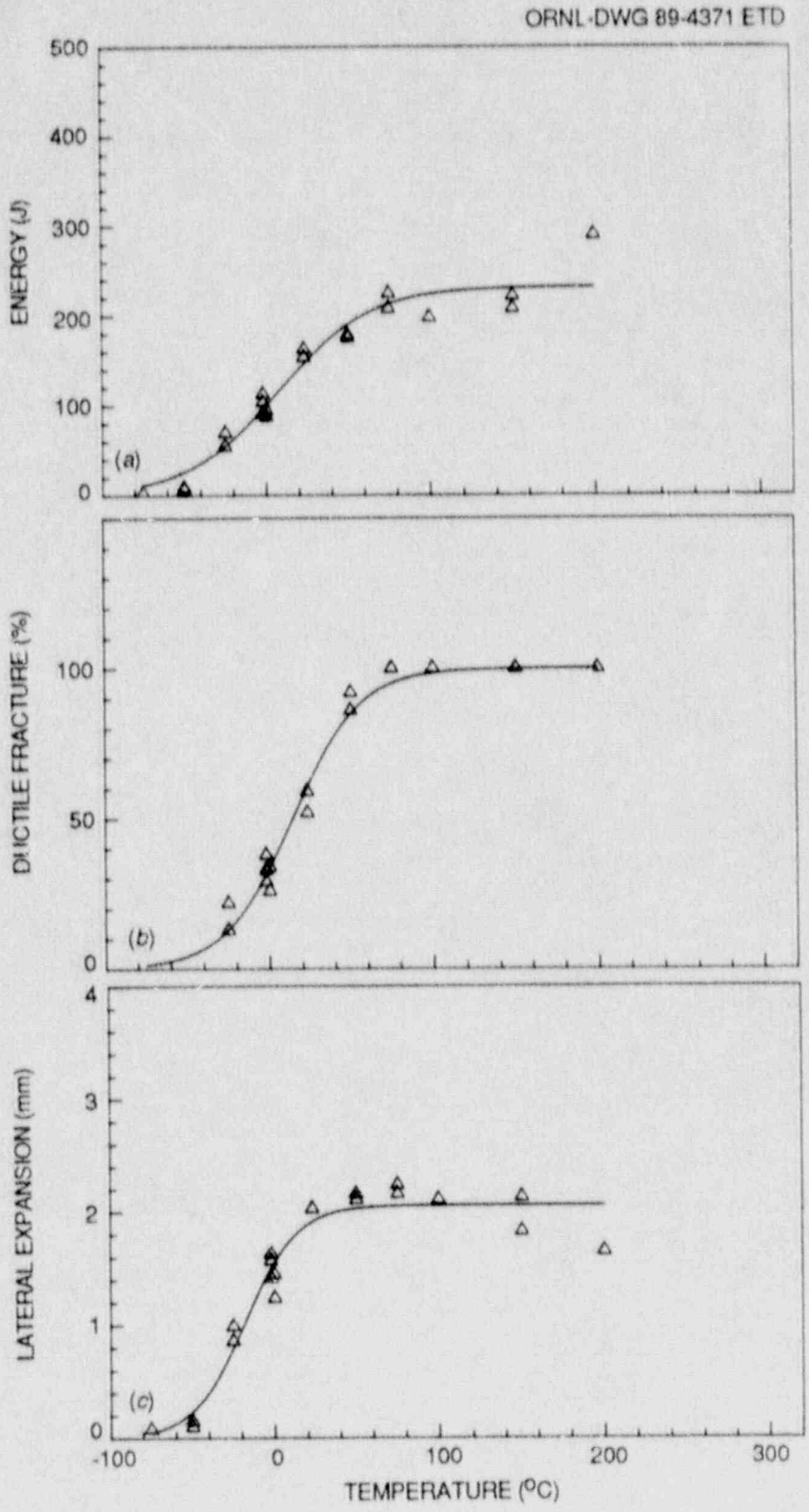

Fig. 3.11. CVN test results in T-L orientation for material obtained from layer 1 of specimen WP-CE-2: (*a*) CVN impact energy, (*b*) percent ductile fracture, and (*c*) lateral expansion.

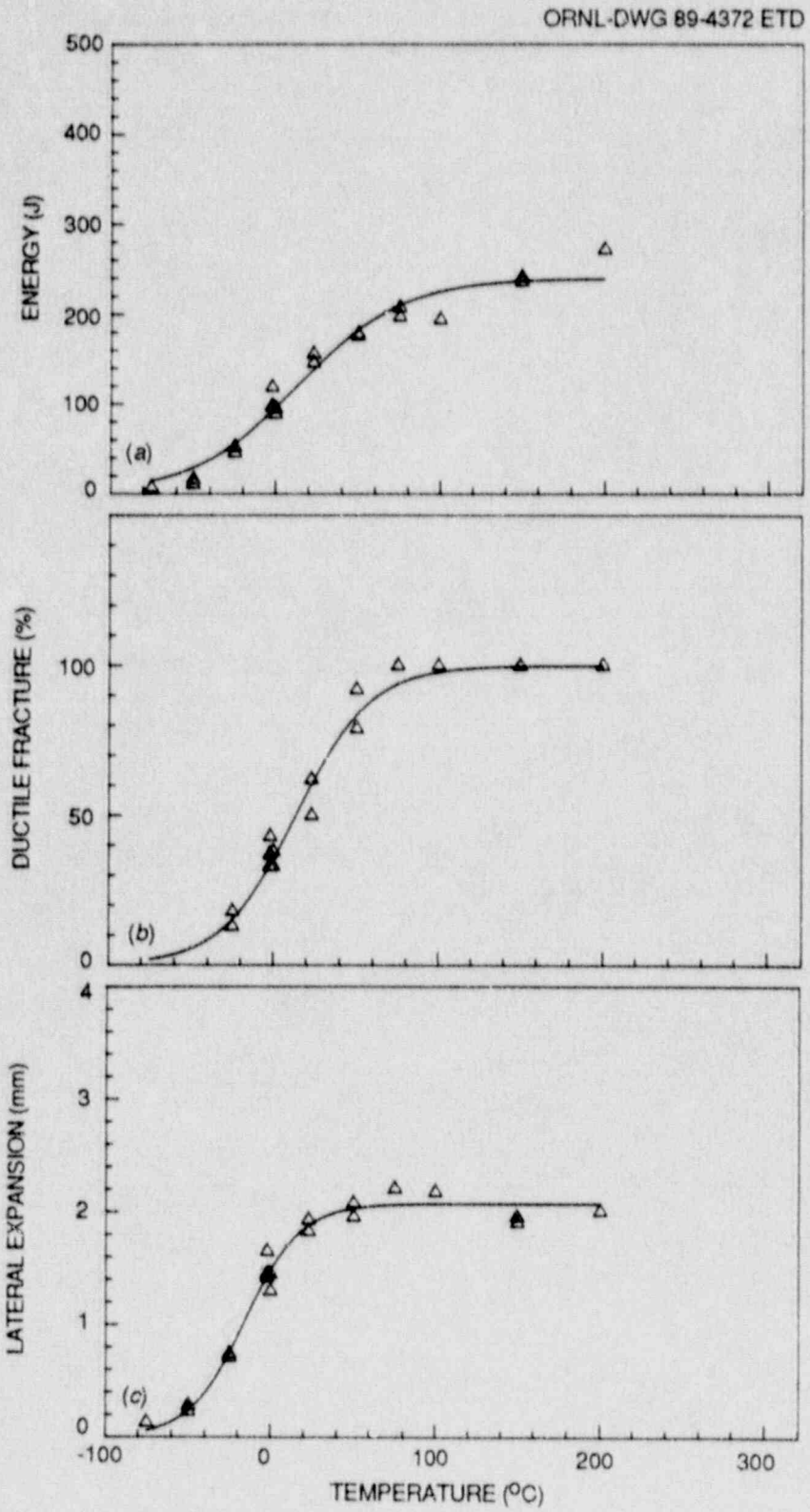

Fig. 3.12. CVN test results in T-L orientation for material obtained from layer 2 of specimen WP-CE-2: (*a*) CVN impact energy, (*b*) percent ductile fracture, and (*c*) lateral expansion.

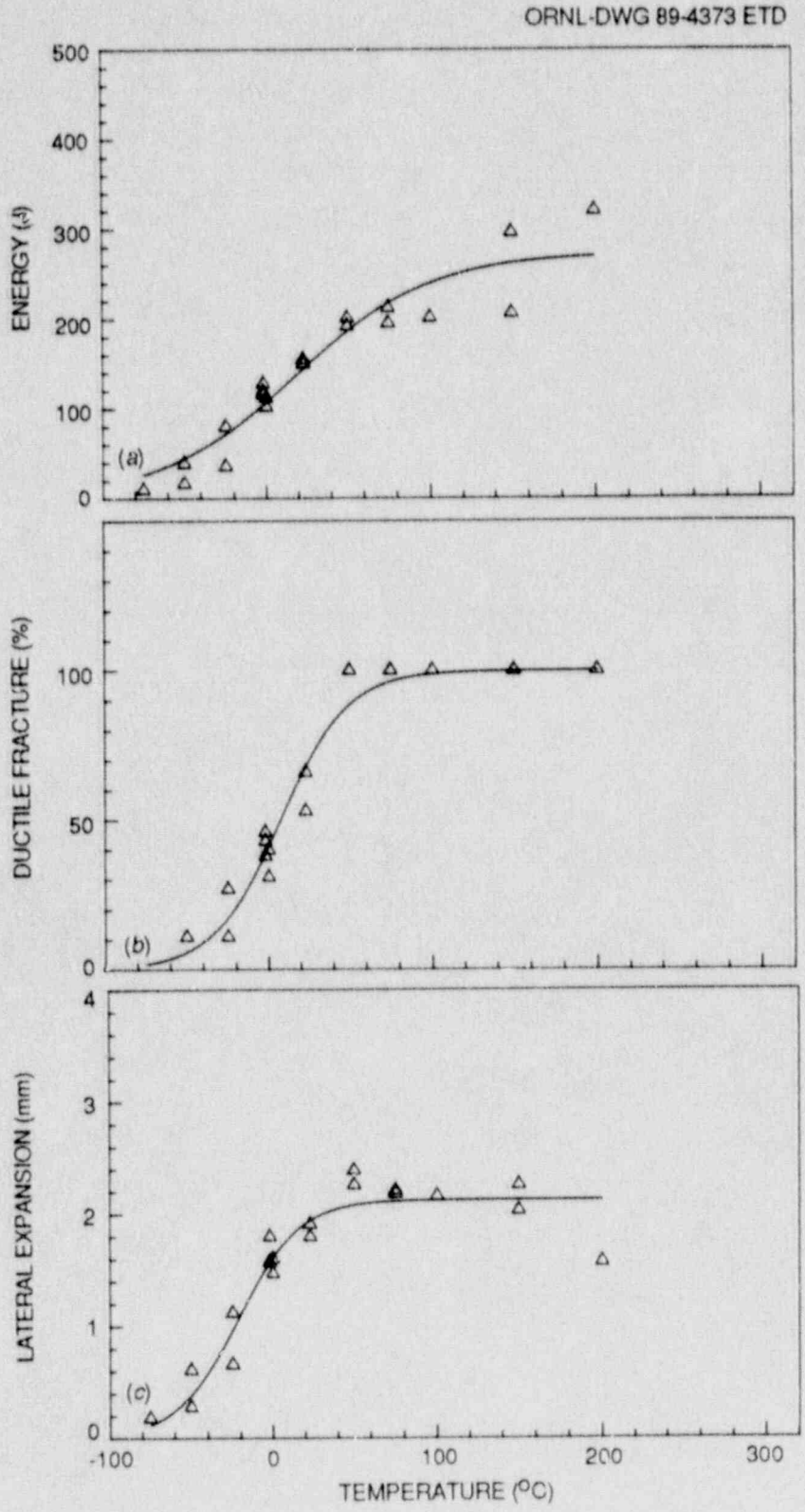

Fig. 3.13. CVN test results in T-L orientation for material obtained from layer 3 of specimen WP-CE-2: (*a*) CVN impact energy, (*b*) percent ductile fracture, and (*c*) lateral expansion.

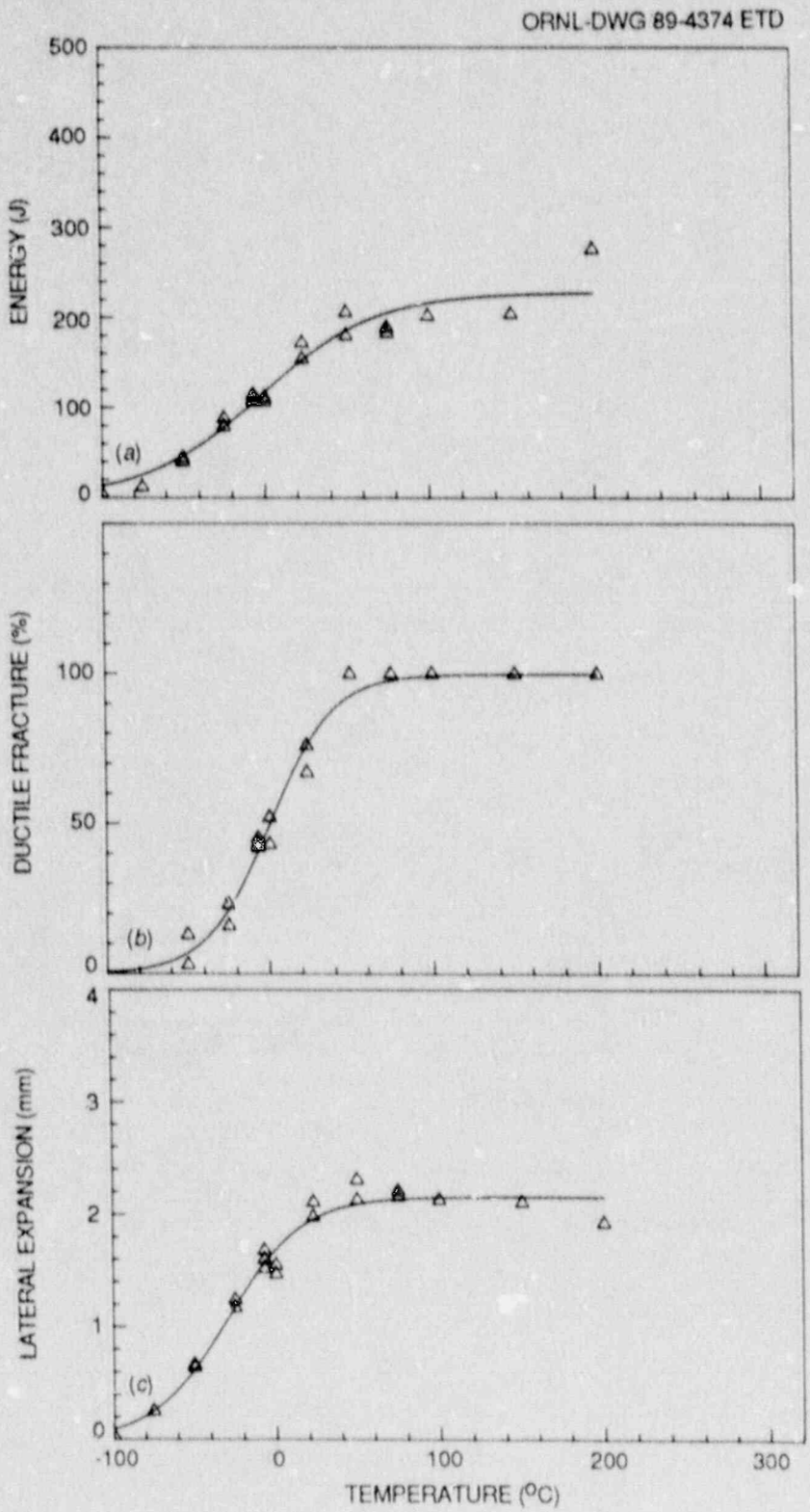

Fig. 3.14. CVN test results in T-L orientation for material obtained from layer 4 of specimen WP-CE-2: (*a*) CVN impact energy, (*b*) percent ductile fracture, and (*c*) lateral expansion.

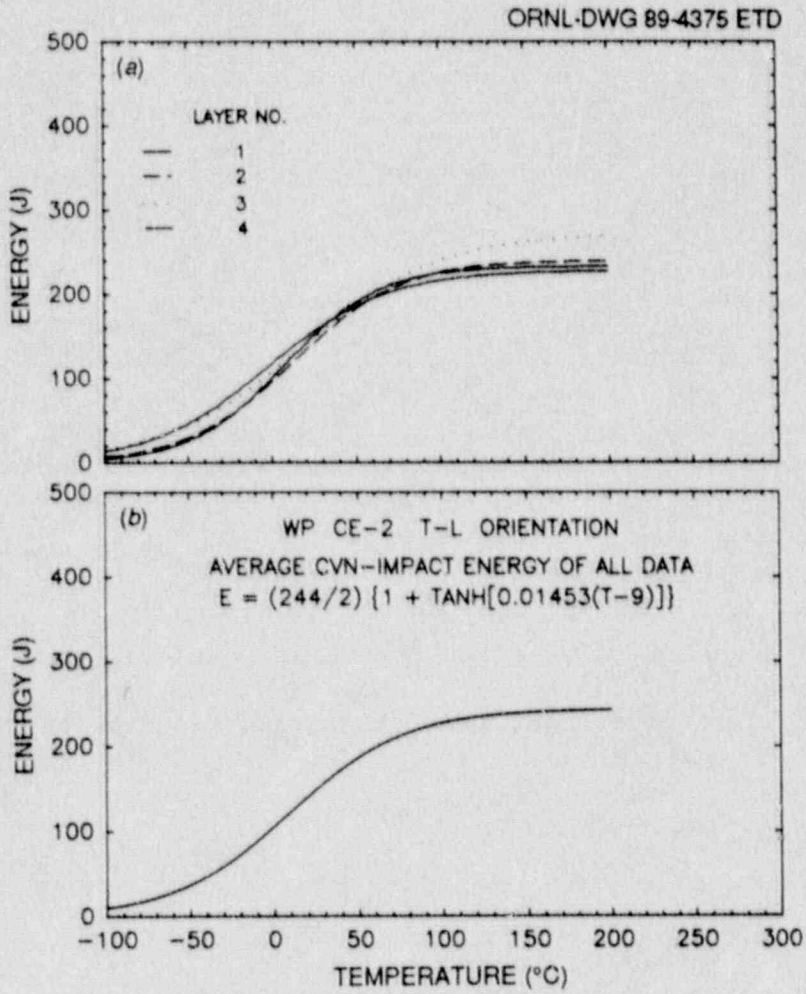

Fig. 3.15. Comparison of T-L orientation CVN regression curve fits to the impact energy: (*a*) for the four layers of material in specimen WP-CE-2 from which results were obtained, and (*b*) average regression curve fit to all CVN-impact energy test data.

upper-shelf impact energies in the T-L orientation from this study are significantly higher than those reported in Ref. 1. For instance, Ref. 1 reported USEs in the range 183 to 203 J, and the present results range from 228 to 273 J. Also, the 68-J transition temperature reported in Ref. 1 is −18°C, whereas present results from the various layers range from −17 to −32°C.

The RT_{NDT} of the SA 533 grade B class 1 material tested is −35°C and was governed by the drop-weight NDT temperature. No significant differences in the CVN impact toughness for the various layers in either of the two orientations tested were found. The average upper-shelf toughness in the L-T orientation for all four layers tested is ~330 J. In the L-T orientation, the onset of upper-shelf as determined by the 100% ductile fracture criterion is ~50°C, and the average 68-J transition temperature for all four layers is −25°C.

The tensile properties from Ref. 1 are given in Table 3.5. The data originated from blocks numbered as 6 and 10 in Ref. 1 (see Fig. 3.1). As mentioned previously, some variation of properties occurs along the 5600-mm length of the plate, and characterization blocks 6 and 10 are the closest to the location where wide-plate specimens WP-CE-1 and -2 were obtained.

3.5 FRACTURE-TOUGHNESS RELATIONS

Fracture-toughness relations for crack initiation and arrest were assumed to be of the same form as those developed for the WP-1 test series that also used A 533 grade B class 1 material but from another heat[2]; that is,

$$K_{Ic} = 51.28 + 51.90e^{0.036^{(T-RT_{NDT})}} , \tag{3.1}$$

$$K_{Ia} = 49.96 + 16.88e^{0.029^{(T-RT_{NDT})}} , \tag{3.2}$$

with units of K and T being megapascals per root meter and degrees Celsius, respectively. As noted previously, drop-weight and CVN test data resulted in an RT_{NDT} of −35°C for the WP-CE material.

The dynamic fracture-toughness relation for the plate material is written as

$$K_{ID} = K_{Ia} + A(T)\dot{a}^2 , \tag{3.3}$$

where K_{Ia} is given by Eq. (3.2). For

$$T - RT_{NDT} > -13.9°C ,$$

$$A(T) = [329.7 + 16.25\ (T - RT_{NDT})] \times 10^{-6}\ MPa \cdot s^2 \cdot m^{-3/2} ,$$

Table 3.5 Room- end elevated-temperature tensile properties of SA 533 grade B class 1 material[a]

Block No.	Location (t)	Specimen code	Test temperature (°C)	Strength		Elongation (%)	Reduction (%)
				Yield (MPa)	Ultimate (MPa)		
6	1/4	253	RT	399	561	29	69
6	3/4	256	RT	390	553	32	74
6	3/4	251	66	423	552	29	71
6	3/4	252	66	401	530	29	72
6	1/4	254	93	404	538	29	70
6	3/4	255	93	421	546	31	70
6	1/4	257	121	395	524	29	73
6	1/4	25A	121	390	517	29	65
10	3/4	2K6	RT	400	554	27	67
10	1/4	2KD	RT	394	555	30	71
10	1/4	2K7	49	382	533	28	73
10	3/4	2KC	49	395	542	29	72
10	1/4	2KE	66	410	558	28	70
10	3/4	2KB	66	422	555	26	68

[a]From EPRI NP-5121SP (No. 130), *Test and Analyses of Crack Arrest in Reactor Vessel Materials*, Appendix G, "Material Characterization."

and for

$$T - RT_{NDT} \leq -13.9°C ,$$

$$A(T) = [121.7 + 1.2962\ (T - RT_{NDT})] \times 10^{-6}\ MPa \cdot s^2 \cdot m^{-3/2} .$$

Units for K_{ID}, $\dot{a}$, and T are megapascals per root meter, meters per second, and degrees Celsius, respectively. The form of the K_{ID} expression in Eq. (3.3) and relations for A(T) are derived from Ref. 3 by estimating that $RT_{NDT} = -6.1°C$ for the material used in that study. Much of the data used in Ref. 3 are presented in Ref. 4.

REFERENCES

1. D. J. Ayres et al., Combustion Engineering, Inc., for Electric Power Research Institute, *Tests and Analyses of Crack Arrest in Reactor Vessel Materials*, Appendix G, "Material Characterization," EPRI NP-5121SP, April 1987.

2. D. J. Naus et al., Martin Marietta Energy Systems, Inc., Oak Ridge Natl. Lab., *Crack-Arrest Behavior in SEN Wide-Plates of Quenched and Tempered A 533 Grade B Steel Tested Under Nonisothermal Conditions*, USNRC Report NUREG/CR-4930 (ORNL-6388), August 1987.*

3. M. F. Kanninen et al., prepared by Battelle-Columbus Laboratories for Martin Marietta Energy Systems, Inc., Oak Ridge Natl. Lab., *Preliminary Analysis of Japanese Wide-Plate Dynamic Crack Propagation Arrest Experiments*, ORNL/Sub/1724C, December 1983.*

4. T. Kanazawa et al., Study on Fast Fracture and Crack Arrest, *Exp. Mech.* 21(2), 78-88 (February 1981).†

---

*Available for purchase from National Technical Information Service, Springfield, Virginia 22161.

†Available in public technical libraries.

4. SPECIMEN PREPARATION, INSTRUMENTATION, AND TESTING PROCEDURE

4.1 SPECIMEN PREPARATION

The WP-CE-1 and -2 test articles (1 × 1 × 0.1 m), shown schematically in Fig. 4.1, were machined and precracked by ORNL before they were sent to the National Institute of Standards and Technology (NIST). The precracking was done by hydrogen charging an electron-beam (EB) weld (Fig. 4.2) located at the base of a premachined notch.[1] The notch (a/w ~ 0.2) is composed of a 25.4-mm-wide gap that is machined to a depth of 187 mm ("X" in Fig. 4.1) plus the EB weld-generated crack that has a depth of ~12.7 mm at the end of the gap. Each face of the specimen is side-grooved to a depth equal to 12.5% of the plate thickness, and the grooves have a 0.025-cm-root radius. The initial crack is perpendicular to the rolling direction. The crack front of each specimen is then cut into a truncated chevron configuration, shown in Fig. 4.3, to reduce the tensile load required to achieve crack initiation. Table 4.1 presents dimensions for test articles WP-CE-1 and -2.

Upon receipt of the test article from ORNL, NIST welded it to pull plates, which were nominally 103 mm thick. The pull tabs at the end of the pull plates were strengthened by being 152 mm thick. Figures 4.4(*a*) and (*b*) give dimensions for each of the test specimens. Before application of the axial load, the out-of-plane deviation of each of the wide-plate assemblies was determined as a function of axial position from the top load pin; the results are presented in Figs. 4.5(*a*) and (*b*).

4.2 INSTRUMENTATION

To obtain pertinent data during each test, the specimens were instrumented with five types of devices: thermocouples, strain gages, crack-opening-displacement (COD) gages, accelermometers, and a displacement transducer. Reference 2 gives more detailed information on specimen instrumentation than that presented below.

Forty thermocouples were positioned on each specimen, as shown in Fig. 4.6. The thermocouples were attached by inserting and gluing them into 1.5-mm-diam by 3-mm-deep holes that had been drilled in each specimen. The hole and thermocouple were then covered with a protective silicone coating. Additional thermocouples, not indicated in Fig. 4.6, were used to control heating and cooling of the wide-plate specimen. All thermocouple lead wires were connected to copper lead wires in an insulated junction box whose temperature was measured by a resistance temperature detector that was monitored by a digital ohmmeter and data logger. The thermocouples were sequentially monitored periodically and corrected for room temperature, and the results were both recorded on magnetic tape and displayed on the computer screen. During the heating and cooling processes, the 20 thermocouples adjacent to the crack plane (0–19 in Fig. 4.6) were displayed graphically in real time to indicate the relationship between the actual and desired thermal gradient across

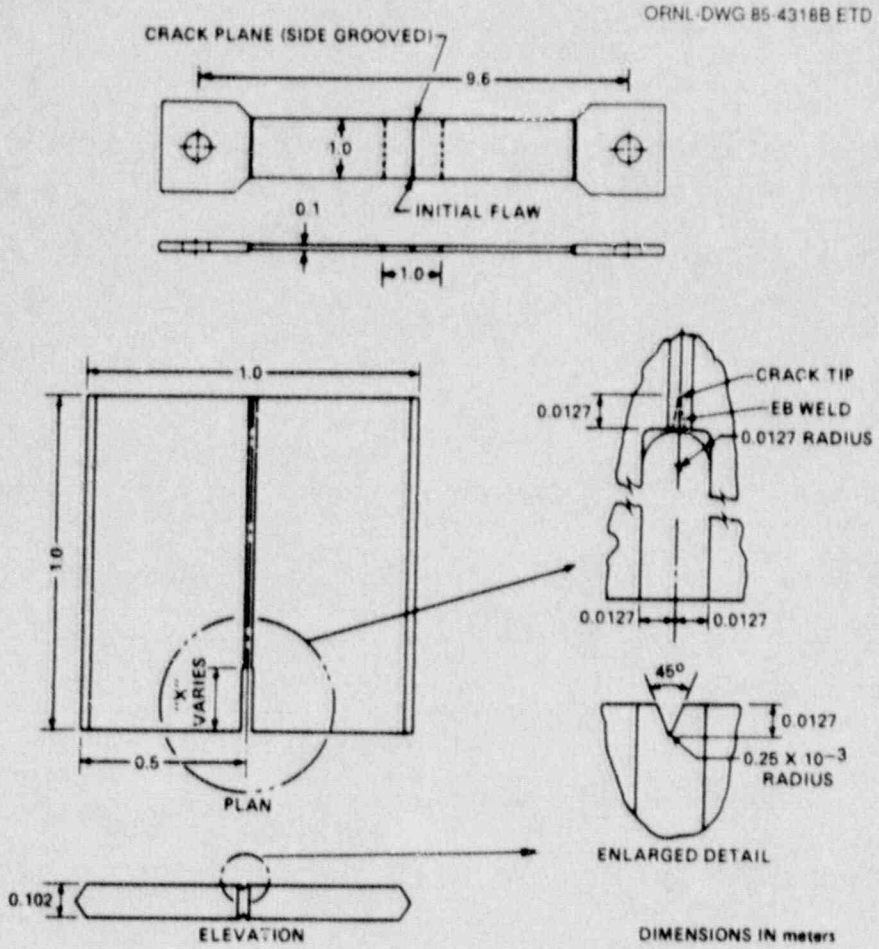

Fig. 4.1. Schematic of HSST wide-plate crack-arrest specimen.

Table 4.1. Detailed dimensions of wide-plate crack-arrest specimens WP-CE-1 and -2

Specimen feature	Symbol[a]	Dimension (mm)	
		WP-CE-1	WP-CE-2
Initial crack length	a_o	200	201
Thickness	B	101.7	101.8
Notch thickness	B_N	76.3	76.2
Chevron thickness (thickness at a_o)	B_C	40.0	40.4
Width	W[b]	1000	999.5

[a]See Fig. 4.3 for definitions of symbols.

[b]Not shown in Fig. 4.3.

ORNL PHOTO 7176-84

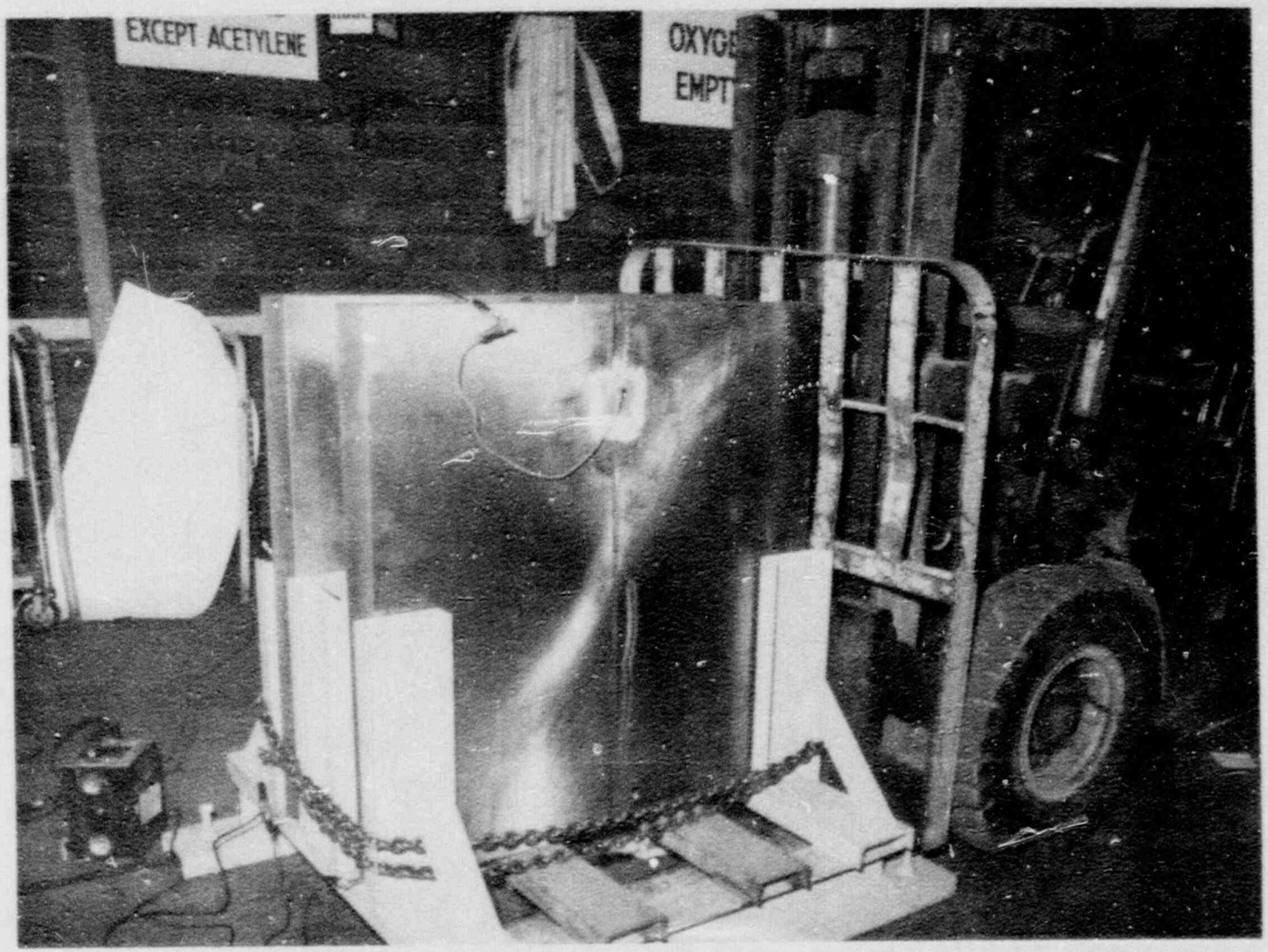

Fig. 4.2. Wide-plate test articles undergoing hydrogen charging of electron-beam weld.

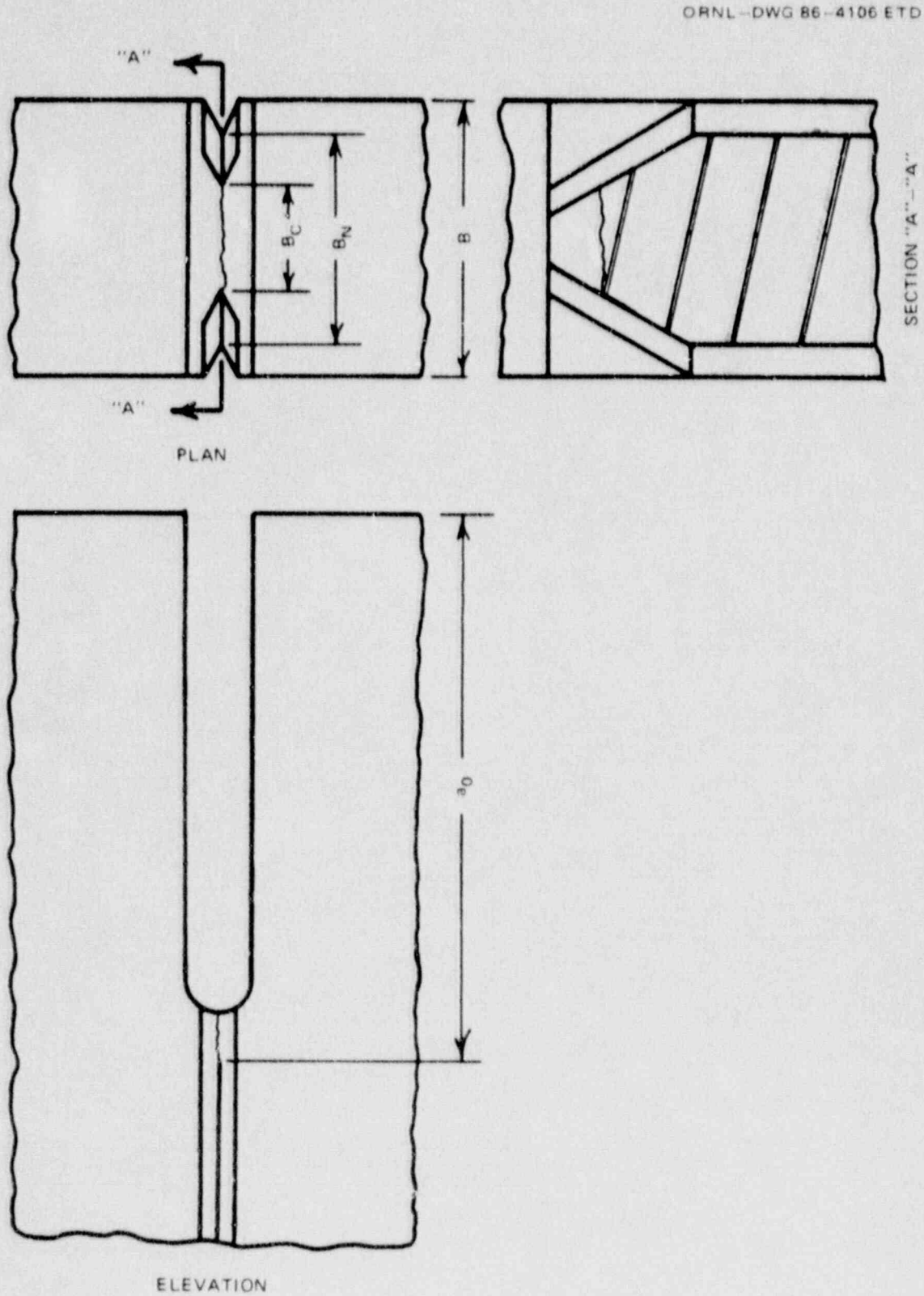

Fig. 4.3. Schematic of chevron configuration of crack front.

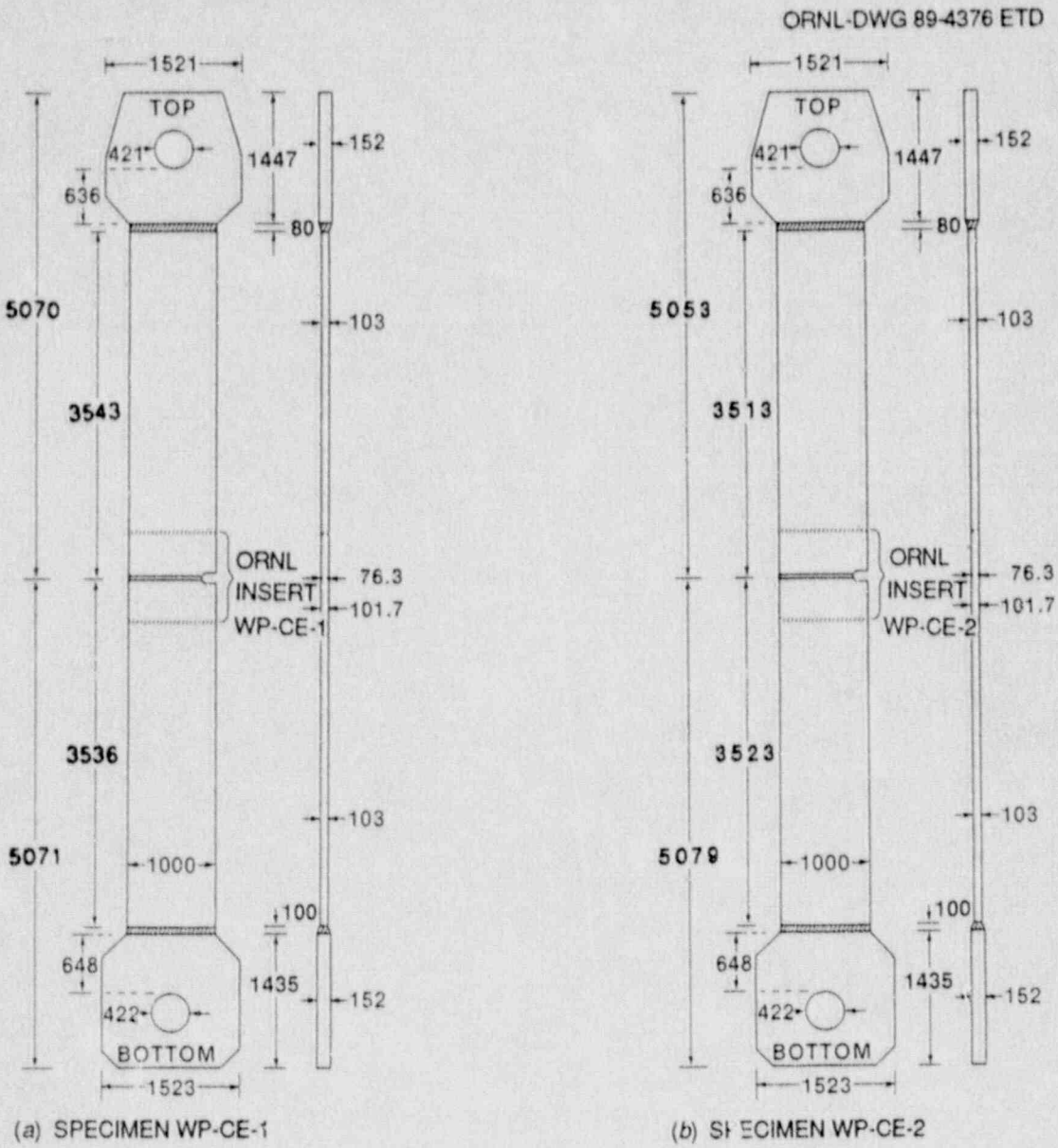

Fig. 4.4. Overall dimensions of HSST wide-plate crack-arrest specimens and pull plates for (*a*) specimen WP-CE-1 and (*b*) specimen WP-CE-2.

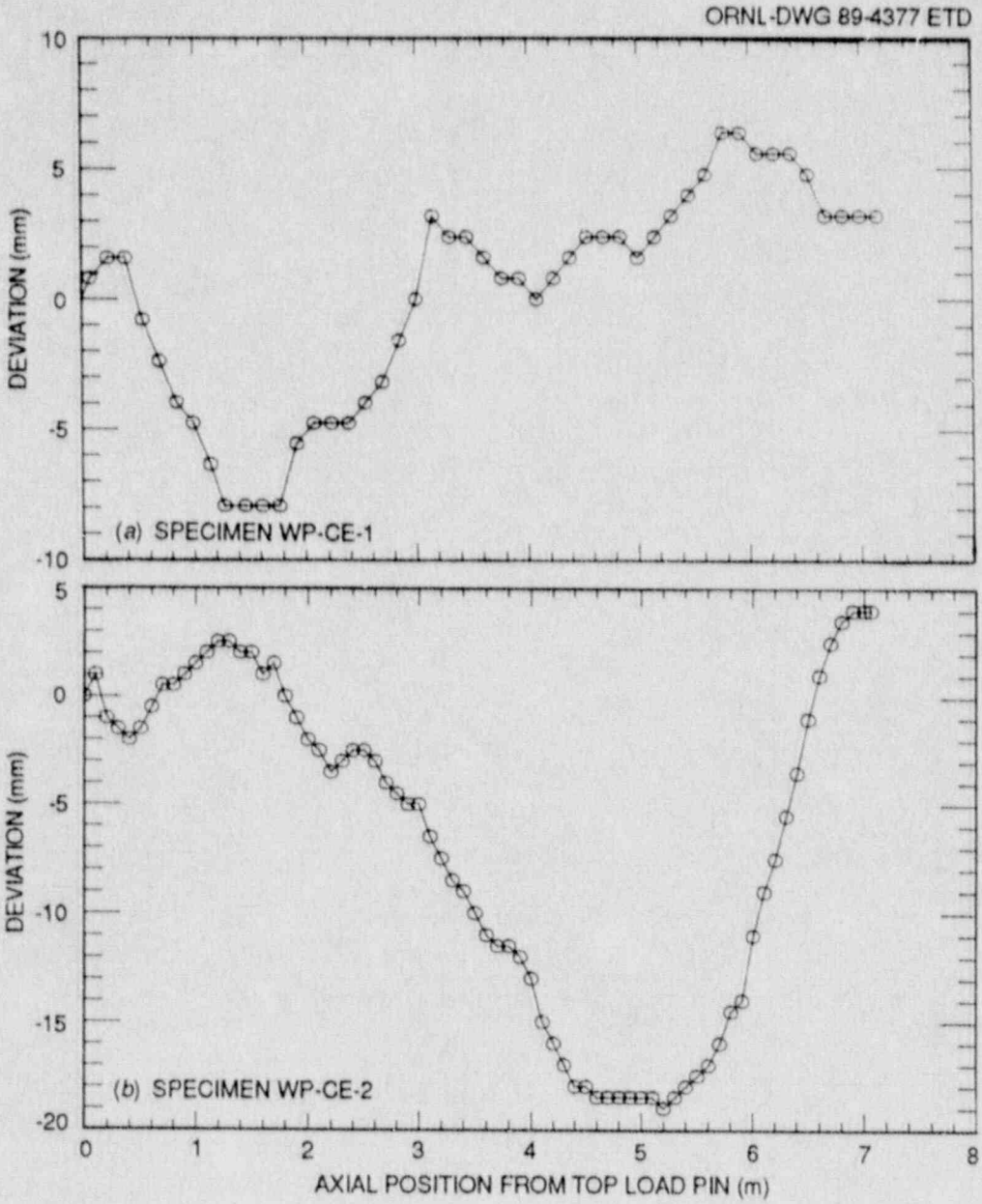

Fig. 4.5. Out-of-place deviation vs axial position from top load pin: tests WP-CE-1 and -2.

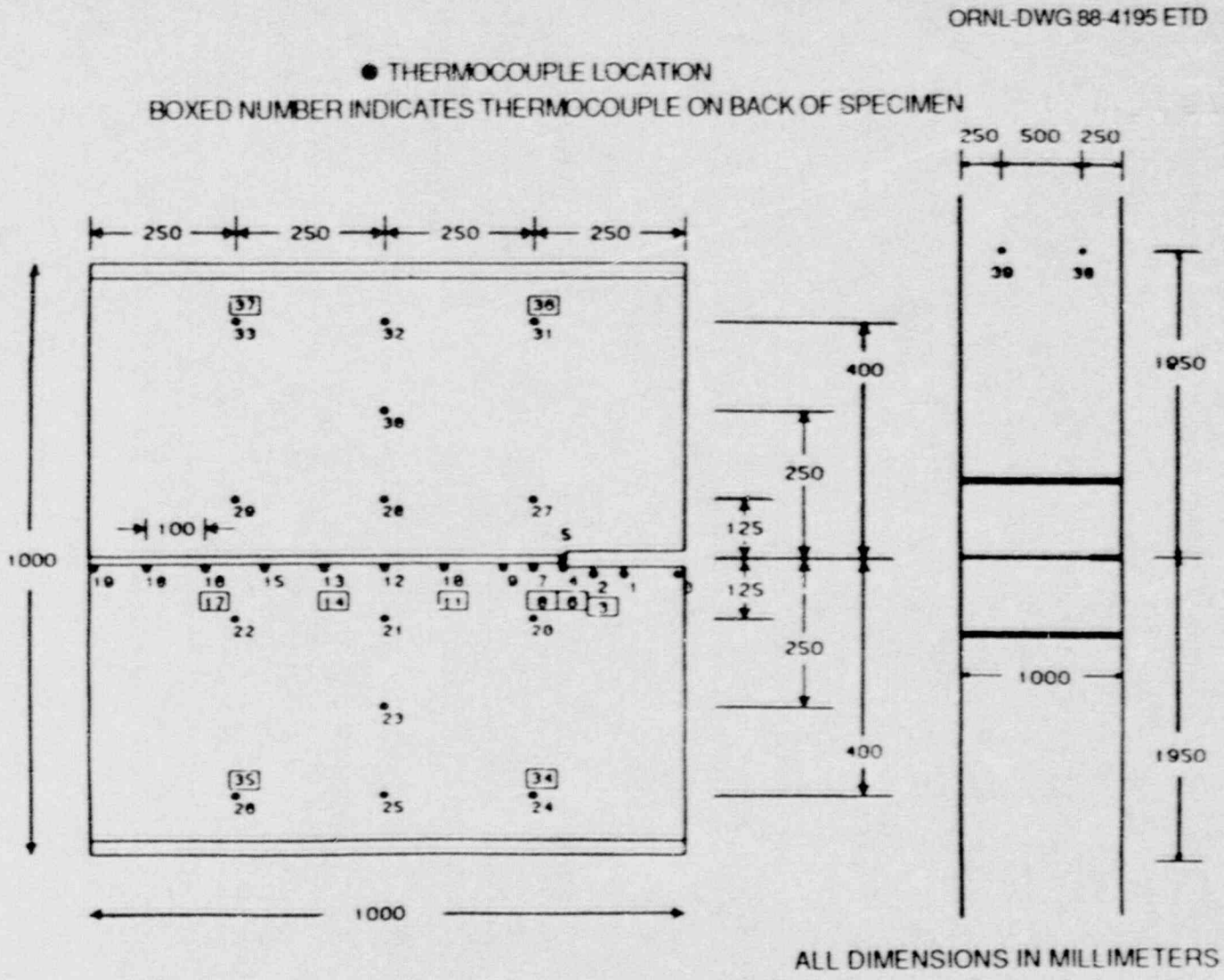

Fig. 4.6. Thermocouple locations for HSST wide-plate, crack-arrest specimens WP-CE-1 and -2.

the specimen width. The other 20 thermocouples were used to indicate the temperature distribution at other positions on the specimen and pull plates during a test for use in posttest analysis.

Twenty-five strain gages were positioned on each specimen to provide dynamic strain-field measurements for determination of crack velocity and to provide far-field strain measurements for assessing boundary conditions. Strain-gage locations used for tests WP-CE-1 and -2 are shown in Fig. 4.7. The crack-line gages (1–20 in Fig. 4.7) were two-element, 45° stacked, 350-Ω Karma alloy (nickel-chromium alloy) gages on a polyimide backing. Outputs of these gages were proportional to the difference between the longitudinal and transverse strains. Near- and far-field strain gages were uniaxial 350-Ω constantan alloy gages on a polyimide backing. The gages were attached to the plates by using an elevated-temperature-cured epoxy. All gages were connected to low-reactance bridges (half-bridge configuration for crack-line gages), the imbalances of which were amplified by wide-band differential amplifiers. The strain-gage signals were recorded by a multichannel, wide-band, frequency-modulated, magnetic tape recorder, shown schematically in Fig. 4.8.

Additional instrumentation included capacitance-based COD gages mounted on the plate front and back faces at a/w = 0.15. The gages measured the displacement between points 30 mm above and 30 mm below the

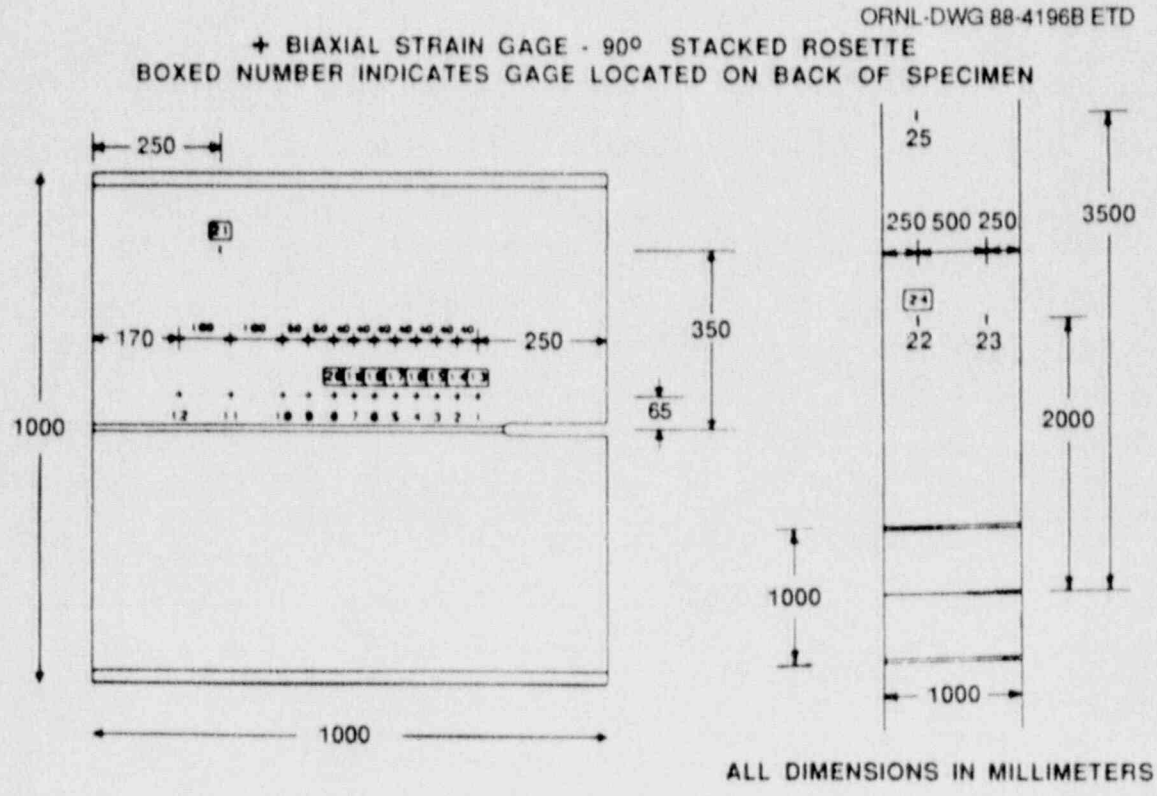

Fig. 4.7. Strain gage locations for HSST wide-plate, crack-arrest specimens WP-CE-1 and -2.

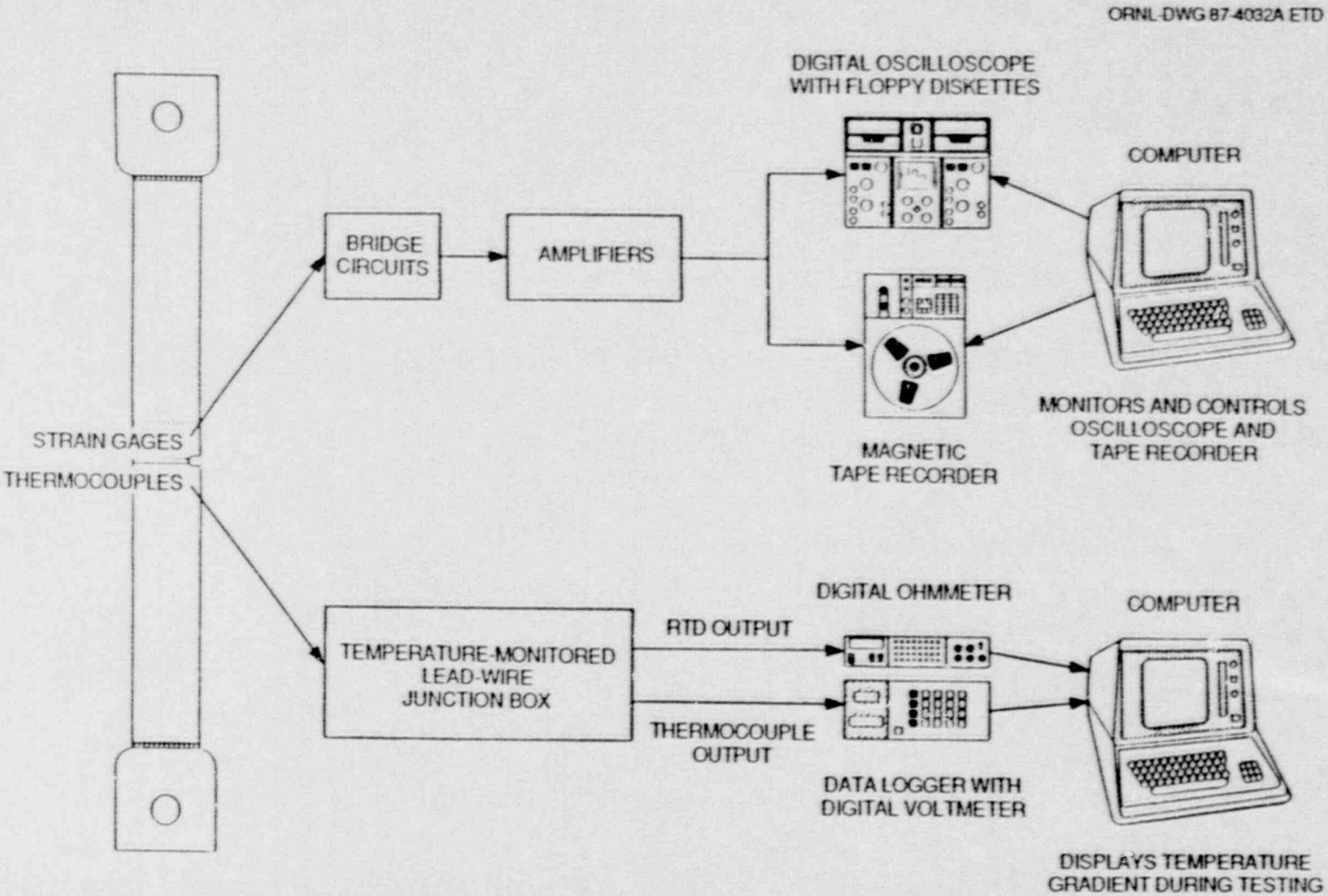

Fig. 4.8. Schematic of HSST wide-plate, crack-arrest data acquisition system.

crack plane. Accelerometers were installed 3.697 m above and 3.711 m below the crack plane on the centerline of specimen WP-CE-1 and 3.714 m above and 3.710 m below the crack plane on the centerline of specimen WP-CE-2. In addition, a displacement gage was mounted in the same location as the lower accelerometer on specimen WP-CE-1. For specimen WP-CE-2, the displacement gage was mounted on the specimen centerline 5 mm above the lower accelerometer. The displacement gage measured the movement of the point on the specimen where it was attached relative to that of the large columns of the testing machine.

4.3 HEATING, COOLING, AND INSULATION SYSTEMS

After the specimen was instrumented, it was placed into the NIST testing machine, as shown in Fig. 4.9, and eight individual electric-resistance strip heaters were attached to the back edge of the plate. Each heater was 2.8 cm wide with a heating element length of 61 cm and was rated at 1.9 W/cm^2. The heaters were attached to the plate in pairs and were backed with 1.3-cm-thick sheets of insulating board (Marinite I) to hold the heaters against the plate surface and to provide insulation. The heating level during a test was controlled by two means: (1) a Variac transformer, which adjusted the power level or output of each heater, and (2) separate on/off temperature controllers, which interacted with thermocouples at the edge of the plate to regulate two zones of heating. The primary heating zone was formed by two pairs of heaters attached to the specimen edge above and below the fracture plane. The second heating zone, consisting of the areas on either side of the first zone, was heated by two outward pairs of heaters. Temperature levels in the two zones were independently controlled to better achieve and maintain a linear thermal gradient across the specimen.

One edge of the specimen was cooled by spraying liquid nitrogen (LN_2) onto the specimen's notched edge. A 2.6-m-long insulated chamber was affixed to the edge, equally spanning both sides of the notch. The LN_2 was pumped into the chamber and sprayed directly onto the specimen surface through a copper-tube manifold consisting of sprayers at 18-cm increments. The cooling level could be controlled by two methods. Initially, when establishing a linear thermal gradient, the temperature was controlled by adjusting the LN_2 flow rate by manually setting a hand valve. When the desired temperature was achieved, that level was maintained by controlling the LN_2 flow with an on/off temperature controller interfaced with a thermocouple at the cold edge of the specimen. The temperature controller powered an electric solenoid gas valve that regulated the flow of LN_2 into the cold chamber.

Two types of thermal insulation were used to insulate the front and back faces of the specimen. On the hot side of the plate, 5-cm-thick, 61-cm-wide mineral wool bats were used. The bats were positioned on the specimen face at the vertical centerline of the specimen and extended beyond the heated edge and the strip heaters. The cold side of the plate was insulated with 61-cm-wide, 5-cm-thick styrofoam sheets, which butted up against the mineral wool at the specimen center and extended beyond the cooled edge or to the cold chamber. The cold chamber was insulated with 2.5-cm-thick styrofoam sheets. All insulation was held

ORNL PHOTO 6718-85

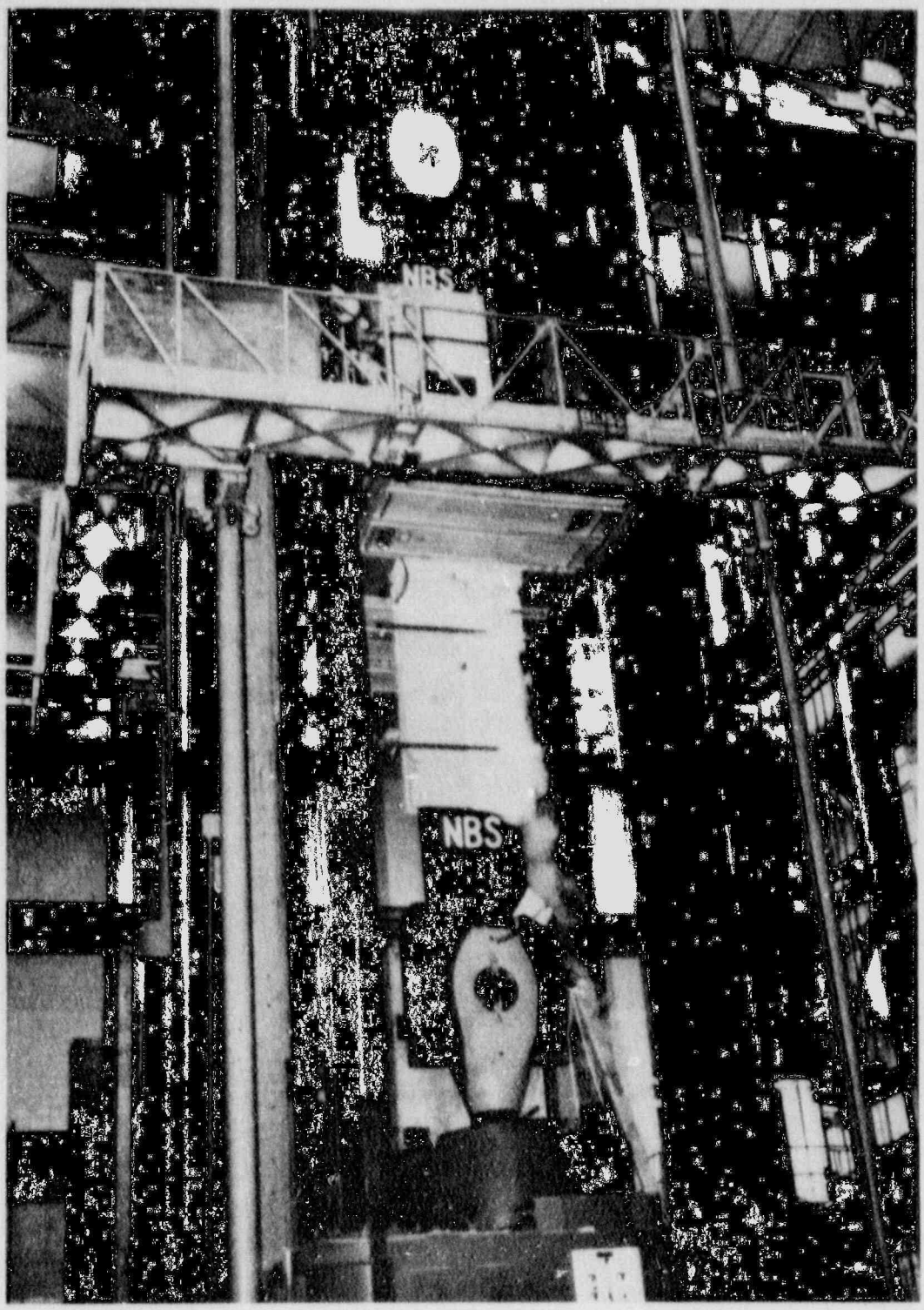

Fig. 4.9. HSST wide-plate, crack-arrest test specimen installed in NIST testing machine just before testing.

tight against the plate surface and, in total, covered an area 3 m above and 3 m below the fracture plane on both the front and back faces. Additional mineral wool and styrofoam insulation were placed on the specimen edges above and below the heaters and cold chamber to cover the same length on the specimen as the back and front face insulation.

4.4 TESTING PROCEDURE

After insulating the specimen, all instrumentation was attached to the data acquisition systems and checked out to demonstrate that all systems were operational. A temperature gradient was imposed across the plate by cooling the notched edge with LN_2 while heating the other edge.* Liquid nitrogen flow and power to the heaters were continuously adjusted to obtain the desired thermal gradient. Final calibrations of strain gages, COD gages, and the load cell were completed just before beginning specimen loading. Tensile load was then applied to the specimen at a rate of 9.6 to 24 kN/s until fracture occurred. Details of each test are presented in the next chapter.

REFERENCES

1. P. P. Holz, Union Carbide Corp. Nuclear Div., Oak Ridge Natl. Lab., *Flaw Preparations for HSST Program Vessel Fracture Mechanics Testing: Mechanical-Cyclic Pumping and Electron-Beam Weld-Hydrogen-Charge Cracking Schemes*, USNRC Report NUREG/CR-1274 (ORNL/NUREG/TM-369), June 1980. Available for purchase from National Technical Information Service, Springfield, Virginia 22161.

2. C. A. Danko et al., *Wide Plate Crack Arrest Tests Instrumentation for Dynamic Strain Measurements*, NBSIR 85-3289, 1985. Available from National Institute of Standards and Technology, Gaithersburg, Maryland.

*Specimen WP-CE-2 was warm prestressed before imposing the thermal gradient. Details are presented in Sect. 5.1.2.

5. SUMMARY OF WIDE-PLATE CRACK-ARREST TESTS WP-CE-1 AND -2

Table 5.1 summarizes the general conditions for wide-plate crack-arrest tests WP-CE-1 and -2 (test specimen dimensions were presented in Table 4.1). Transverse temperature profiles at the approximate time of crack-initiation events are summarized in Fig. 5.1. Figure 5.2 presents the fracture surface for each specimen. The remainder of this section is a brief summary of each test and pertinent results.

5.1 TEST DESCRIPTION SUMMARY

5.1.1 Test WP-CE-1

Test WP-CE-1 was the first wide-plate crack-arrest test that used the A 533 grade B class 1 material provided by CE.[1] After obtaining a satisfactory thermal gradient (Fig. 5.3), the specimen was loaded at an average rate of 24 kN/s. At a load of 10.14 MN, cleavage crack propagation initiated with a stable arrest occurring at $a/w = 0.37$ on the plate front face and at $a/w = 0.42$ on the plate back face. After holding the load constant for 150 s, loading was reinitiated at 24 kN/s. At a load of 15.26 MN, fibrous crack propagation began and was then followed by a rapid drop in load to ~4.4 MN (Fig. 5.4). After maintaining the load at this value for ~30 s, loading was reinitiated at 24 kN/s until at a load of 6.34 MN, complete separation of the plate occurred. Examining the fracture surface and strain-gage records indicated that one cleavage crack run-arrest event occurred before the onset of ductile tearing.

5.1.2 Test WP-CE-2

Before testing, specimen WP-CE-2 was warm prestressed at room temperature (~25°C) by slowly loading it to 14 MN, holding the load constant at this value for 5 min, and slowly reducing the load to 5 MN. Figure 5.5 presents the load history and load vs COD results during warm prestressing. While maintaining the load constant at 5 MN, the thermal gradient was developed. After obtaining a satisfactory temperature profile (Fig. 5.6), the specimen was loaded at an average rate of 9.6 kN/s. At a load of 14.6 MN, cleavage crack propagation initiated, and within a 4-ms interval, three crack run-arrest events occurred. After the third crack run-arrest event, the load rapidly decreased to 7.9 MN, followed by a slow continued drop in load with time, as shown in Fig. 5.7. While the load was slowly decreasing, an attempt was made to increase specimen loading; however, ductile tearing occurred. Final separation of the plate occurred 55 s after the three crack run-arrest events.

Table 5.1. Summary of HSST wide-plate crack-arrest test conditions for A 533 grade B class 1 steel: tests WP-CE-1 and -2

Test No.	Crack location (cm)	Crack-tip temperature (°C)	Initiation load (MN)	Arrest location (cm)	Arrest temperature (°C)	Arrest $T - RT_{NDT}$ (°C)
WP-CE-1	20.0[a]	−34	10.14	42.0[b]	36	71
WP-CE-2A	20.0[a,c]	−40	14.60	46.6[d]	42	77
WP-CE-2B	46.6	42	14.60	50.4[d]	53	88
WT-CE-2C	50.4	53	14.60	52.5[d]	60	95

[a]Crack front cut to truncated chevron configuration.

[b]Plate back-face location. The arrest location at the plate front face was at $a/w = 0.37$ where $T - RT_{NDT} = 58°C$.

[c]Specimen was warm prestressed to 14 MN at 25°C.

[d]Plate front-face location.

5.2 TEST RESULT SUMMARY

5.2.1 Test WP-CE-1

Figure 5.2 shows the fracture surface of specimen WP-CE-1. Note that one cleavage crack run-arrest event occurred during the test, with clear delineation of the cleavage arrest. Also note that the fibrous fracture appearance for this material more closely resembles that obtained with the WP-2 series material (low-upper-shelf)[2] than with the WP-1 series material (A 533 grade B class 1).[3,4] The entire fracture surface produced by this test remained in the plane of the side grooves. The reduction-in-thickness contour map for the specimen is presented in Fig. 5.8. As noted in the figure, the greatest reduction-in-thickness measured was 10%, the largest value obtained so far in any of the wide-plate crack-arrest tests. Also, as previous tests have shown, significant reductions-in-thickness occur only after the location corresponding to the arrest point (i.e., a/w > 0.37 for test WP-CE-1).

Figures 5.9 and 5.10 present strain histories for companion crack-line gages mounted on the front and back surfaces of the plate. Figure 5.9 shows the cleavage crack passing strain gages 1–4 and 13–16. Figure 5.10 shows the crack arresting before reaching strain gage 5 at the plate front face and passing strain gage 17 but arresting before reaching strain gage 18 at the plate back face. Figure 5.11 presents highly amplified strain histories for crack-line gages 9–12 mounted on the plate front face. Strain histories for near- and far-field gages 21–24 are presented in Fig. 5.12. Long-time (60-ms) strain histories for near- and far-field gages 21–24 are presented in Fig. 5.13. Short- (6-ms) and long- (60-s) time strain output from far-field gage 25 is presented in Fig. 5.14. Long-time (60-ms) records for strain gages 5–8 in Fig. 5.15 and strain gages 17–20 in Fig. 5.16 provide some indications of reinitiation and arrest events, but the fracture surface does not clearly reflect their occurrence. Figures 5.17–5.21 present strain histories for selected gages for the period of ductile tearing. (Results for strain gages 5–10, 15, and 17–20 are not available because of the large amount of plasticity that occurred following arrest to render the gages either inoperable or uninterpretable.) Note that although the time scales in Figs. 5.17–5.21 have been synchronized, the time zero does not necessarily correspond to the onset of ductile fracture because it could not be unambiguously identified.

The strain-gage records and fracture surface were used to deduce the crack length (apparent position of crack front) during the fracture process, and the results are summarized in Table 5.2. In the table, the strain-gage positions are modified from those shown in Fig. 4.7 to account for the fact that the peak strain occurs at an angle of 72° in front of the crack tip. Figure 5.22 presents a plot of crack position vs time derived from the front-face and back-face strain-gage results up to the time corresponding to arrest of the cleavage crack propagation. (Because of the large amount of plasticity that occurred after arrest, many strain gages became inoperative or uninterpretable; therefore, the crack-front position vs time could not be evaluated during fibrous fracture.) Results (a/w > 0.229) indicate that the crack front advance at comparable elapsed times during the cleavage crack run-arrest event was

Table 5.2. Crack position vs time and velocity: test WP-CE-1

Indicator[a]	Position (mm)	Time (ms)	Velocity[b] (m/s)
Front-face measurements			
Initial crack	200	0	
			853
SG1	229	0.034	
			741
SG2	269	0.088	
			690
SG3	309	0.146	
			526
SG4	349	0.222	
			244
Cleavage arrest	370	0.308	
Back-face measurements			
Initial crack	200	0	
			853
SG13	229	0.034	
			1538
SG14	269	0.060	
			952
SG15	309	0.102	
			513
SG16	349	0.180	
			435
SG17	389	0.272	
			337
Cleavage arrest	420	0.364	

[a]Strain gage positions in the table are all reduced by 21 mm from the actual gage position shown in Fig. 4.7 to account for the fact that the peak strain occurs at an angle of 72° in front of the crack tip.

[b]Velocity is an average calculated velocity for crack propagation between indicator points.

more rapid near the back face of the plate than near the front face. As noted earlier, no results are available for the period of ductile tearing.

Front- and back-face COD (F- and B-COD) histories for both short (6-ms) and long (60-ms) times are presented in Fig. 5.23. Longitudinal

accelerations recorded by "damped" accelerometers mounted on the specimen's centerline at 3.714 m above (top) and 3.710 m below (bottom) the crack plane are presented in Figs. 5.24 and 5.25, respectively. Dynamic displacement of the specimen, relative to that of the large columns of the testing machine, as measured 3.710 m below the crack plane, is presented in Fig. 5.26 for several time resolutions.

5.2.2 Test WP-CE-2

Figure 5.2 shows the fracture surface of specimen WP-CE-2. There are three distinct cleavage crack run-arrest events, with the third event being composed of two events (i.e., one event at the plate front and one at the plate back face). As the crack propagated, it deviated from the side grooves, reaching ~1 cm from the plane of the side grooves at the furthest extent of cleavage crack propagation. After loss of cleavage, crack propagation returned to the plane of the side grooves. Figure 5.27 is the posttest reduction-in-thickness contour map.

Figure 5.28 presents strain histories for companion crack-line gages mounted on the front and back faces of the specimen. The strain gage records show cleavage crack propagation past the companion crack-line gages. Figure 5.29 shows the cleavage crack passing gages 5 and 6 on the plate front face and gages 17 and 18 on the back face. Strain histories for gages 6 and 18 also show arrest of cleavage crack propagation just past the gages, as well as evidence of additional cleavage crack run-arrest events. Reinitiation of cleavage crack propagation at $t \approx 2$ ms with the crack propagating past gages 7 and 19 with arrest occurring before gages 8 and 20 is shown in Fig. 5.30. Also shown in the figure is reinitiation of cleavage crack propagation at $t \sim 4$ ms at the back face. The crack appears to pass gages 8 and 20 before arresting, but interpretation of the strain results is difficult because of plasticity effects. Long-time strain histories (70 s) presented in Fig. 5.31 for companion crack-line gages 7–8 and 19–20 show that the strain levels indicated for these gages were fairly constant before reloading and the occurrence of ductile tearing. Short-time records for gages 9–12 shown in Fig. 5.32 indicate that gages 9–11 broke sequentially several milliseconds after the last arrest, apparently because of the occurrence of an extensive plastic zone. Gage 12 however, did not break until ~24 s after the arrest event, with the break occurring during reloading while ductile tearing was taking place. Figure 5.33 (*a*) and (*b*) presents the strain histories for intermediate-field gage 21 during the cleavage crack run-arrest events and while ductile tearing was occurring. Figure 5.34 presents strain histories for far-field gages 22–25 during the cleavage crack run-arrest events, and Fig. 5.35 presents strain histories for these gages while ductile tearing was taking place.

The strain-gage records and fracture surface were used to deduce the crack length (apparent position of crack front) during the fracture process, and the results are summarized in Table 5.3. In the table, the strain-gage positions are modified from those shown in Fig. 4.7 to account for the fact that the peak strain occurs at an angle of 72° in front of the crack tip. Figure 5.36 presents a plot of strain-gage-

Table 5.3. Crack position vs time and velocity: test WP-CE-2

Indicator[a]	Position (mm)	Time (ms)	Velocity[b] (m/s)
Front-face measurements			
Initial crack	201	0	
			1333
SG1	229	0.021	
			2500
SG2	269	0.037	
			976
SG3	309	0.078	
			1111
SG4	349	0.114	
			851
SG5	389	0.161	
			714
SG6	429	0.217	
			451
First arrest	466	0.299	
			0
Reinitiation	466	1.899	
			100
SG7	469	1.929	
			530
Second arrest	504	1.995	
			0
Reinitiation	504	3.753	
			71
SG8	509	3.823	
			178
Third arrest	525	3.913	
Back-face measurements			
Initial crack	201	0	
			823
SG13	229	0.034	
			2857
SG14	269	0.048	
			952
SG15	309	0.090	
			1143
SG16	349	0.125	
			833
SG17	389	0.173	
			833
SG18	429	0.221	
			375
First arrest	456	0.293	
			0
Reinitiation	456	1.927	
			464
SG19	469	1.955	
			875
Second arrest	504	1.995	
			0
Reinitiation	504	7.961	
			167
SG20	509	7.991	
			247
Third arrest	546	8.141	

[a]Strain-gage positions in the table are all reduced by 21 mm from the actual gage position shown in Fig. 4.7 to account for the fact that the peak strain occurs at an angle of 72° in front of the crack tip.

[b]Velocity is an average calculated velocity for crack propagation between indicator points.

derived crack-front position vs time from the front-face and back-face strain-gage results up to the time corresponding to arrest of the third cleavage crack propagation. This figure indicates that the crack front advance was consistent at the two plate faces up to arrest of the second cleavage crack propagation. Also as noted in the figure, reinitiation of crack propagation after the second cleavage crack run-arrest event occurred first at the plate front face.

F-COD and B-COD histories at two time resolutions are presented in Fig. 5.37. Longitudinal accelerations recorded by "damped" accelerometers mounted on the specimen's centerline at 3.697 m above (top) and 3.711 m below (bottom) the crack plane are presented in Fig. 5.38. Dynamic displacement of the specimen, relative to that of the large columns of the testing machine, as measured 3.706 m below the crack plane, is presented in Fig. 5.39 for several time resolutions.

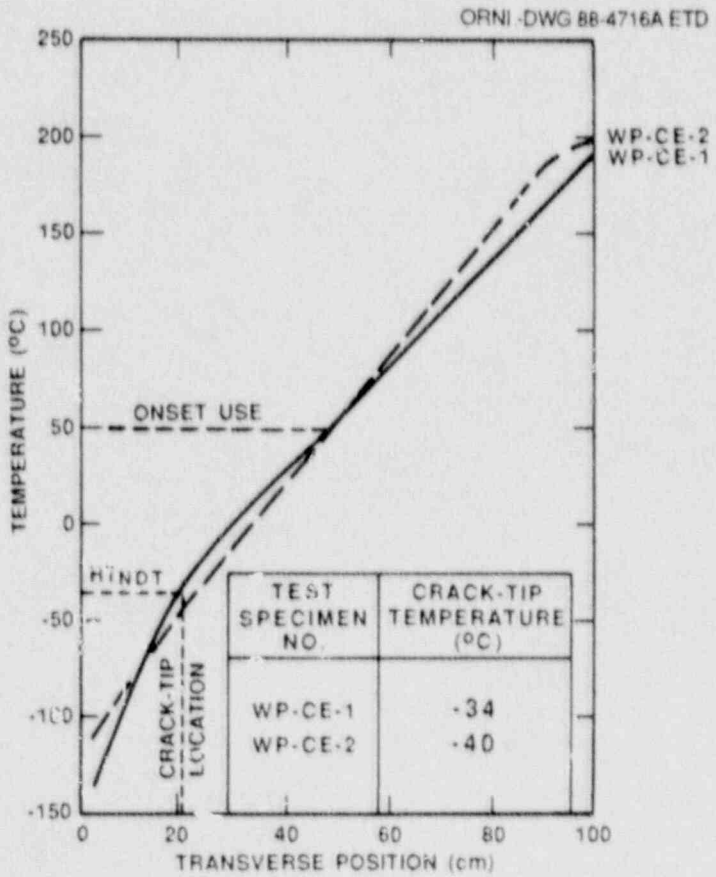

Fig. 5.1. Transverse temperature profiles at approximate time of crack initiation-arrest events: tests WP-CE-1 and -2.

ORNL-PHOTO 6809-88A

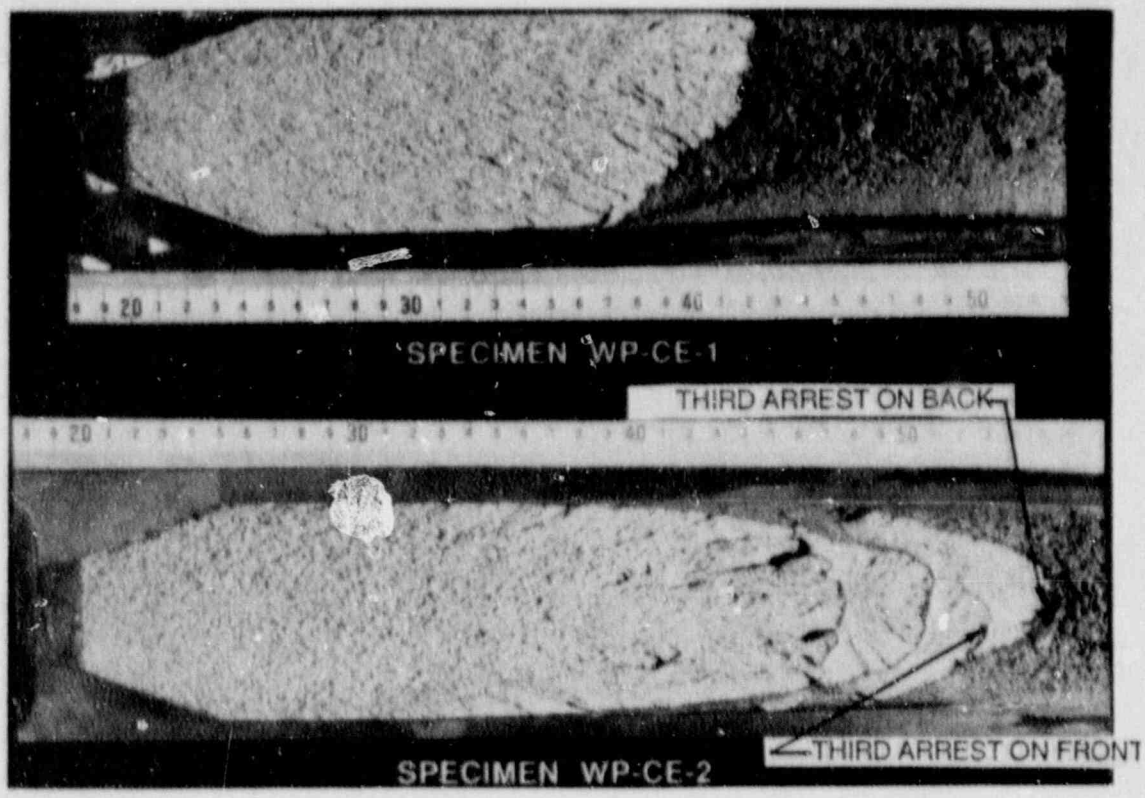

Fig. 5.2. Fracture surfaces for specimens WP-CE-1 and -2.

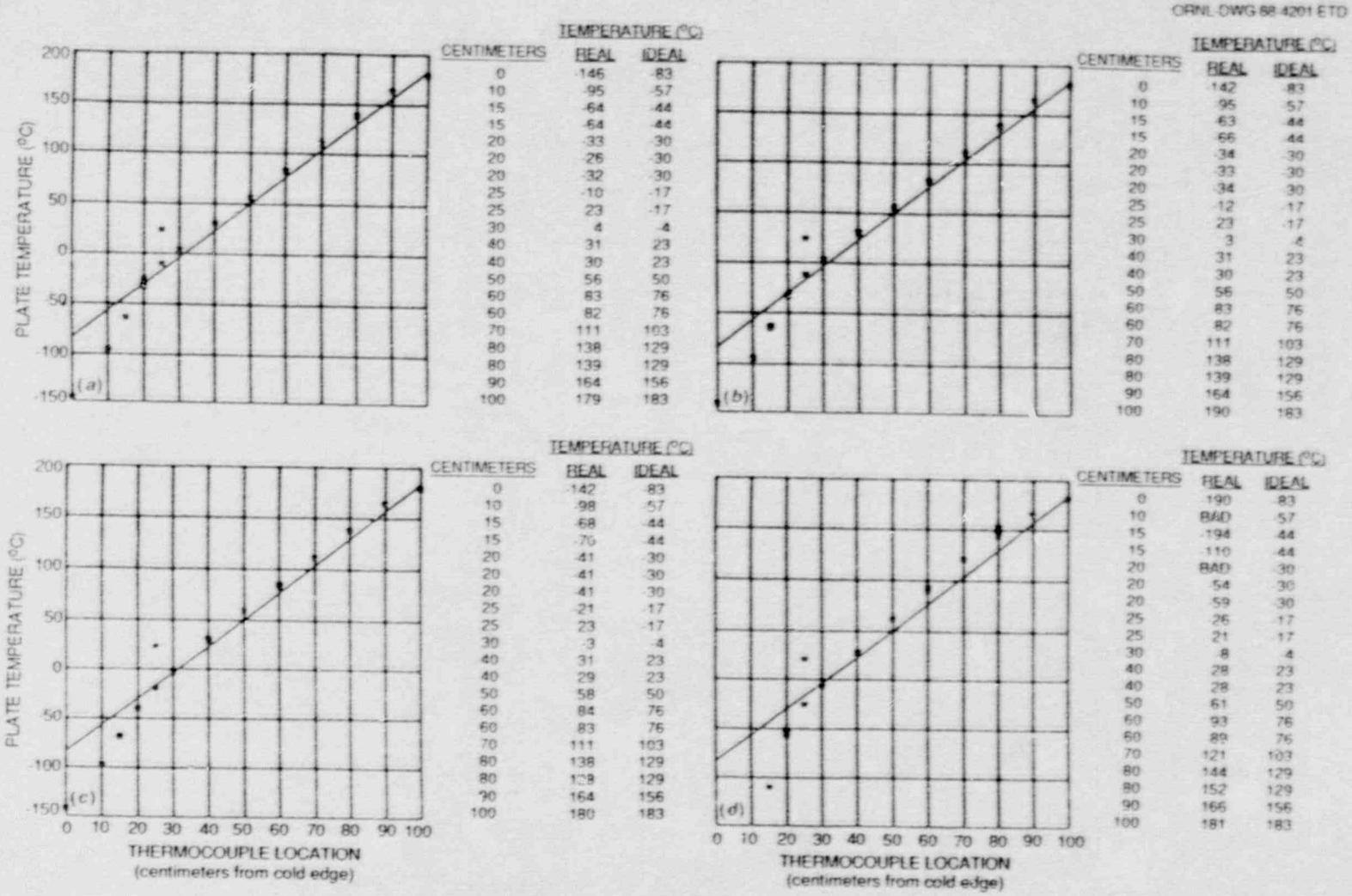

CENTIMETERS	TEMPERATURE (°C) REAL	IDEAL
0	146	83
10	95	57
15	64	44
15	64	44
20	33	30
20	26	30
20	32	30
25	10	17
25	23	17
30	4	4
40	31	23
40	30	23
50	56	50
60	83	76
60	82	76
70	111	103
80	138	129
80	139	129
90	164	156
100	179	183

CENTIMETERS	TEMPERATURE (°C) REAL	IDEAL
0	142	83
10	95	57
15	63	44
15	66	44
20	34	30
20	33	30
20	34	30
25	12	17
25	23	17
30	3	4
40	31	23
40	30	23
50	56	50
60	83	76
60	82	76
70	111	103
80	138	129
80	139	129
90	164	156
100	190	183

CENTIMETERS	TEMPERATURE (°C) REAL	IDEAL
0	142	83
10	98	57
15	68	44
15	70	44
20	41	30
20	41	30
20	41	30
25	21	17
25	23	17
30	3	4
40	31	23
40	29	23
50	58	50
60	84	76
60	83	76
70	111	103
80	138	129
80	139	129
90	164	156
100	180	183

CENTIMETERS	TEMPERATURE (°C) REAL	IDEAL
0	190	83
10	BAD	57
15	194	44
15	110	44
20	BAD	30
20	54	30
20	59	30
25	26	17
25	21	17
30	8	4
40	28	23
40	28	23
50	61	50
60	93	76
60	89	76
70	121	103
80	144	129
80	152	129
90	166	156
100	181	183

Fig. 5.3. Actual and ideal temperature distributions across specimen width at (*a*) start of loading, (*b*) initiation of cleavage crack run-arrest event, (*c*) onset of ductile fracture, and (*d*) final separation of plate: test WP-CE-1.

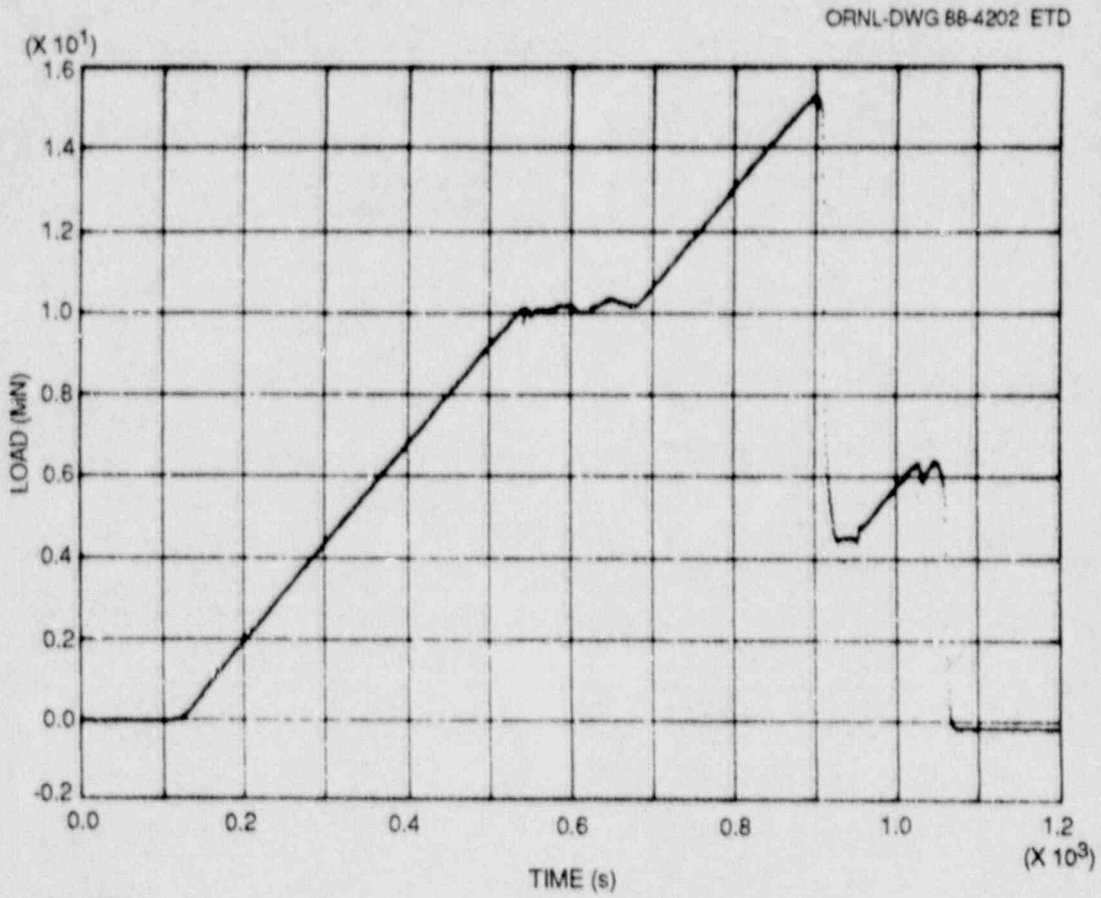

Fig. 5.4. Load vs time relationship: test WP-CE-1.

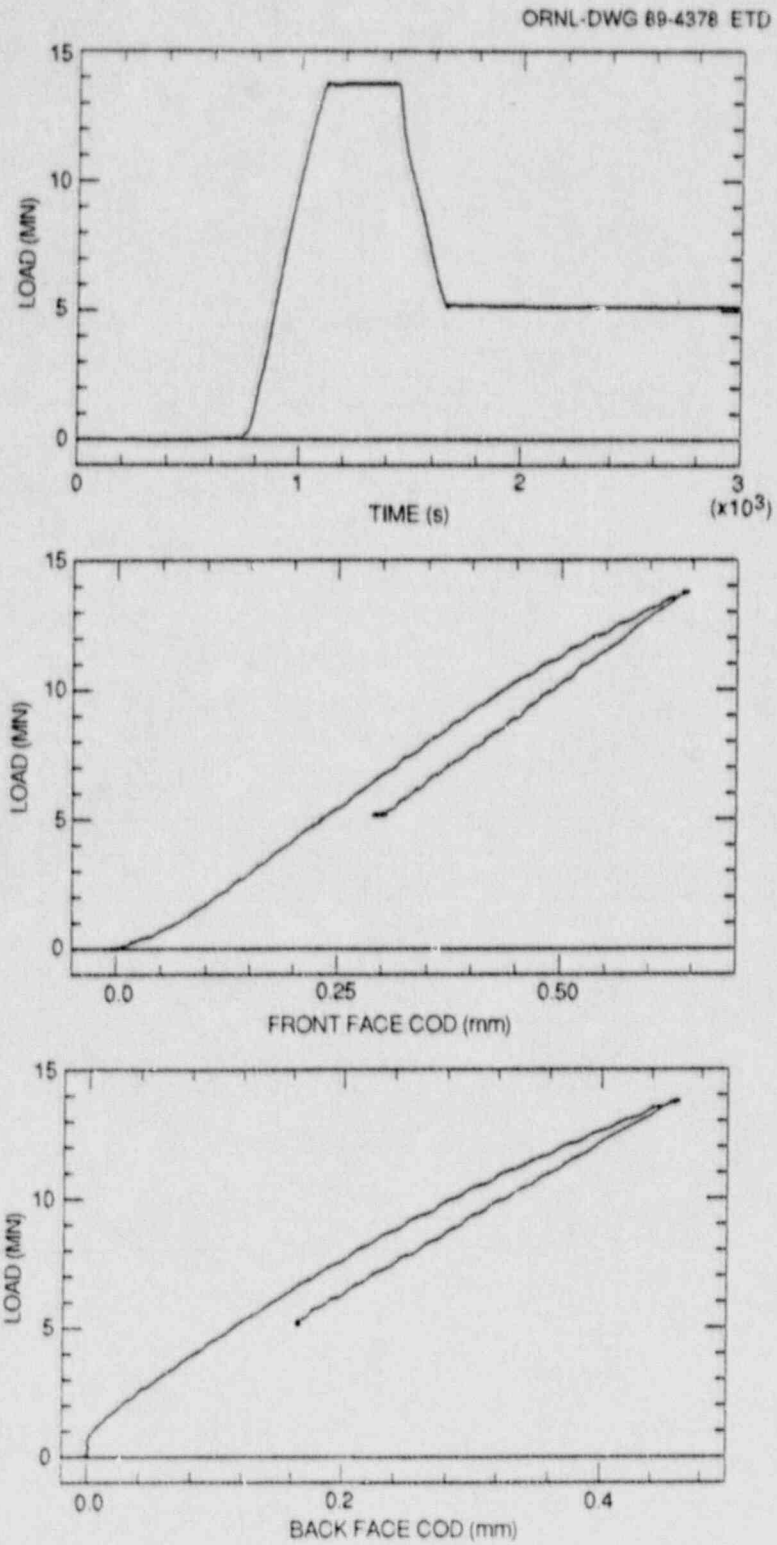

Fig. 5.5. Load history and load vs F-COD- and B-COD results during warm prestressing: test WP-CE-2.

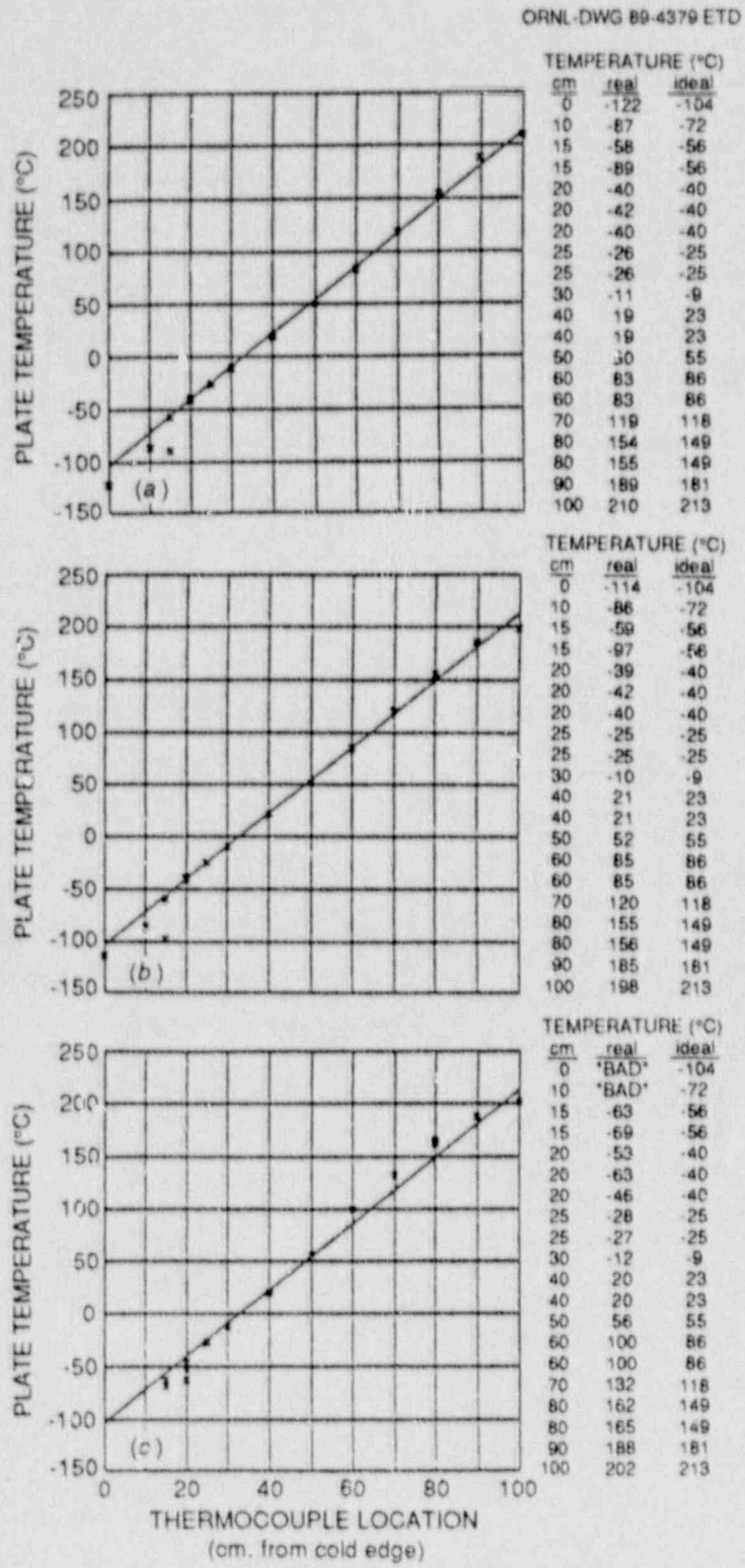

TEMPERATURE (°C)		
cm	real	ideal
0	-122	-104
10	-87	-72
15	-58	-56
15	-89	-56
20	-40	-40
20	-42	-40
20	-40	-40
25	-26	-25
25	-26	-25
30	-11	-9
40	19	23
40	19	23
50	50	55
60	83	86
60	83	86
70	119	118
80	154	149
80	155	149
90	189	181
100	210	213

TEMPERATURE (°C)		
cm	real	ideal
0	-114	-104
10	-86	-72
15	-59	-56
15	-97	-56
20	-39	-40
20	-42	-40
20	-40	-40
25	-25	-25
25	-25	-25
30	-10	-9
40	21	23
40	21	23
50	52	55
60	85	86
60	85	86
70	120	118
80	155	149
80	156	149
90	185	181
100	198	213

TEMPERATURE (°C)		
cm	real	ideal
0	"BAD"	-104
10	"BAD"	-72
15	-63	-56
15	-69	-56
20	-53	-40
20	-63	-40
20	-46	-40
25	-28	-25
25	-27	-25
30	-12	-9
40	20	23
40	20	23
50	56	55
60	100	86
60	100	86
70	132	118
80	162	149
80	165	149
90	188	181
100	202	213

Fig. 5.6. Actual and ideal temperature distributions across specimen width at (*a*) start of loading, (*b*) just before initiation of cleavage crack run-arrest events, and (*c*) near the end of tearing fracture: test WP-CE-2.

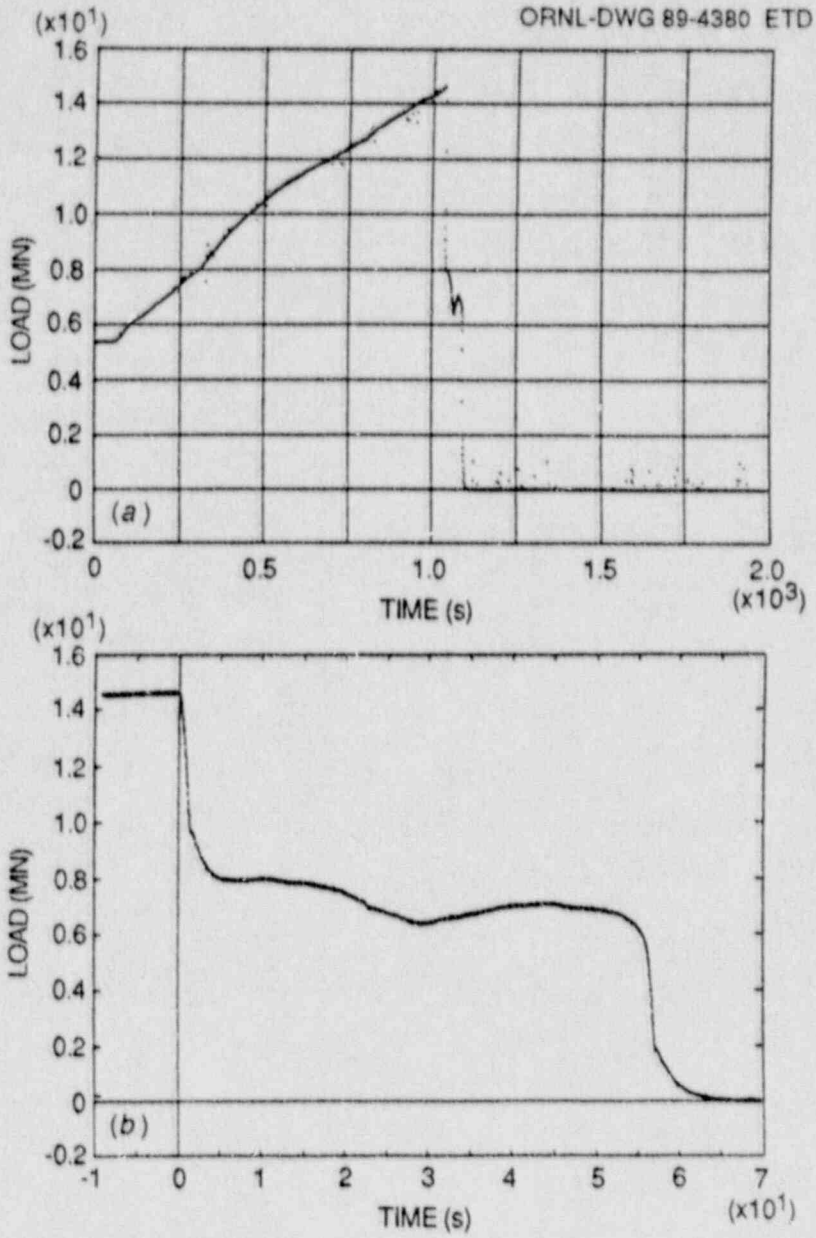

Fig. 5.7. Load history for (*a*) test duration and (*b*) during tearing fracture after cleavage arrest (time zero): test WP-CE-2.

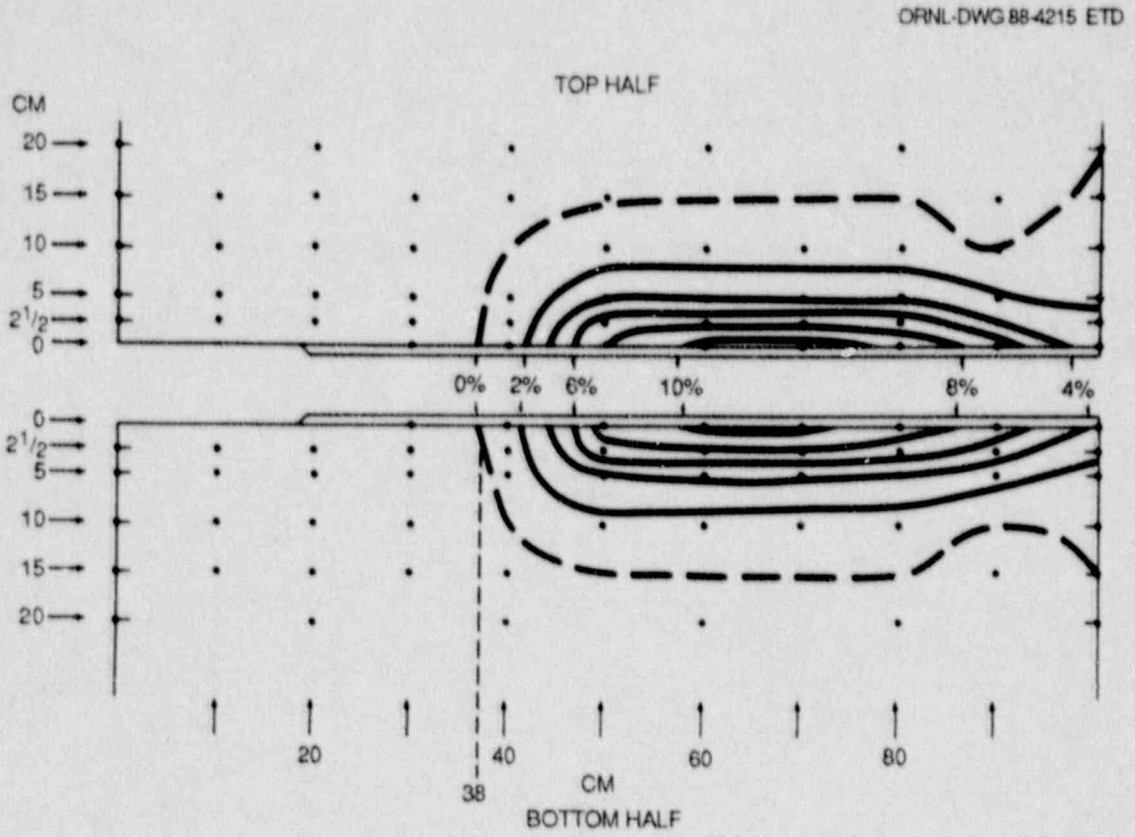

Fig. 5.8. Reduction-in-thickness contour map for specimen WP-CE-1.

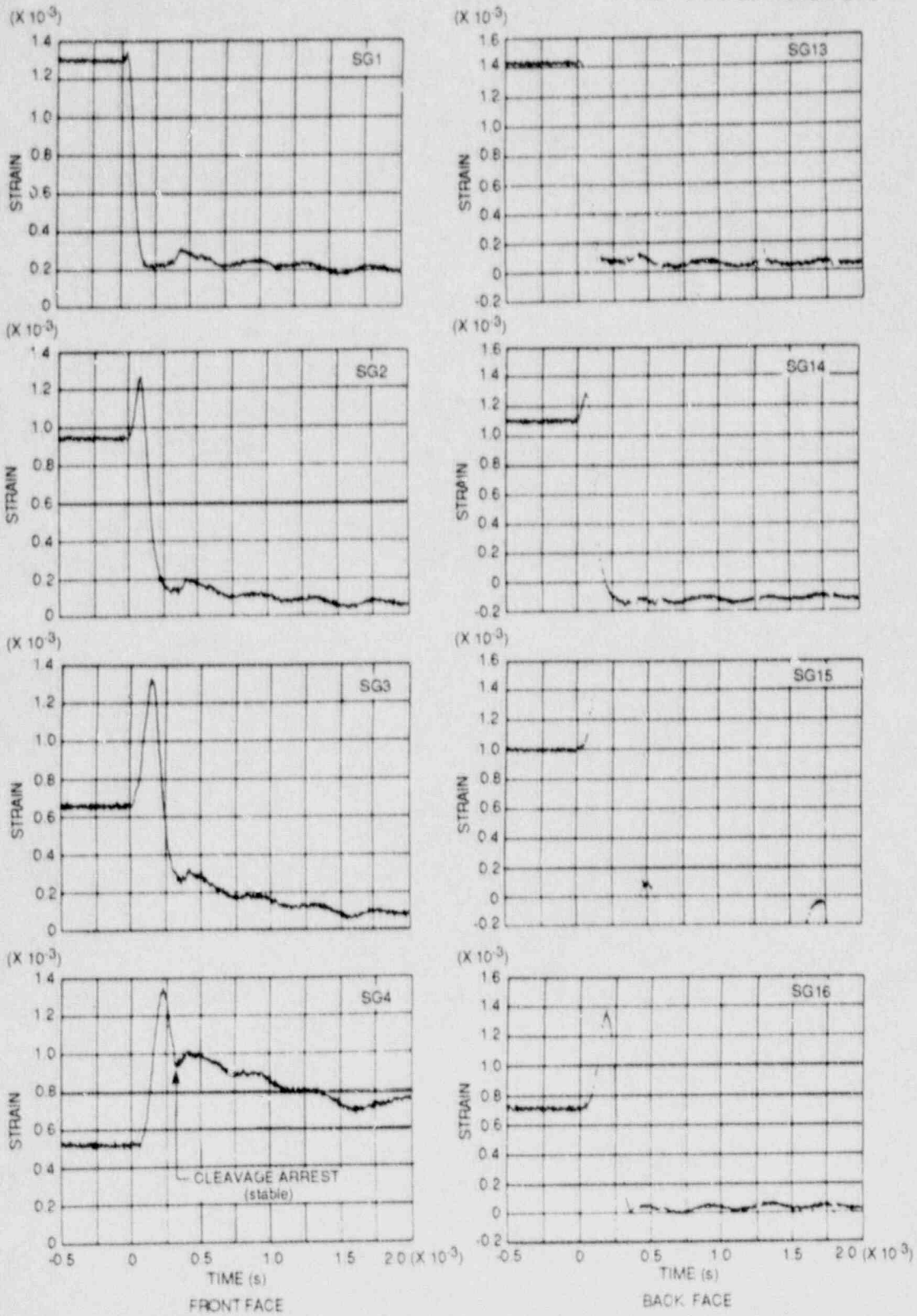

Fig. 5.9. Strain histories for companion crack-line gages showing the cleavage crack passing these gages: test WP-CE-1 (strain gages 1-4 and 13-16).

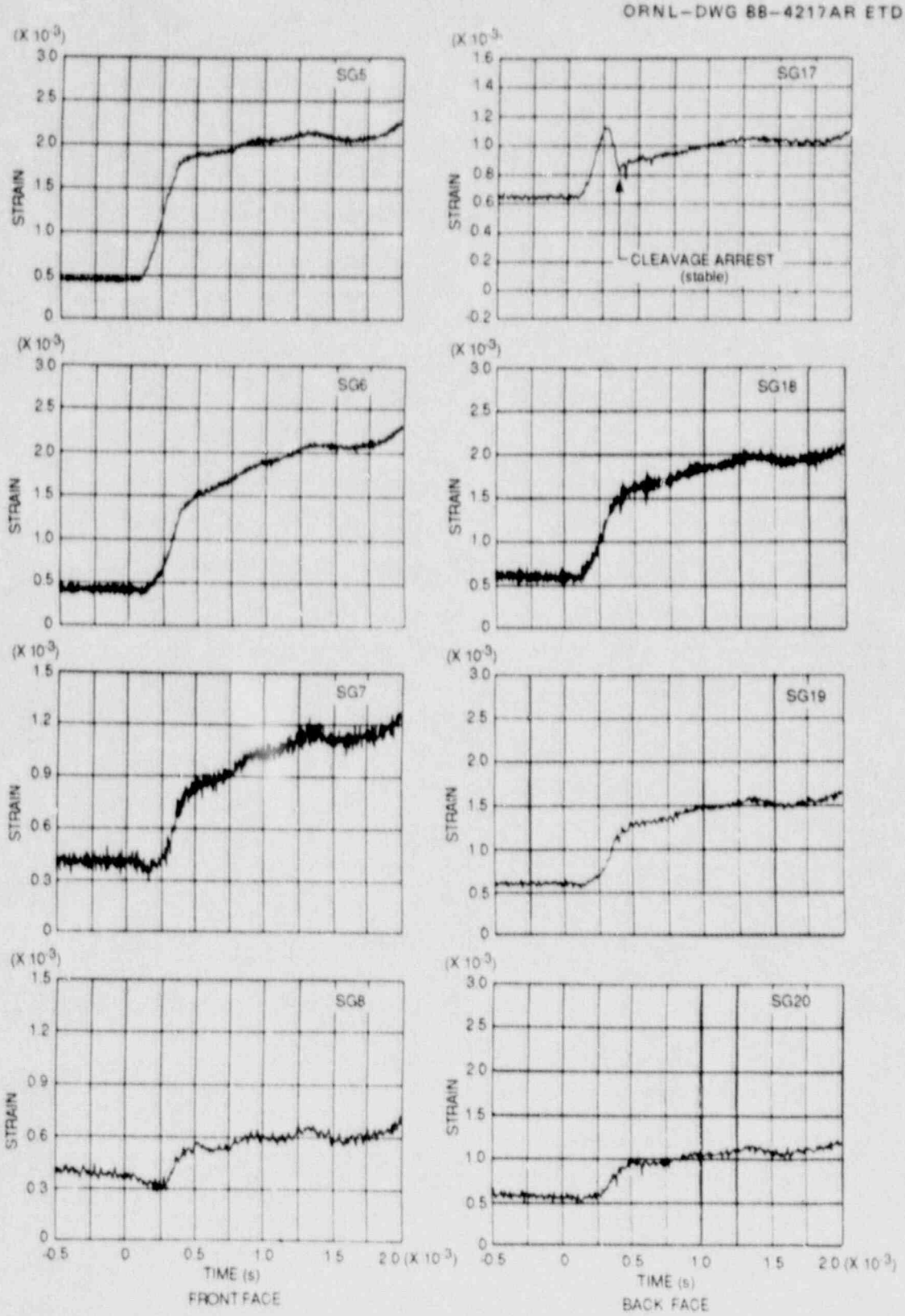

Fig. 5.10. Strain histories for companion crack-line gages showing the crack arresting before reaching gage 5 at plate front face and gage 18 at plate back face: test WP-CE-1 (strain gages 5-8 and 17-20).

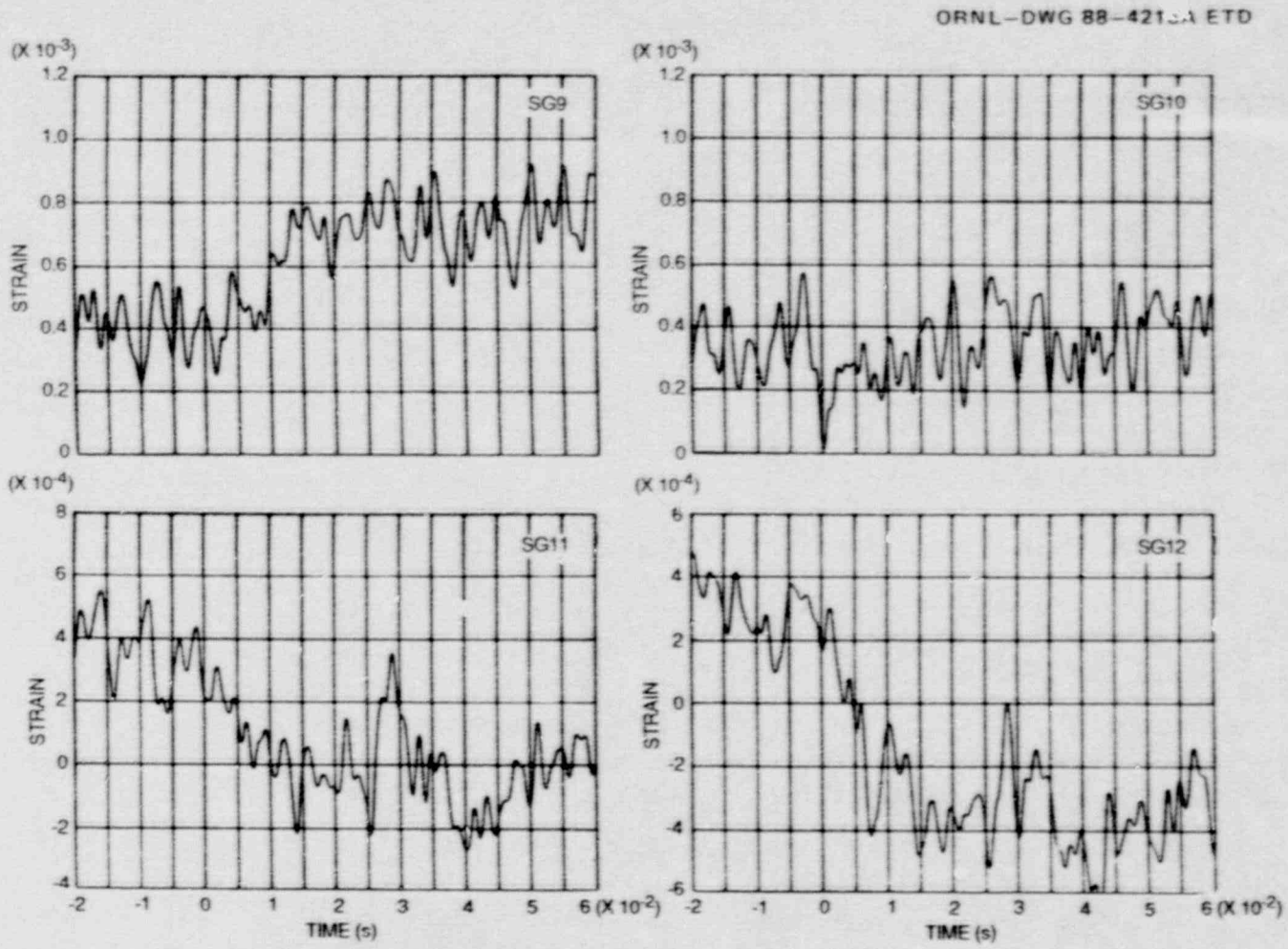

Fig. 5.11. Highly amplified strain histories for front-face gages: test WP-CE-1 (strain gages 9–12).

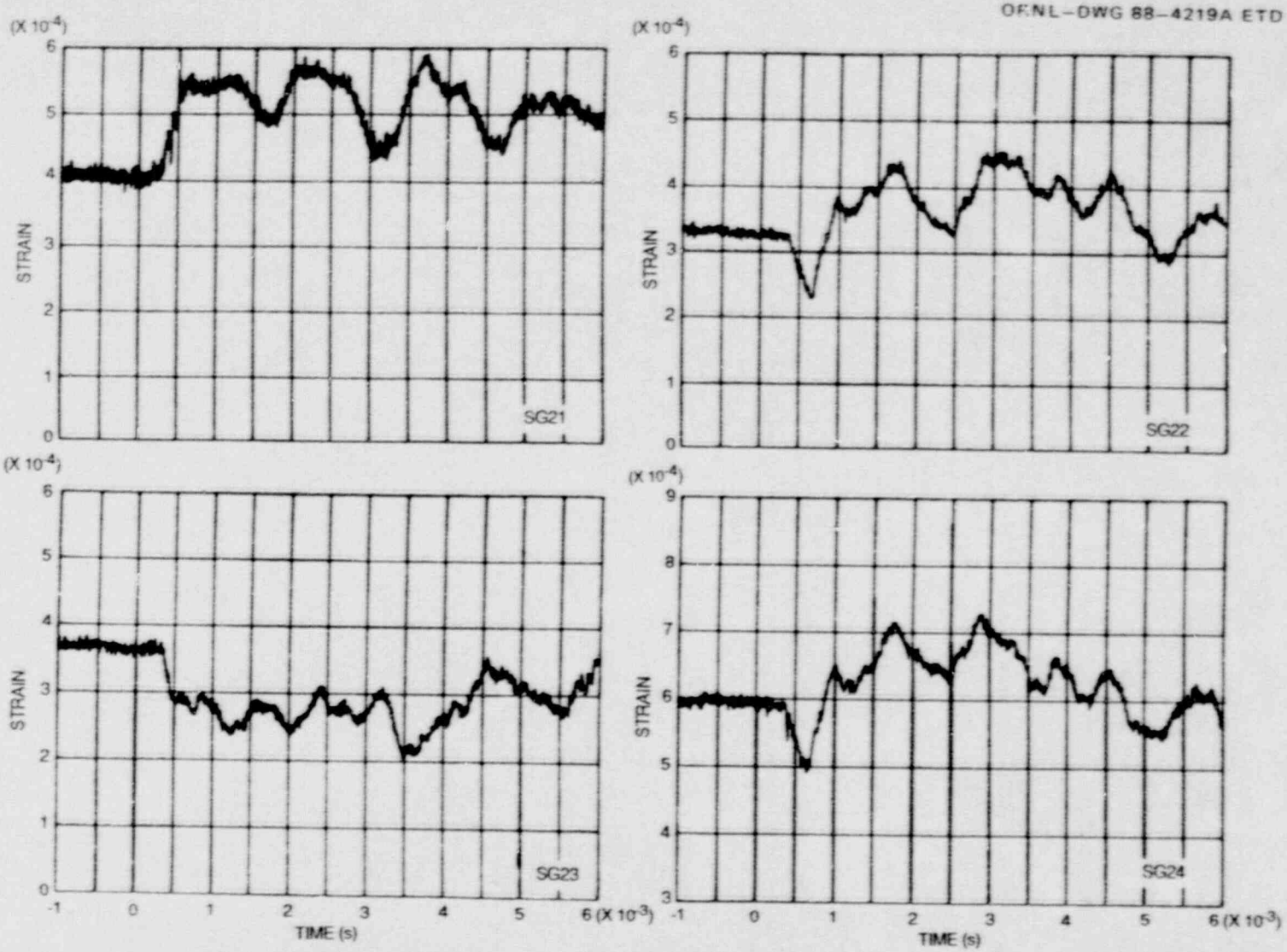

Fig. 5.12. Strain histories for near- and far-field gages recorded just after arrest of the cleavage crack propagation: test WP-CE-1 (strain gages 21-24).

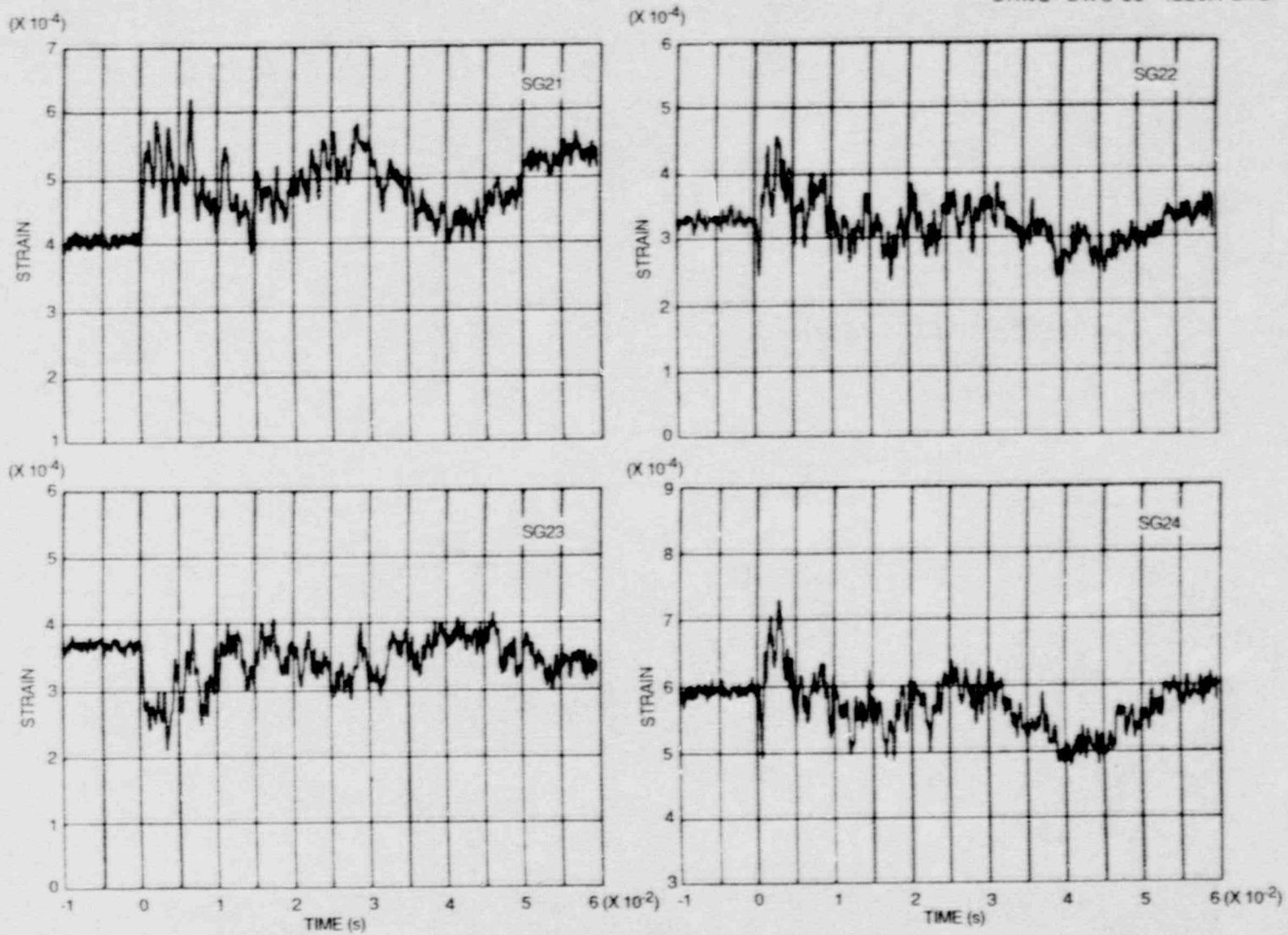

Fig. 5.13. Long-time (60-ms) strain histories for near- and far-field gages: test WP-CE-1 (strain gages 21-24).

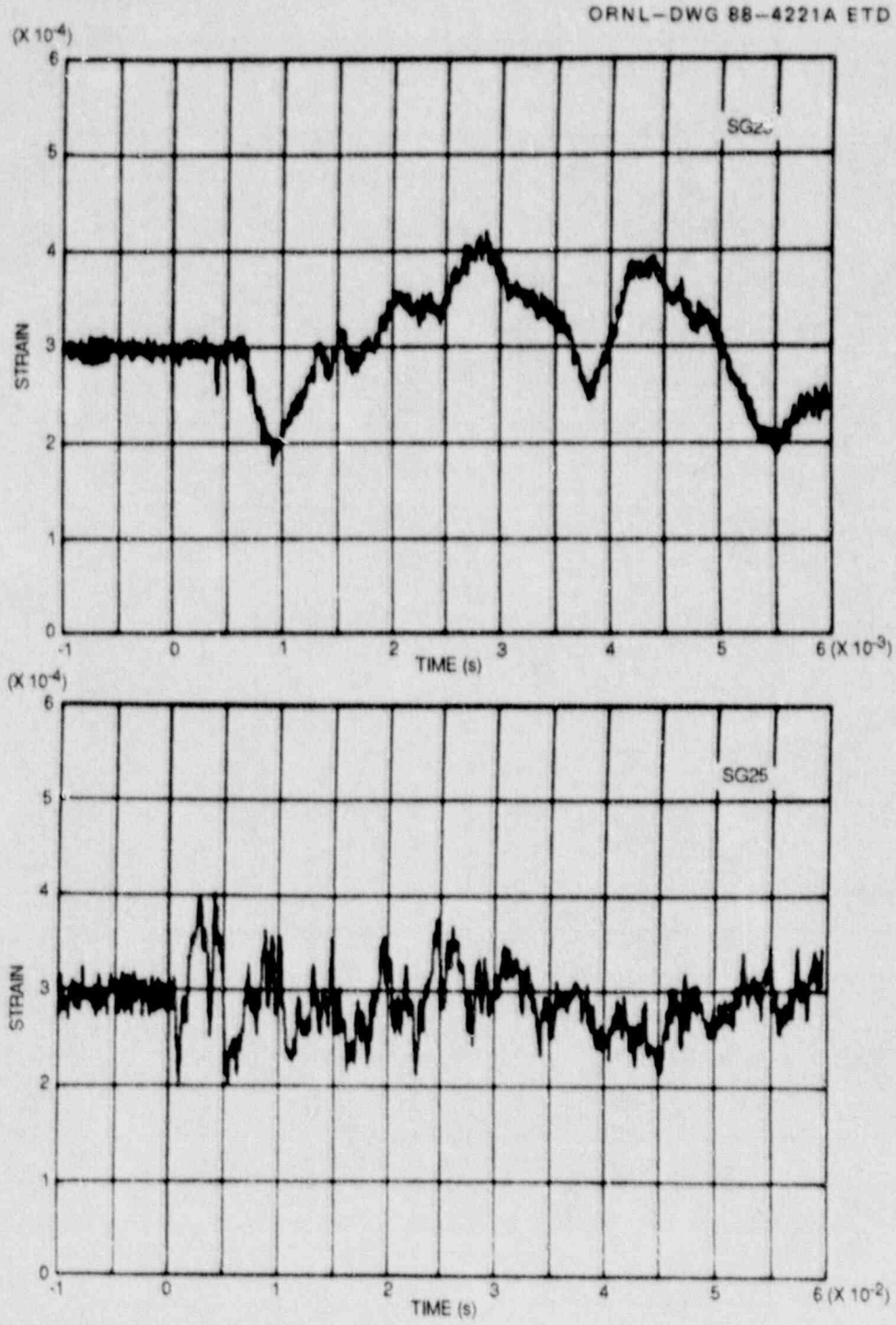

Fig. 5.14. Short- (6-ms) and long- (60-ms) time strain histories for far-field gage 25: test WP-CE-1.

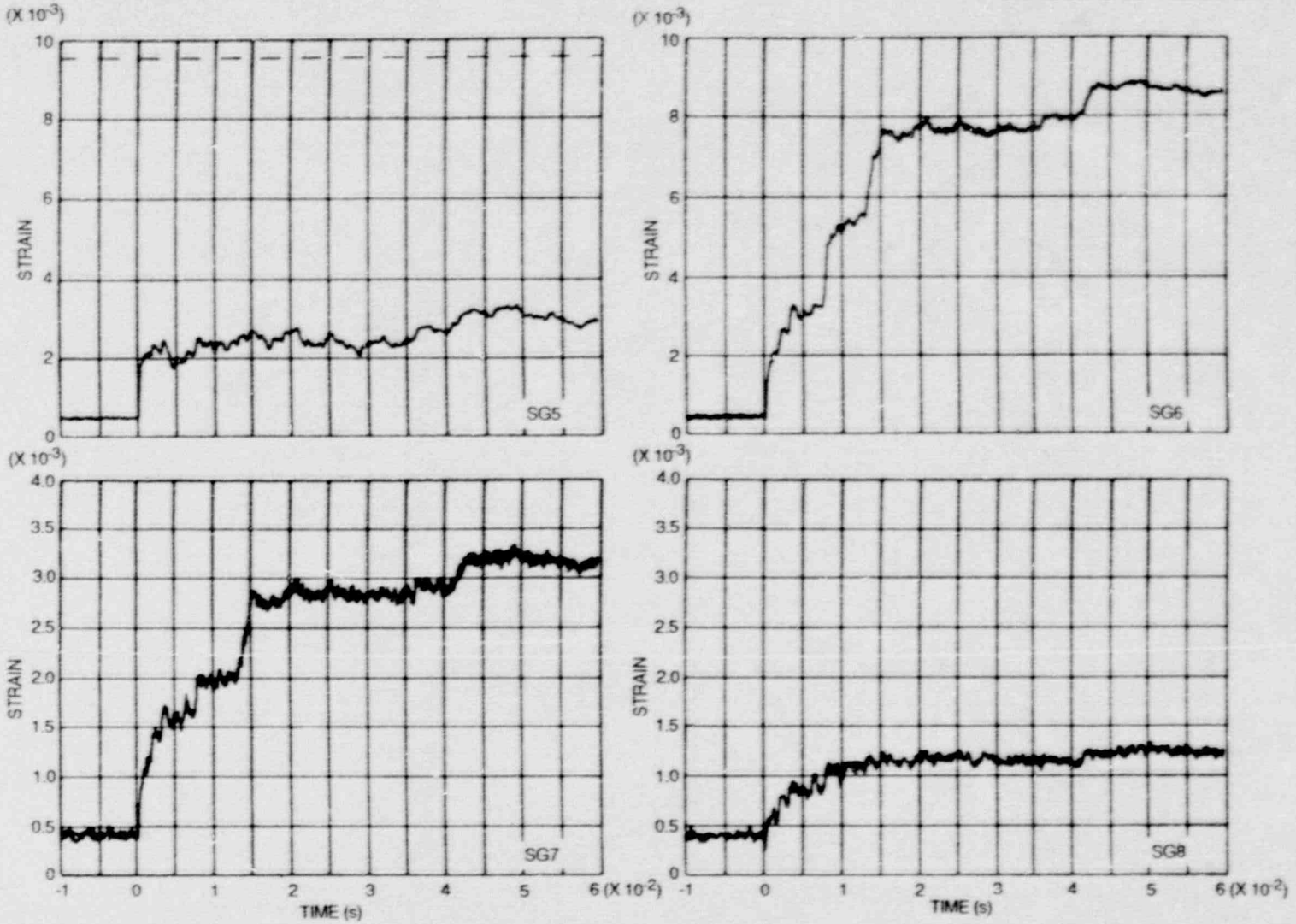

Fig. 5.15. Long-time (60-ms) strain histories for front-face crack-line gages, suggesting some incremental movement of the crack toward gages 5 and 6: test WP-CE-1 (strain gages 5-8).

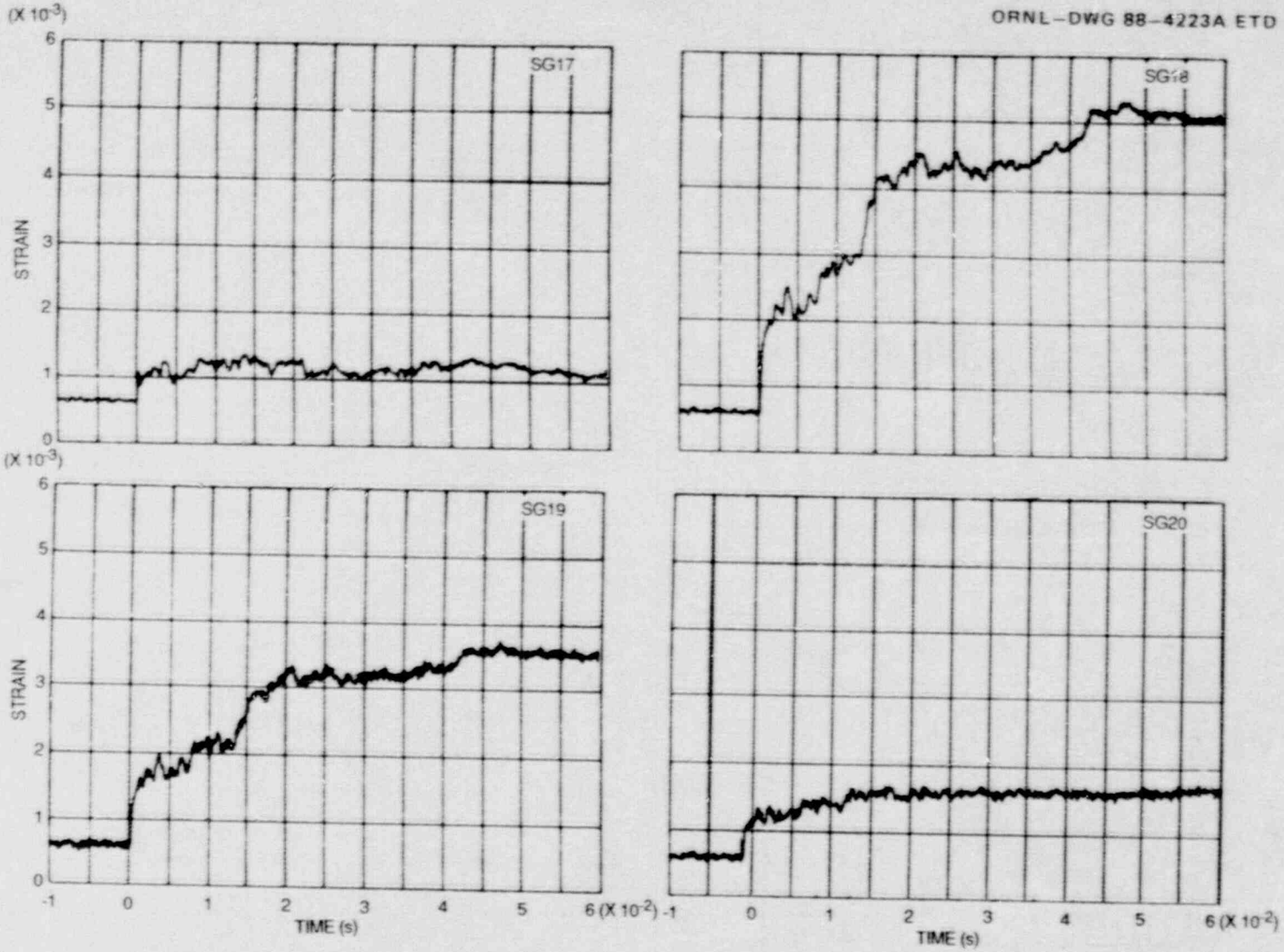

Fig. 5.16. Long-time (60-ms) strain histories for back-face crack-line gages, suggesting some incremental movement of the crack toward gages 18 and 19: test WP-CE-1 (strain gages 17-20).

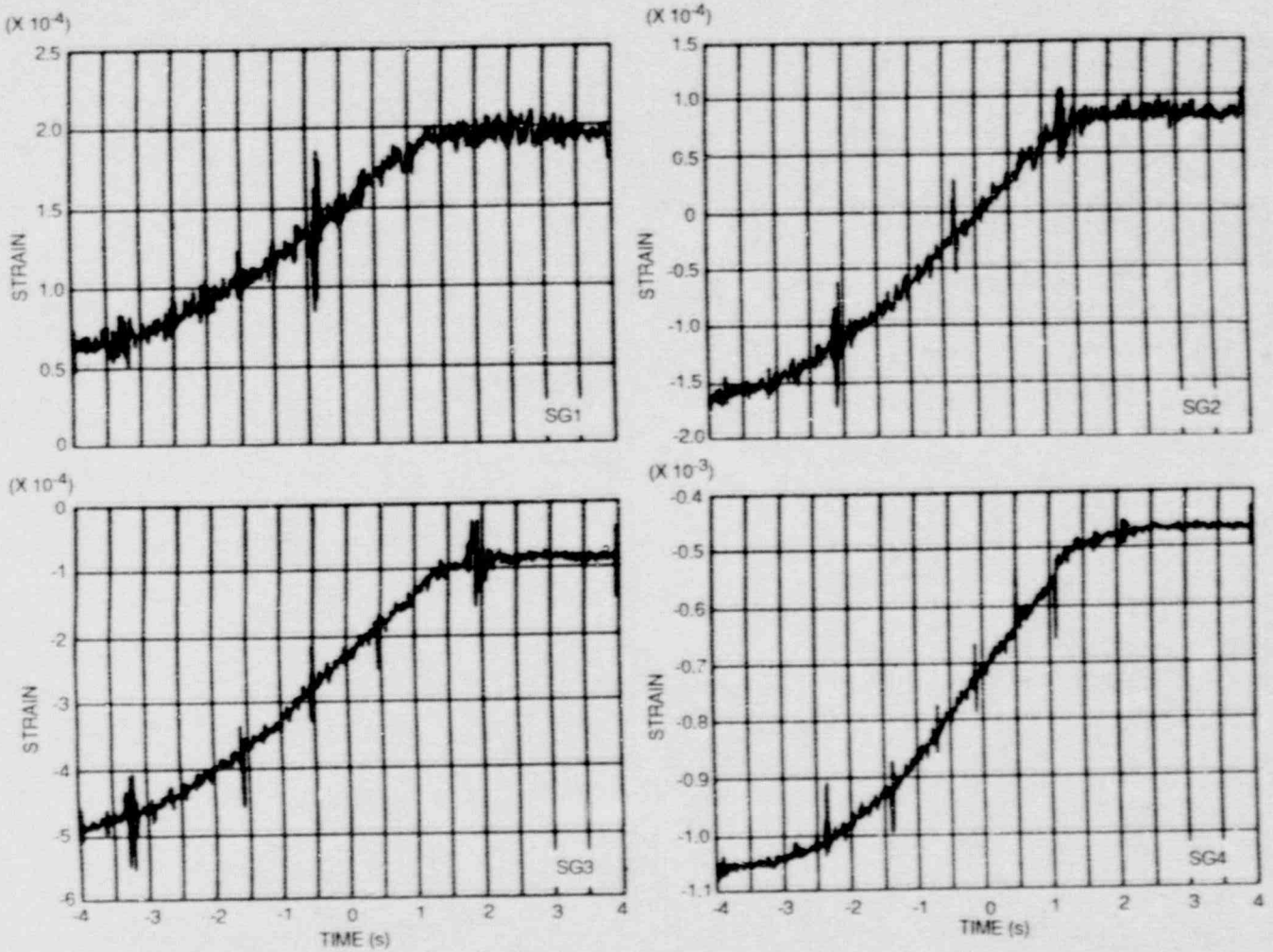

Fig. 5.17. Strain histories for front-face crack-line gages during ductile tearing: test WP-CE-1 (strain gages 1-4).

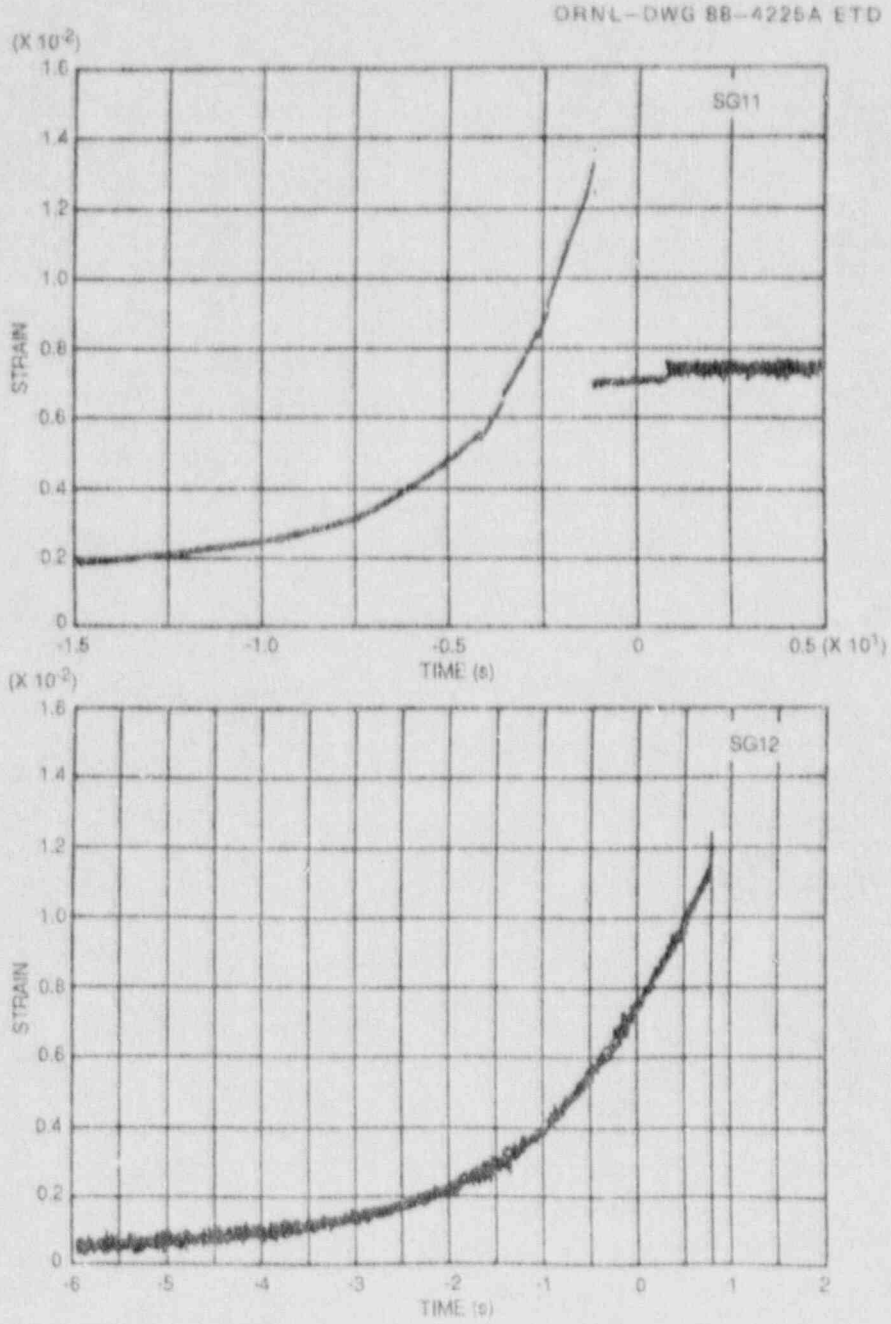

Fig. 5.18. Plasticity and fibrous crack extension as detected by front-face crack-line gages: test WP-CE-1 (strain gages 11-12).

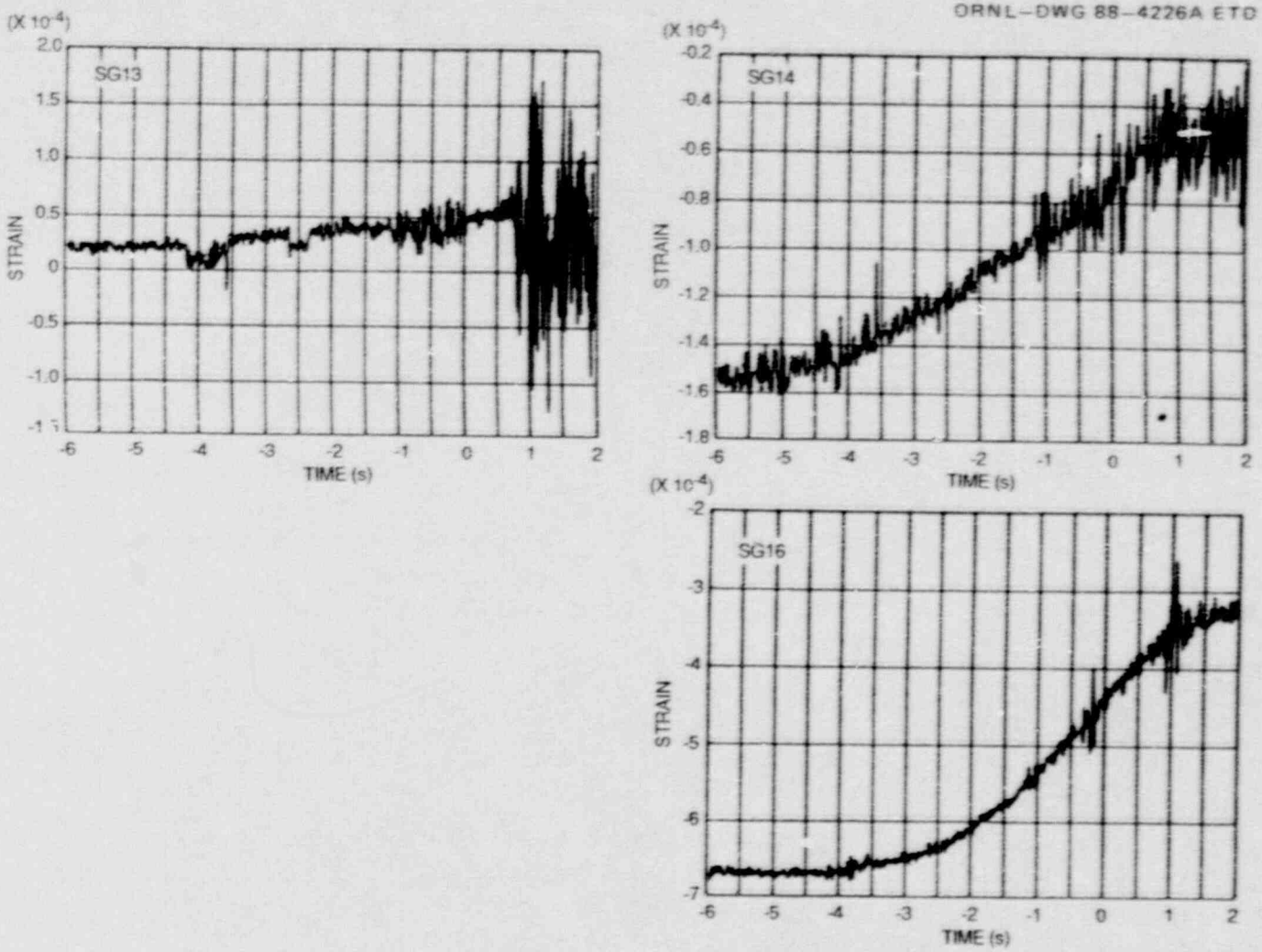

Fig. 5.19. Strain histories for back-face crack-line gages during period while ductile fracture was occurring: test WP-CE-1 (strain gages 13-14 and 16).

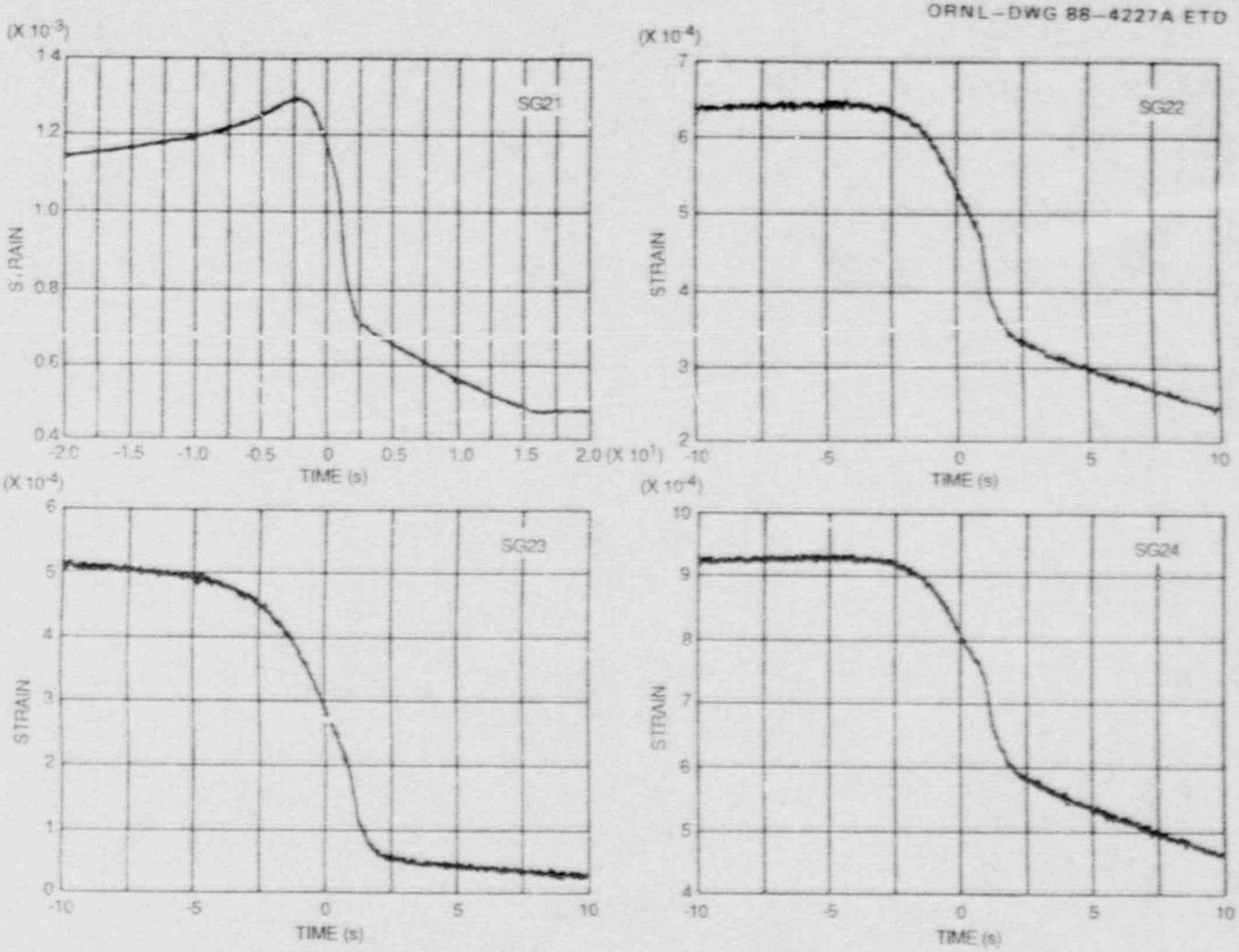

Fig. 5.20. Strain histories for near- and far-field gages during period while ductile failure was occurring: test WP-CE-1 (strain gages 21–24).

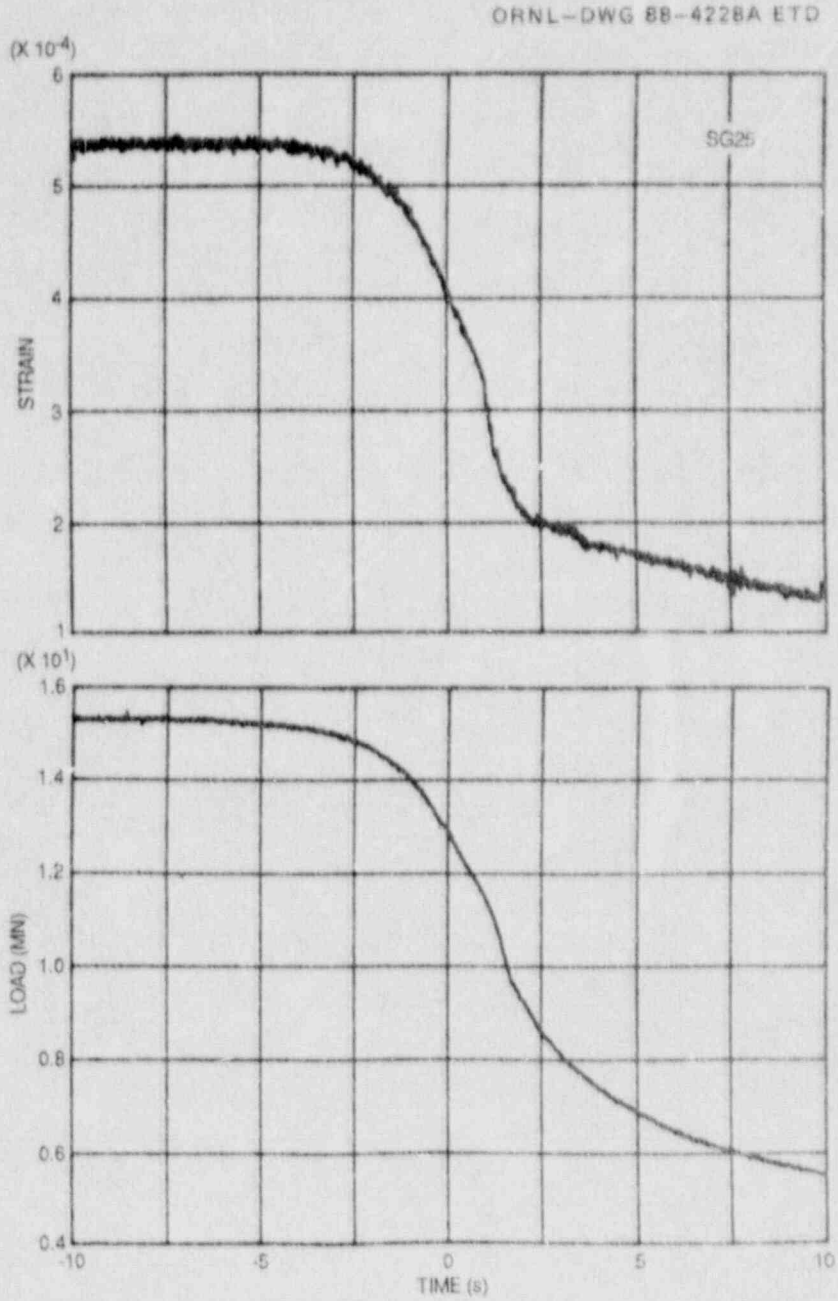

Fig. 5.21. Load and far-field strain (gage 25) histories during period while ductile tearing was occurring: test WP-CE-1.

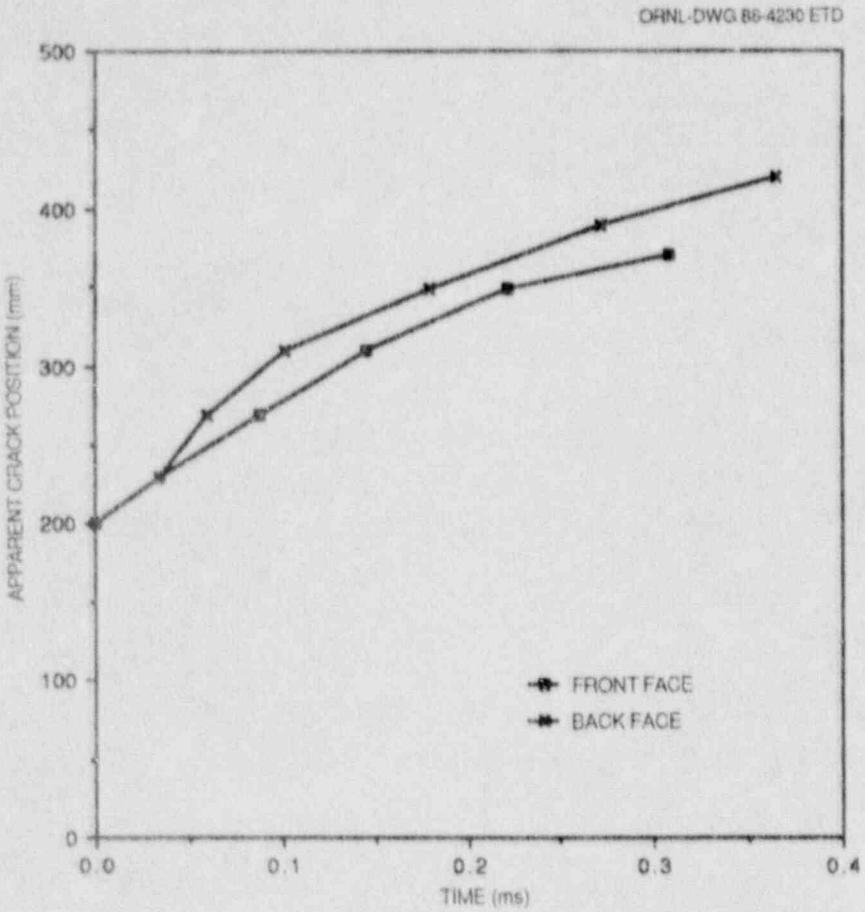

Fig. 5.22. Apparent crack-front position history: test WP-CE-1.

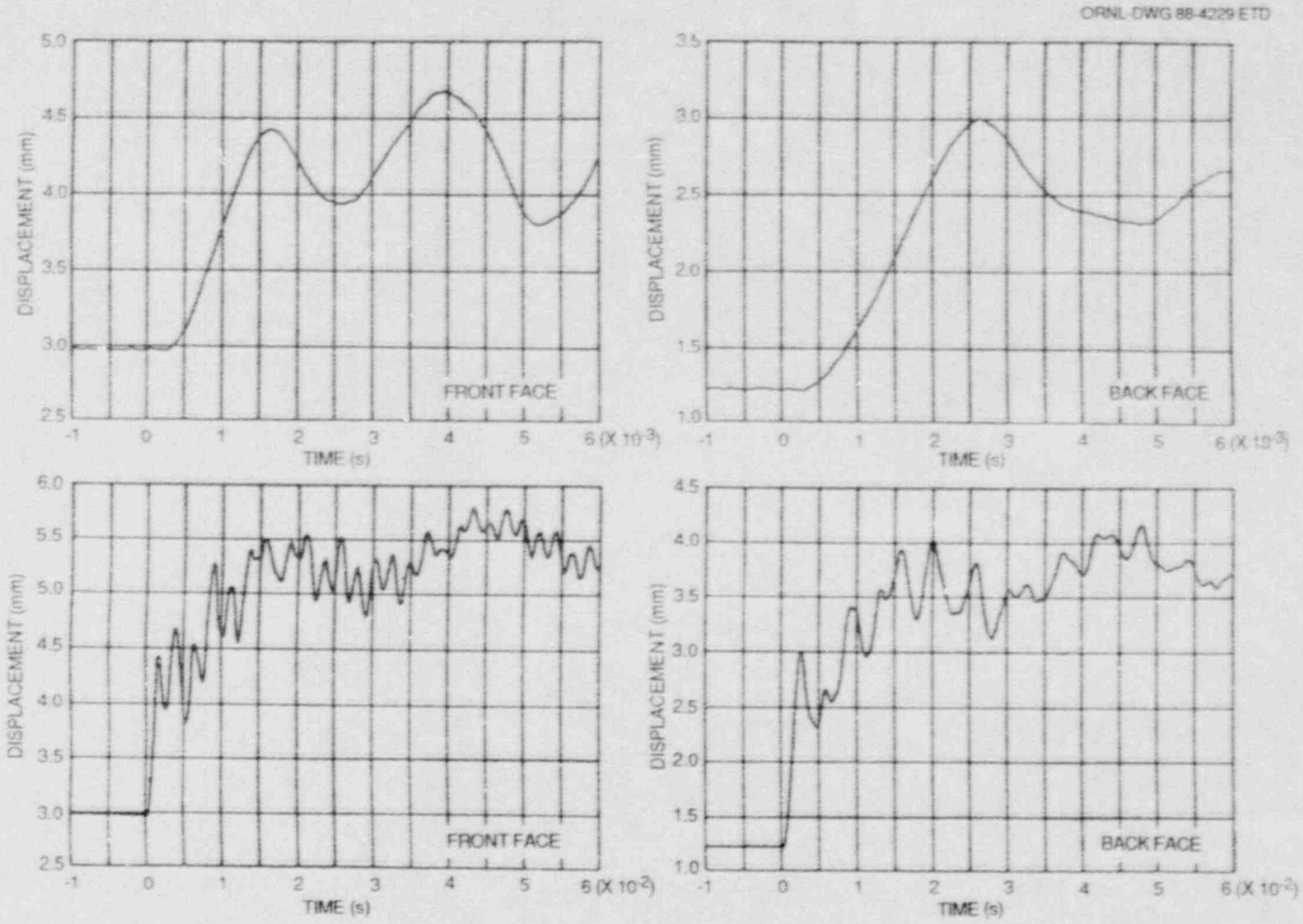

Fig. 5.23. F-COD and B-COD histories for both short (6-ms) and long (60-ms) time periods: test WP-CE-1.

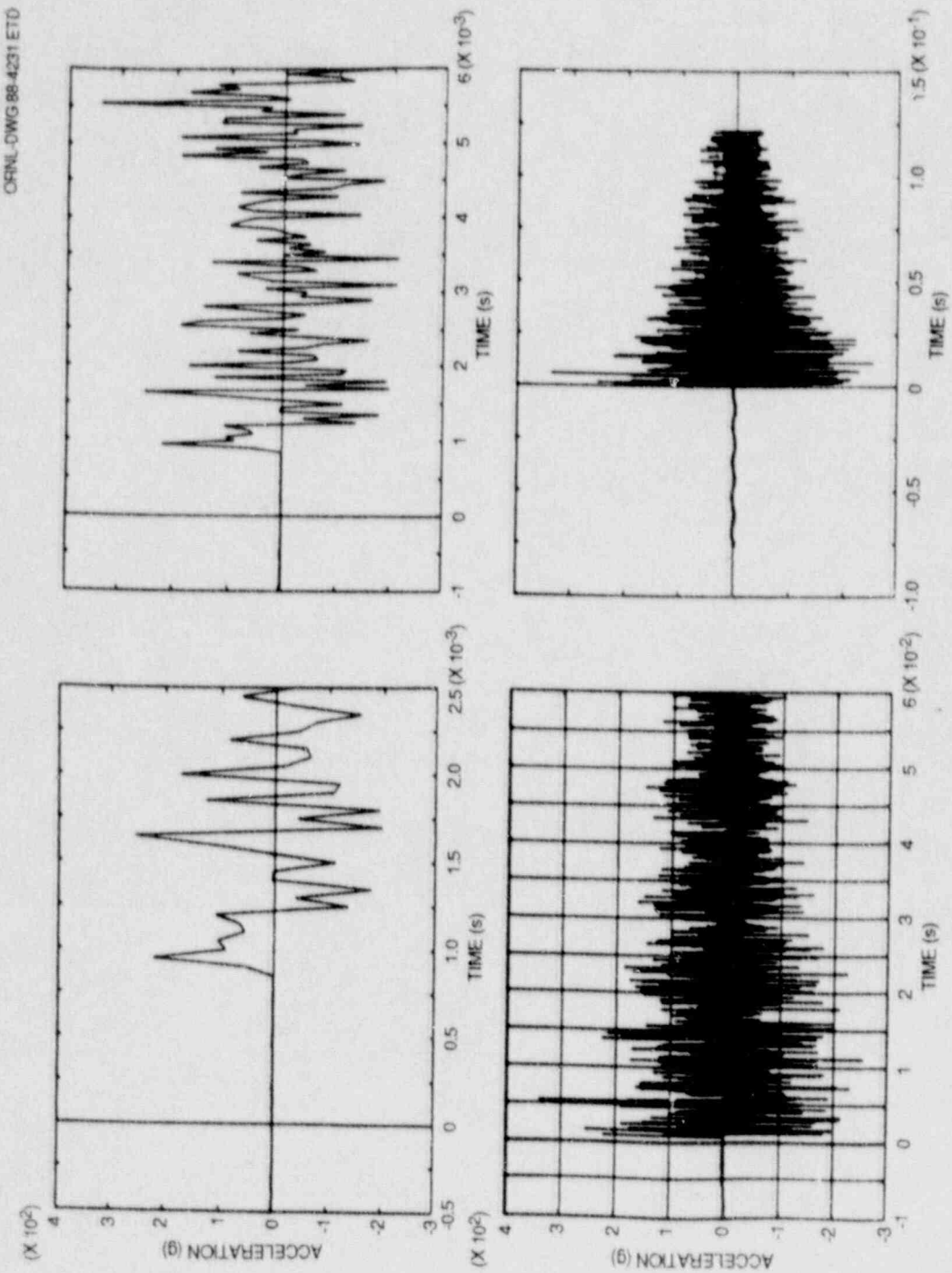

Fig. 5.24. Longitudinal acceleration results of various time resolutions measured by top "damped" accelerometer mounted 3.714 m above crack plane: test WP-CE-1.

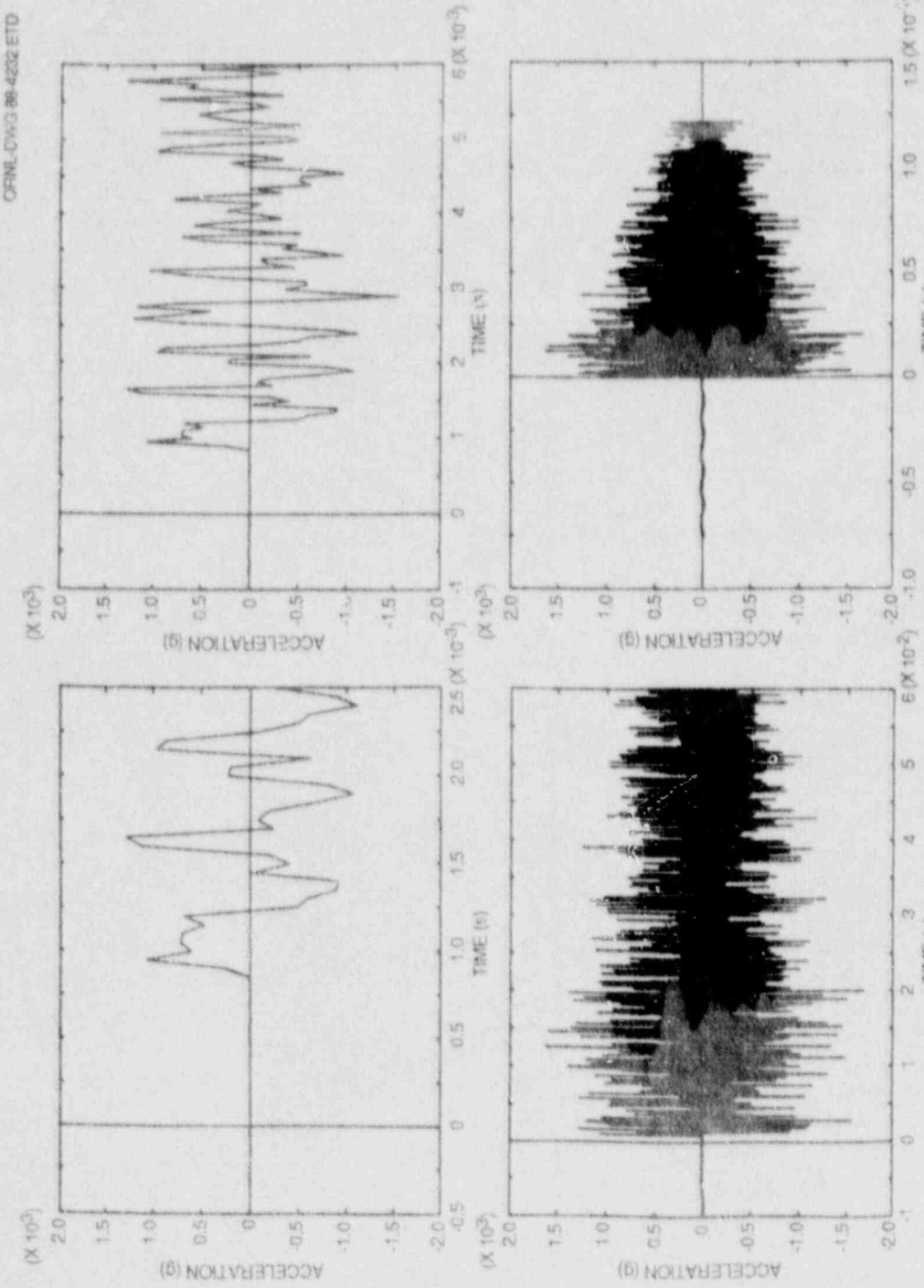

Fig. 5.25. Longitudinal acceleration results at various time resolutions measured by bottom "damped" accelerometer mounted 3.710 m below crack plane: test WP-CE-1.

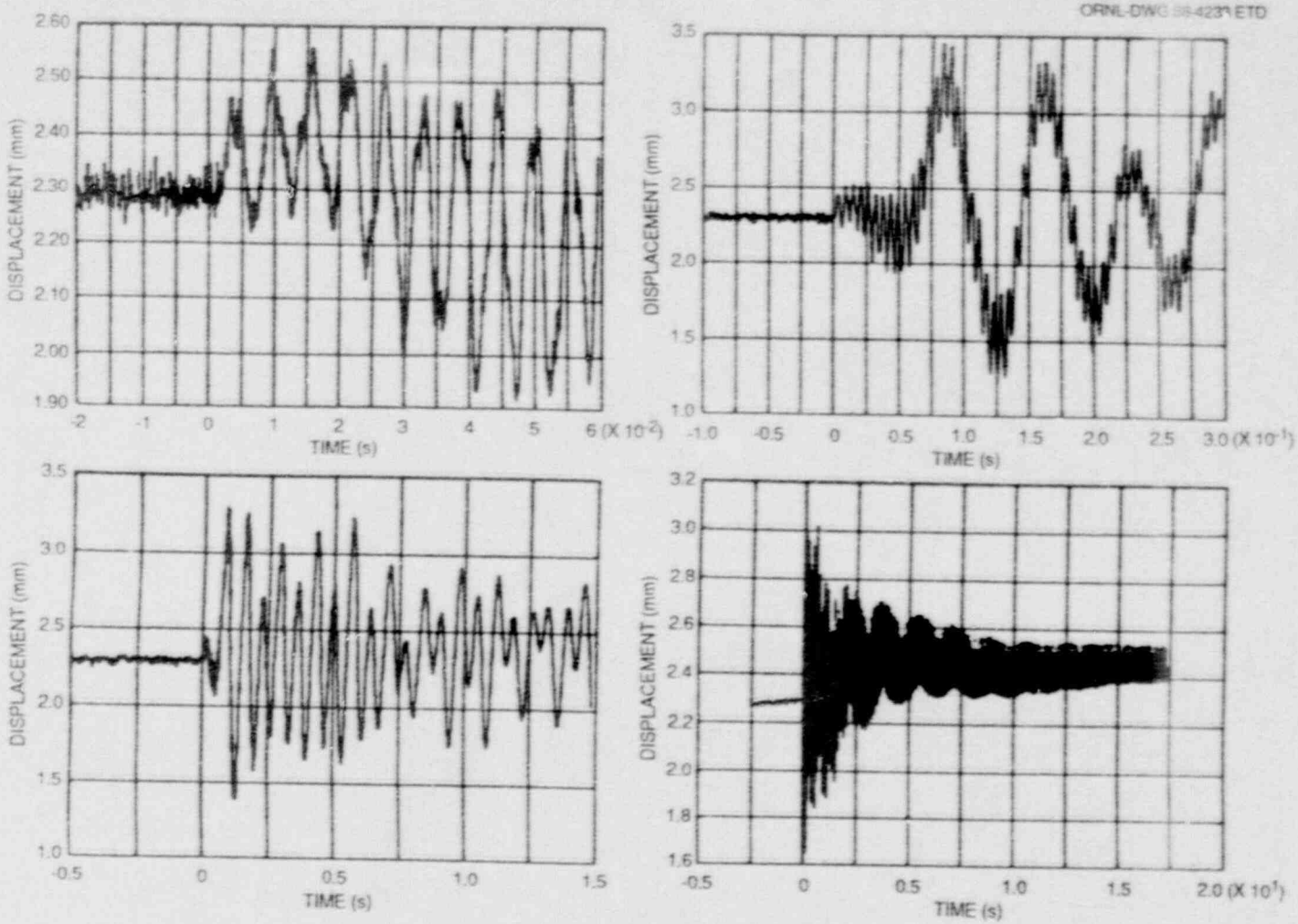

Fig. 5.26. Dynamic displacement results at several time resolutions of specimen relative to that of large columns of testing machine as measured 3.710 m below crack plane: test WP-CE-1.

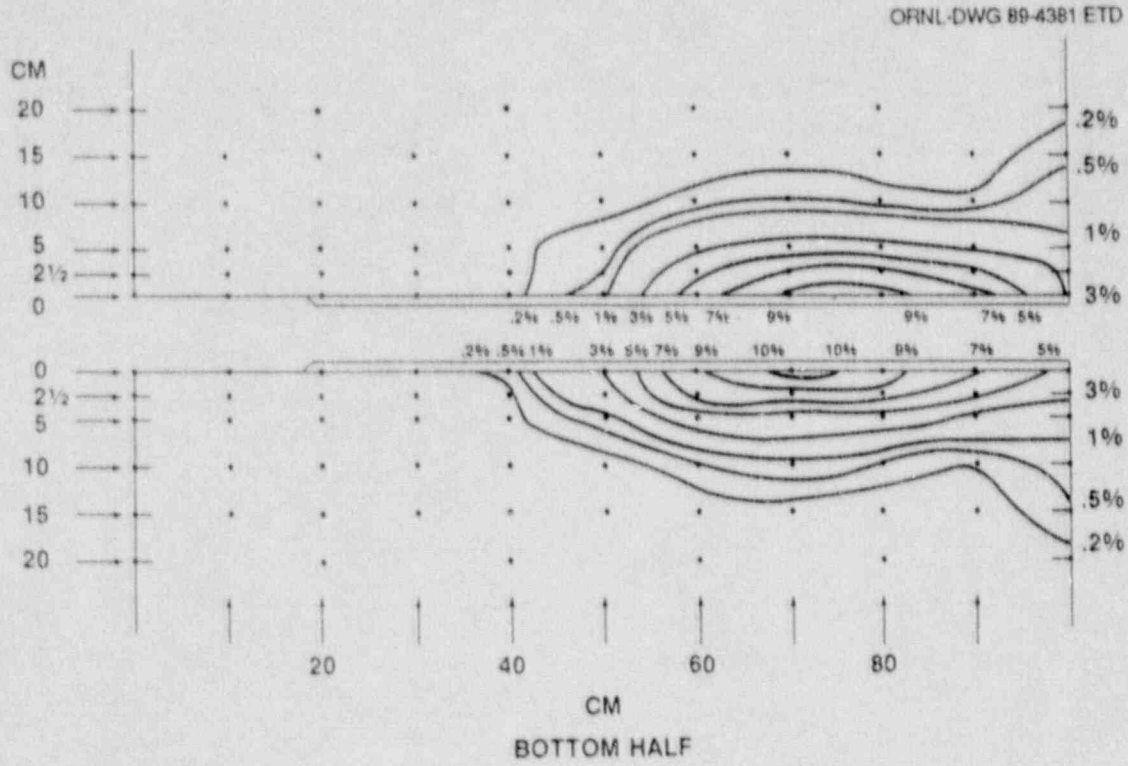

Fig. 5.27. Reduction-in-thickness contour map for specimen WP-CE-2.

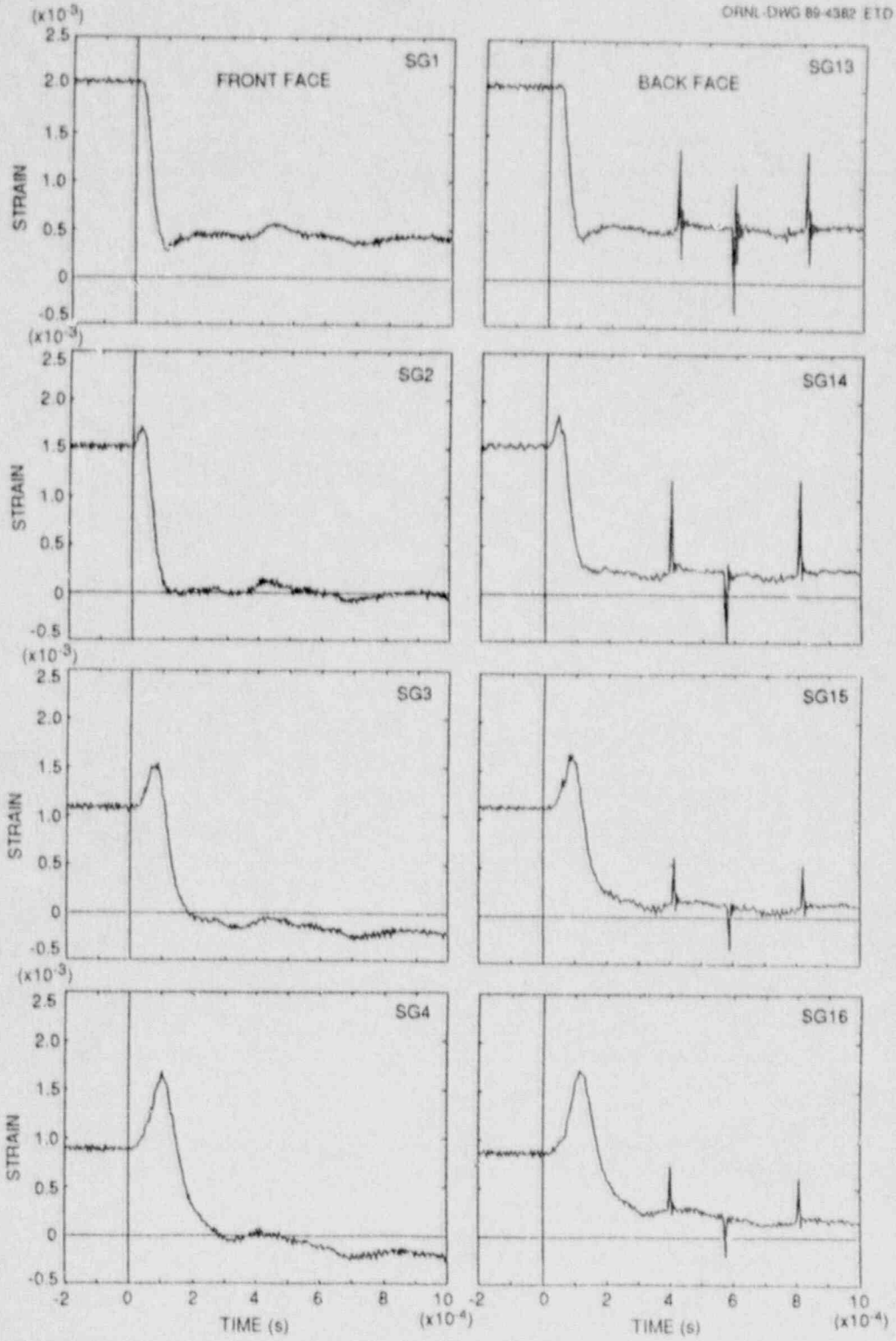

Fig. 5.28. Strain histories for companion crack-line gages showing cleavage crack passing gages 1–4 on plate front face and gages 13–16 on plate back face: test WP-CE-2.

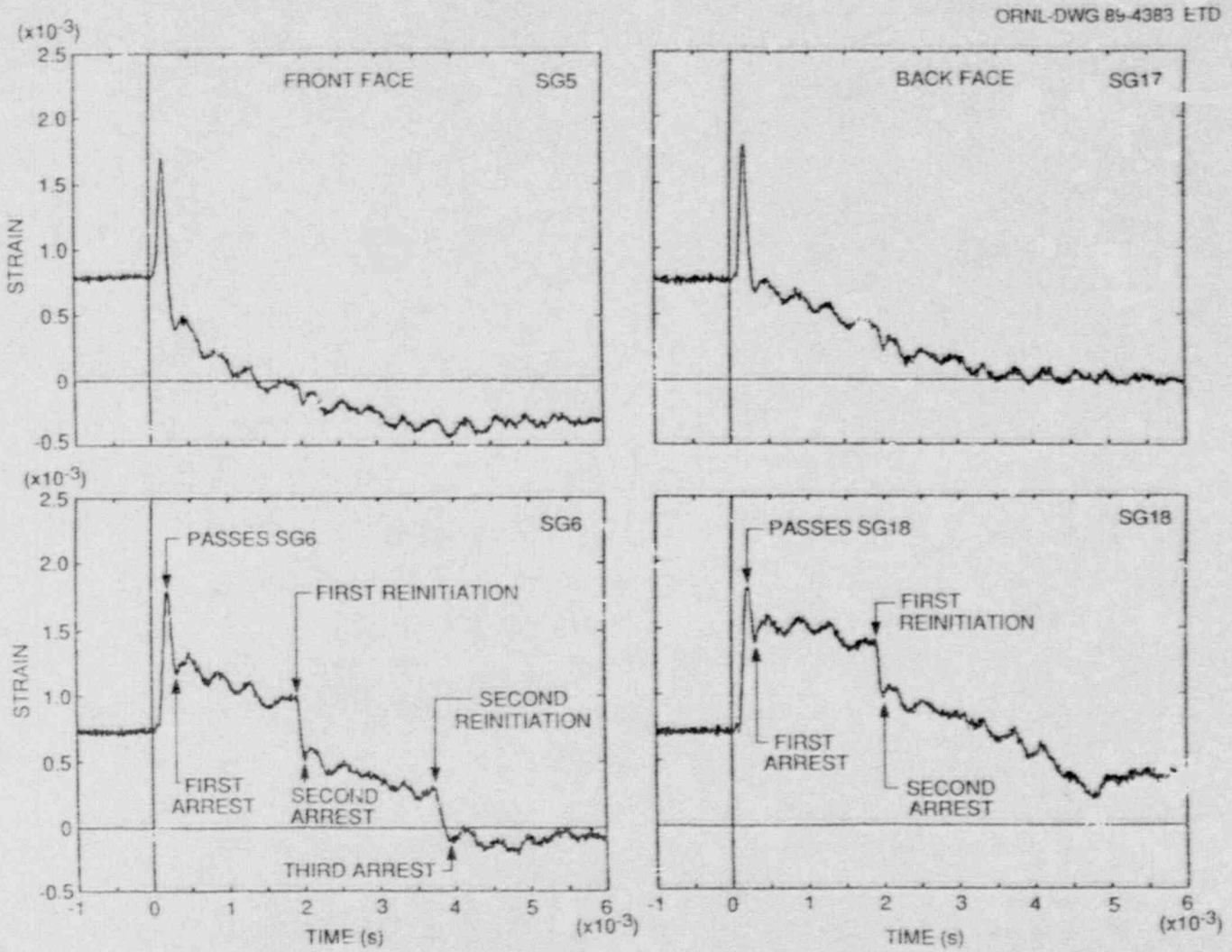

Fig. 5.29. Strain histories for companion crack-line gages showing cleavage crack passing gages 5 and 6 on plate front face and gages 17 and 18 on plate back face: test WP-CE-2.

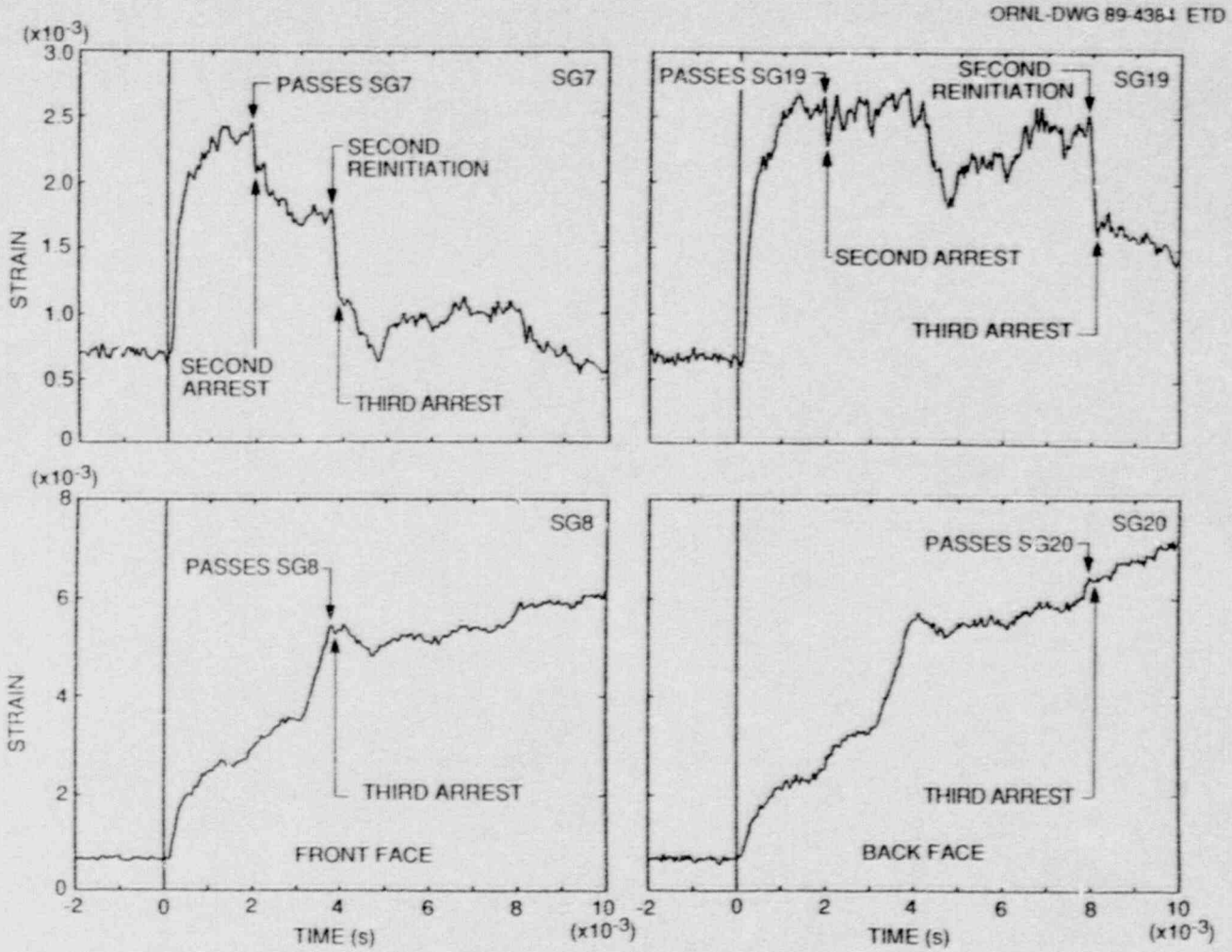

Fig. 5.30. Strain histories for companion crack-line gages showing second and third arrest events: test WP-CE-2 (strain gages 7–8 and 19–20).

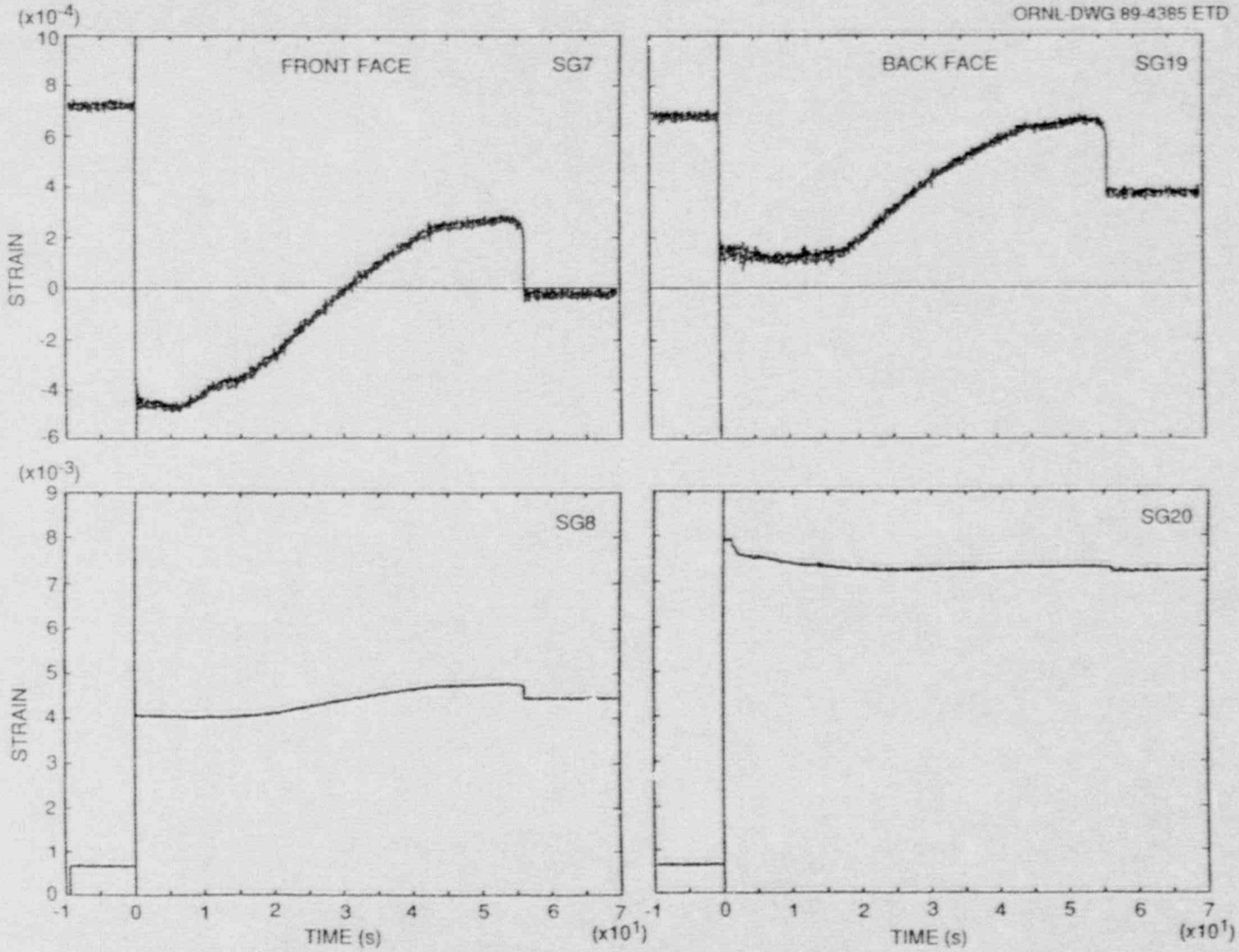

Fig. 5.31. Long-time (70-s) strain histories for companion crack-line gages during ductile tearing: test WP-CE-2 (strain gages 7-8 and 19-20).

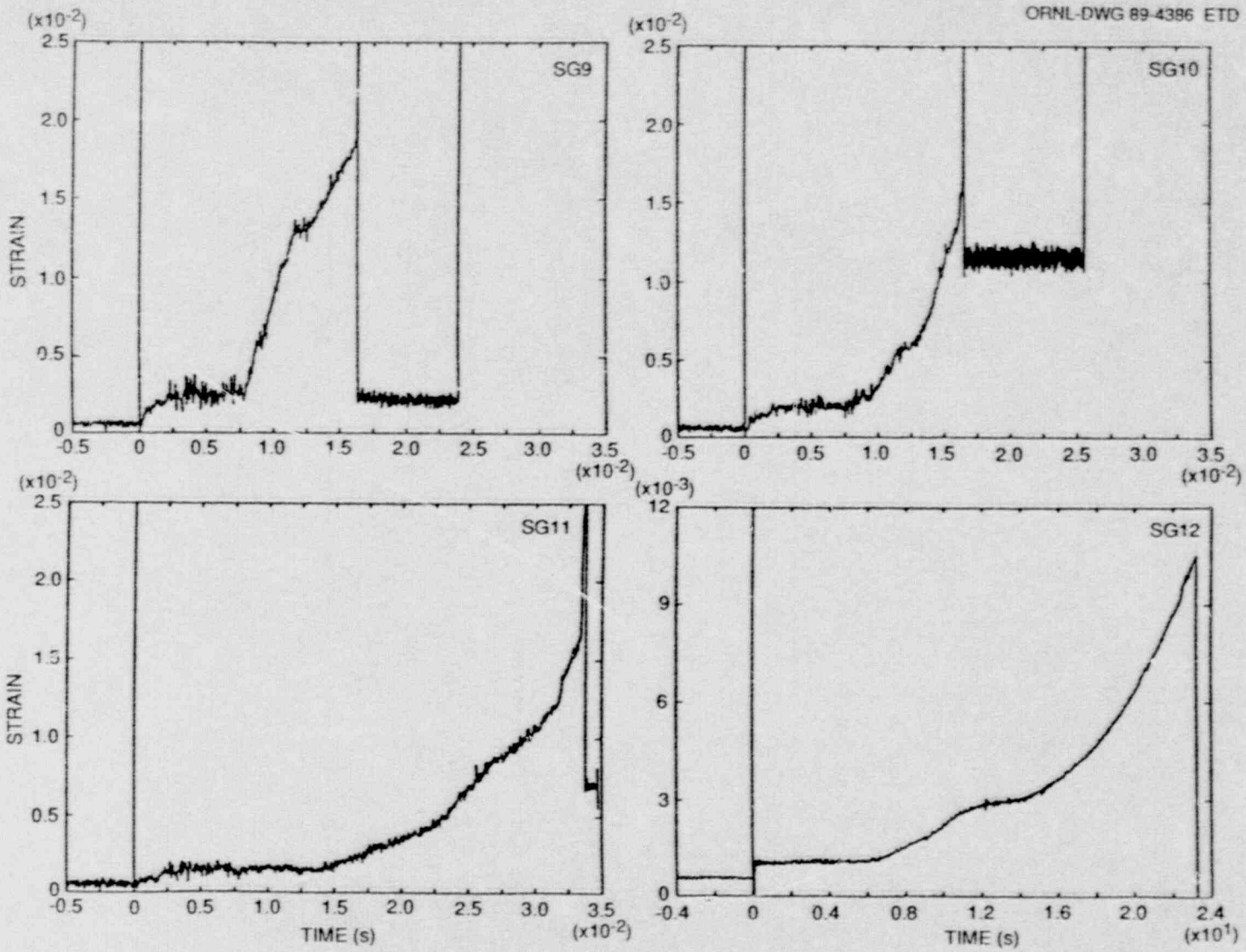

Fig. 5.32. Strain histories for front-face crack-line gages 9–12: test WP-CE-2.

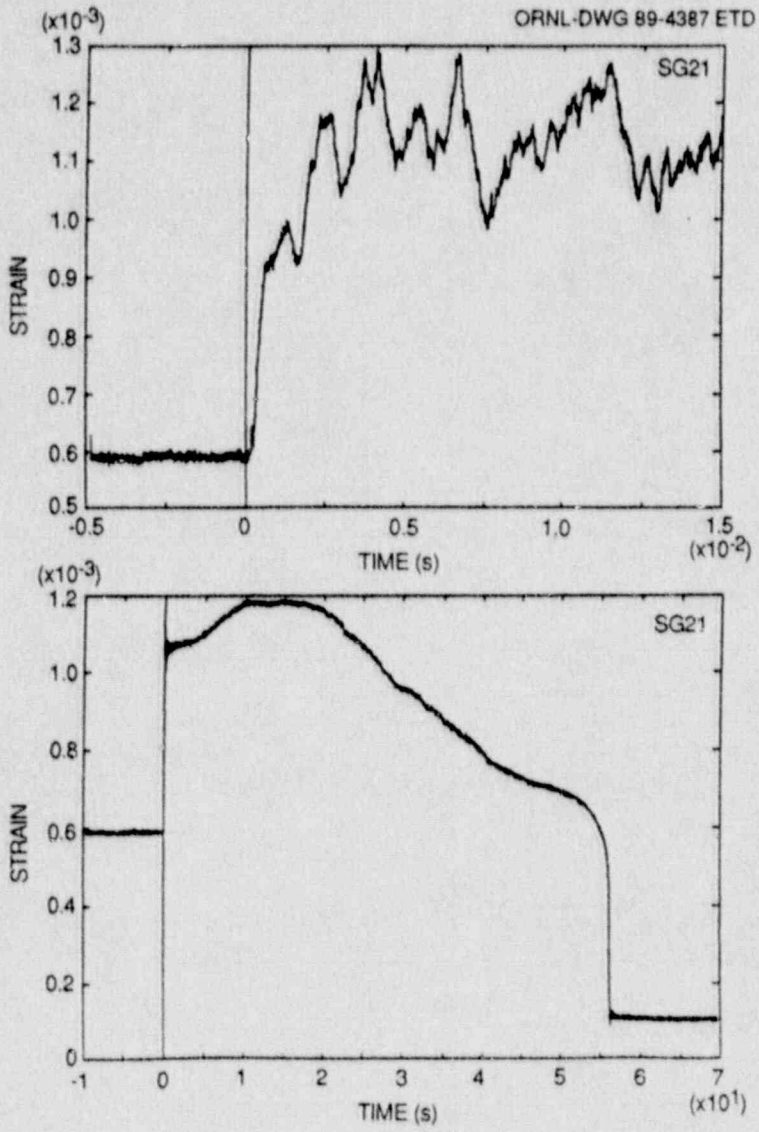

Fig. 5.33. Strain history at two time resolutions for intermediate-field gage 21 during cleavage crack run-arrest events and ductile tearing: test WP-CE-2.

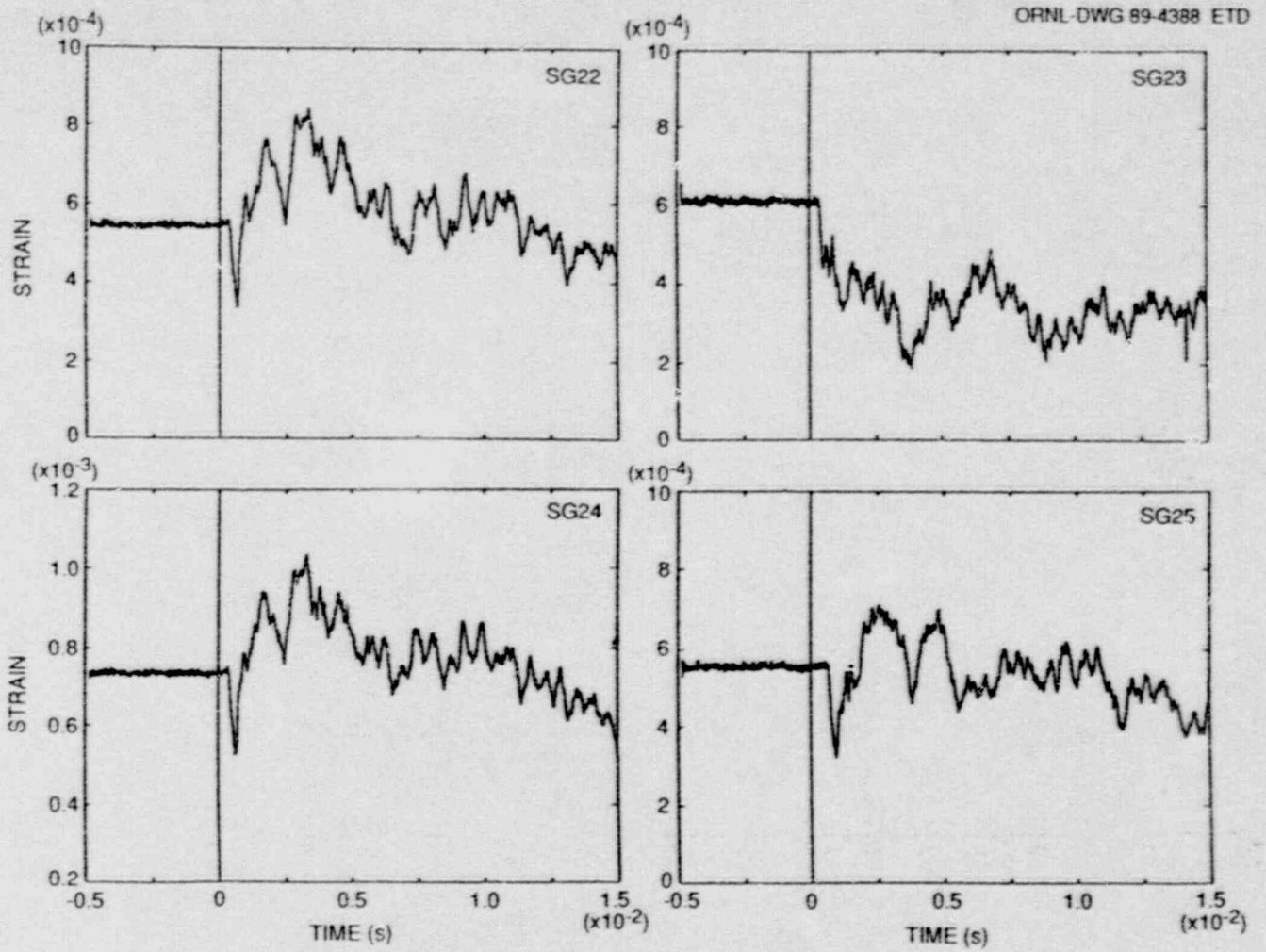

Fig. 5.34. Strain histories for far-field gages 22–25 during cleavage crack run-arrest events: test WP-CE-2.

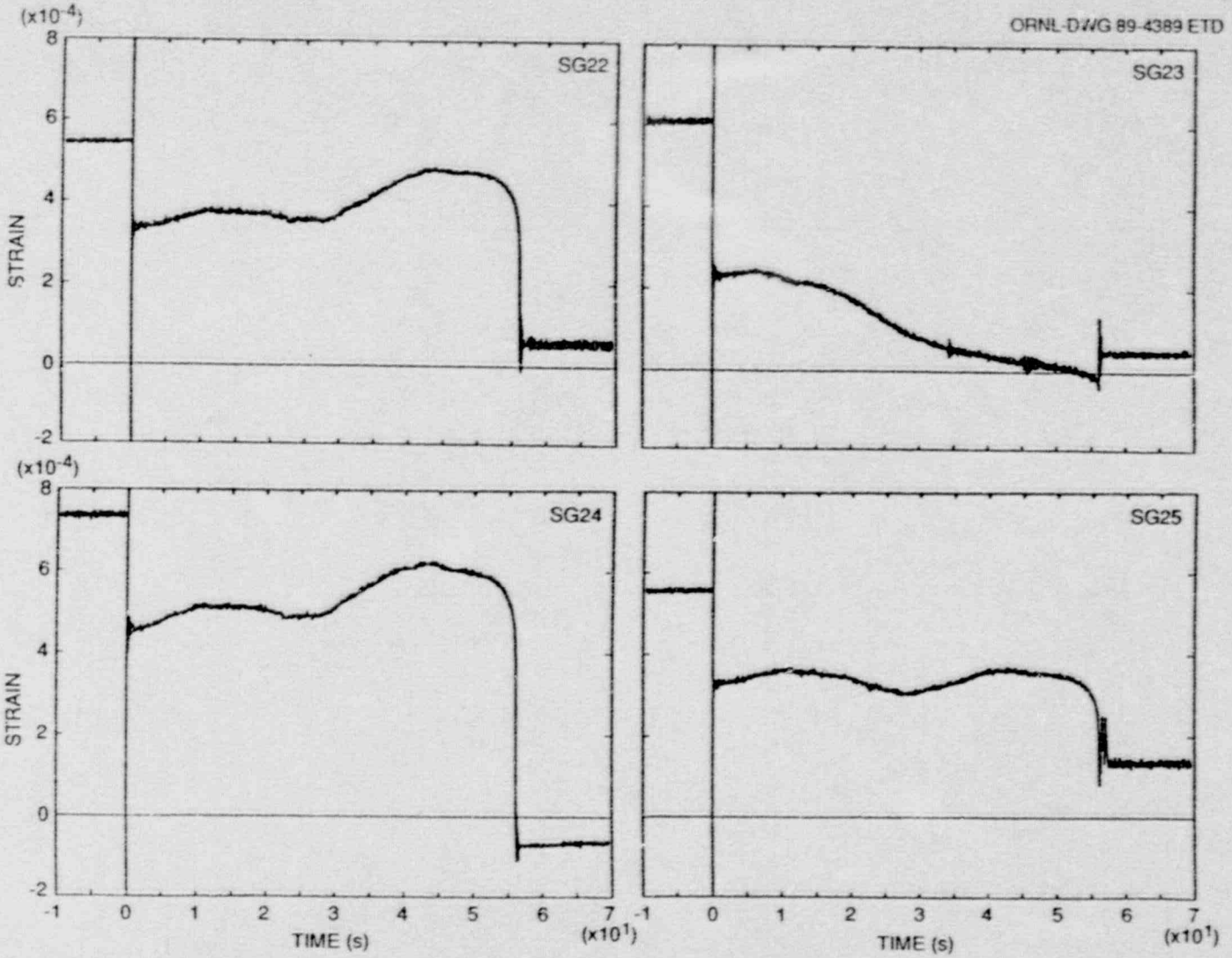

Fig. 5.35 Strain histories for far-field gages 22–25 during ductile tearing: test WP-CE-2.

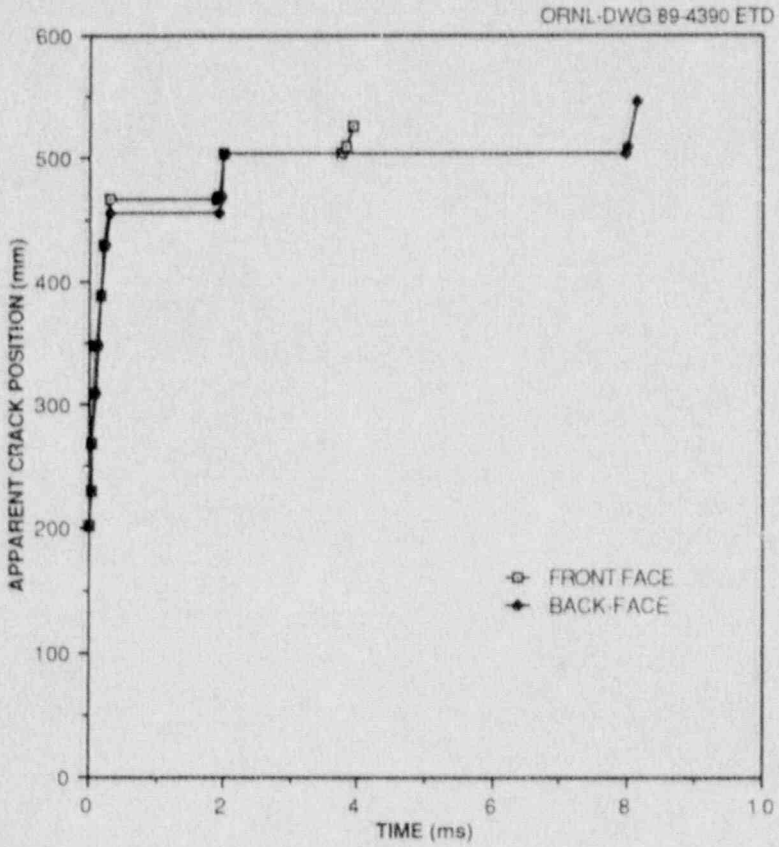

Fig. 5.36. Apparent crack-front position history: test WP-CE-2.

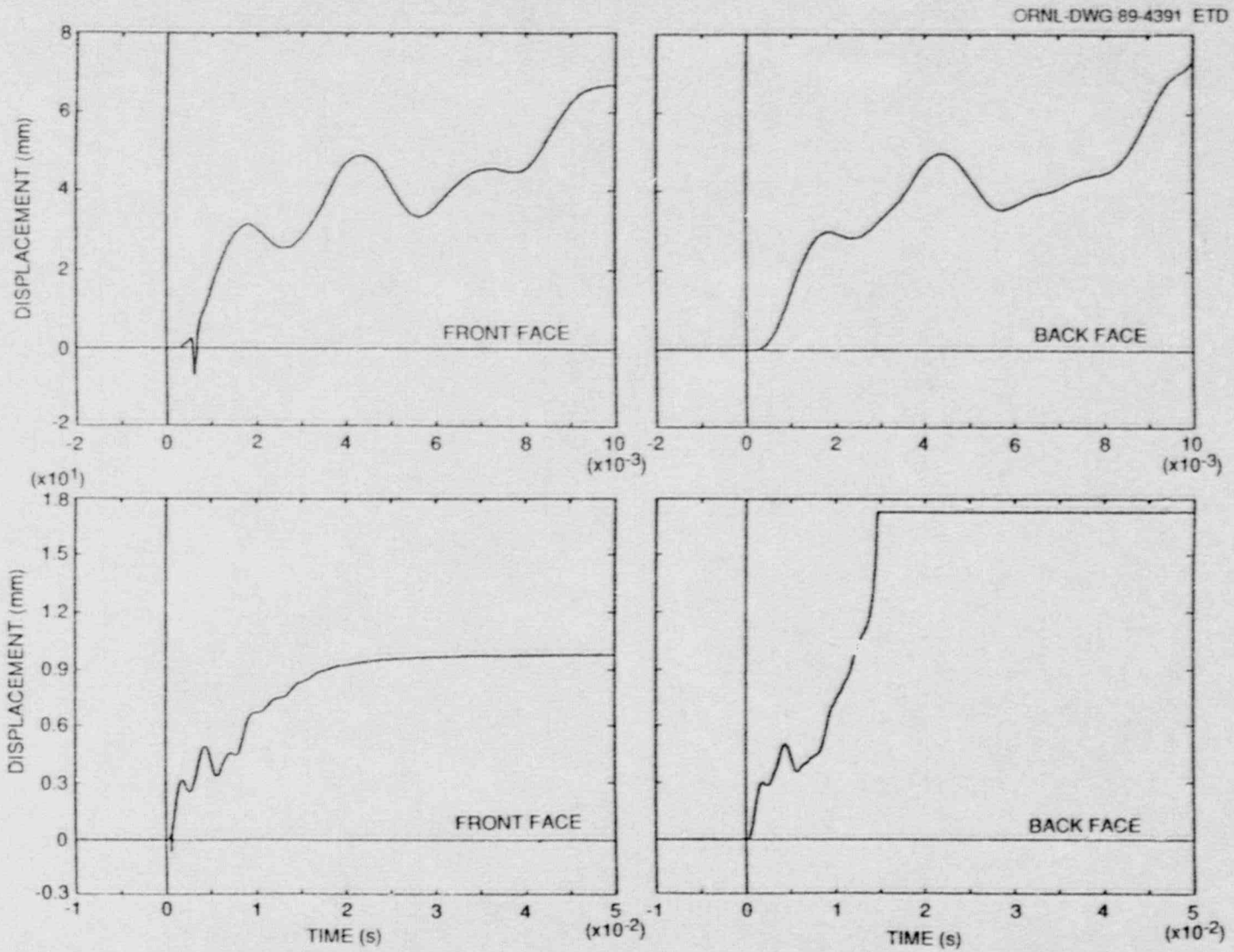

Fig. 5.37. F-COD and B-COD histories for both short (10-ms) and long (50-ms) time periods: test WP-CE-2.

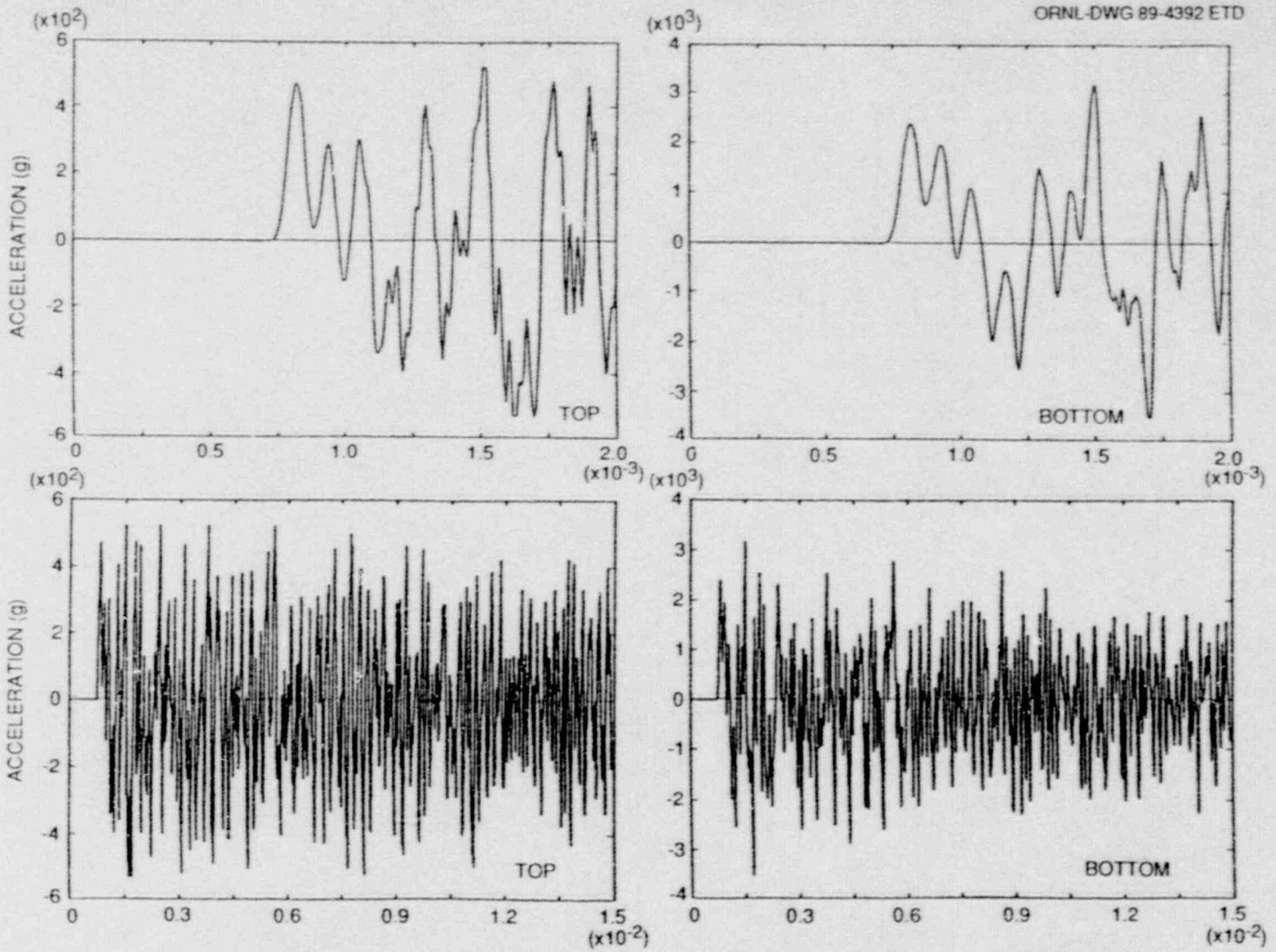

Fig. 5.38. Short (2-ms) and long (15-ms) duration longitudinal acceleration results measured by accelerometers mounted on specimen's centerline 3.697 m above (top) and 3.711 m below (bottom) crack plane: test WP-CE-2.

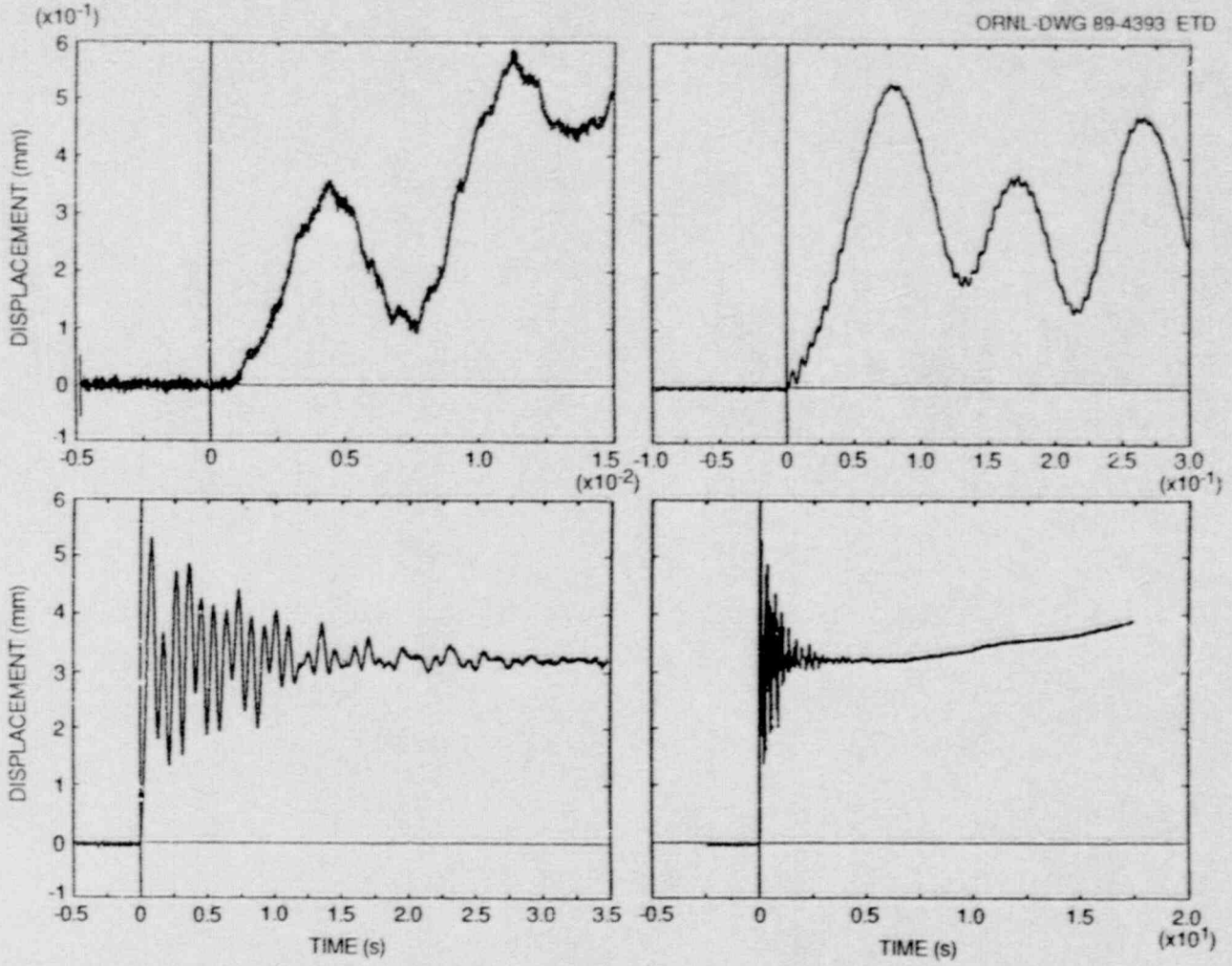

Fig. 5.39. Dynamic displacement results at several time resolutions of specimen relative to that of large columns of testing machine as measured 3.706 m below crack plane: test WP-CE-2.

REFERENCES

1. D. J. Ayres et al., Combustion Engineering, Inc., for Electric Power Research Institute, *Tests and Analysis of Crack Arrest in Reactor Vessel Materials*, Appendix C, "Material Characterization" EPRI NP-5121SP, April 1987.

2. D. J. Naus et al., "HSST Wide-Plate Test Results and Analysis," pp. 291-317 in *Proceedings of the United States Nuclear Regulatory Commission Sixteenth Water Reactor Safety Information Meeting held at National Institute of Standards and Technology, Gaithersburg, MD*, USNRC Conference Proceeding NUREG/CP-0097, Vol. 2, March 1989.*

3. D. J. Naus et al., Martin Marietta Energy Systems, Inc., Oak Ridge Natl. Lab., *Crack-Arrest Behavior in SEN Wide-Plates of Quenched and Tempered A 533 Grade B Class 1 Steel Tested under Nonisothermal Conditions*, USNRC Report NUREG/CR-4930 (ORNL-6388), August 1987.*

4. D. J. Naus, et al., Martin Marietta Energy Systems, Inc., Oak Ridge Natl. Lab., *High-Temperature Crack-Arrest Behavior in 152-mm-Thick SEN Wide-Plates of Quenched and Tempered A 533 Grade B Class 1 Steel*, USNRC Report NUREG/CR-5330 (ORNL/TM-11083), March 1989.*

---

*Available for purchase from National Technical Information Service, Springfield, Virginia 22161.

6. POSTTEST ANALYSES, CRACK-ARREST TOUGHNESS RESULTS, AND COMPARISON OF DATA WITH OTHER LARGE-SCALE TEST RESULTS

6.1 POSTTEST ANALYSES

Posttest analyses were conducted for wide-plate crack-arrest tests WP-CE-1 and -2 to investigate the interaction of parameters (plate geometry, material properties, temperature profile, and mechanical loading) that affect the crack run-arrest events. Three-dimensional (3-D), static, finite-element analyses were performed to determine the static stress-intensity factor at the time of crack initiation. These analyses were conducted using the ORMGEN/ORVIRT fracture analysis system[1,2] in conjunction with the ADINA-84 finite-element code.[3] Quasistatic analyses use the ORNL computer code WPSTAT[4] to evaluate static stress-intensity factors as a function of crack length and temperature differential across the plate. WPSTAT also categorizes arrested crack lengths in terms of three types of instability limits: reinitiation, tearing instability, and tensile instability. Two-dimensional (2-D) elastodynamic analyses were carried out using the ADINA/VPF dynamic crack analysis code.[5] This code is capable of performing both application-mode and generation-mode analyses. In the application-mode analysis, the crack tip is propagated incrementally when K_I, the dynamically computed stress-intensity factor, equals the specified dynamic fracture-toughness value K_{ID}, which depends on the crack velocity $\dot{a}$ and the temperature T [Eq. (3.3)]. In the generation-mode analysis, the crack tip is propagated incrementally according to a prescribed crack-position-vs-time relationship, and values of fracture toughness are determined from the dynamically computed K_I. For both modes of analysis, the dynamic stress-intensity factor is determined in each time step from the dynamic J-integral containing the appropriate inertial and thermal terms.

6.1.1 Posttest Analyses of Test WP-CE-1

6.1.1.1 Posttest 3-D static analyses

The 3-D finite-element model incorporated a segment of the plate assembly that was 4.6930 m long from the crack plane to the top of the load-pin hole. The crack-tip region of the model included the chevron cutout, the side grooving, and the edge notch, the dimensions of which are shown in Table 4.1. Based on symmetry conditions that neglected out-of-plane eccentricity, one-quarter of the partial pull-plate assembly was modeled using 3751 nodes and 720 20-noded isoparametric elements.

The thermal deformations computed from a posttest 2-D analysis were superimposed on a 3-D finite-element model to account for the in-plane thermal bending effect in the 3-D analyses. The 2-D thermoelastic analysis used a temperature distribution from a heat conduction analysis based on assumptions that the heated and cooled edges of the plate were fixed at T_{max} = 205.5°C and T_{min} = -93.5°C, respectively, along a 2.4-m

length (centered relative to the crack plane) and that the pull-tab edges were maintained at T = 20.0°C. The edge temperatures were selected to yield a temperature distribution in the crack plane that agreed (approximately) with the measured values presented in Fig. 5.3(*b*). The remaining surfaces of the assembly were assumed to be insulated. The in-plane thermal bending produced a load-line eccentricity (through the top of the load-pin hole) of 2.26 cm relative to the geometric center of the plate.

In the 3-D analysis, thermal stress effects were neglected, and a uniform line load statically equivalent to the WP-CE-1 test initiation load of 10.14 MN was applied at the location corresponding to the top of the load-pin hole. This analysis resulted in a static stress-intensity factor of K_I = 166.2 MPa·$\sqrt{m}$ at the center plane of the plate at the time of the first crack initiation. A ratio of K_I/K_{Ic} = 1.59 results from comparing this computed K_I value with the static initiation value of K_{Ic} = 104.5 MPa·$\sqrt{m}$ evaluated from Eq. (3.1) by using a crack-tip temperature of −33.7°C.

6.1.1.2 Posttest 2-D static analyses

Posttest quasistatic 2-D analyses for both crack arrest and crack stability were done using the ORNL computer code WPSTAT.[4] As described in Ref. 4, the WPSTAT code evaluates static stress-intensity factors as a function of crack length a and temperature differential $\Delta T = T_{max} - T_{min}$ across the plate. These factors are computed for fixed force conditions K_I^F (a, ΔT) and for fixed load-pin displacement conditions K_I^{DSP} (a, ΔT) by superimposing contributions from tension and bending finite-element and handbook solutions. Also, WPSTAT categorizes arrested crack lengths in terms of the three types of instability limits described below.

For test WP-CE-1, the proposed temperature profile was defined by specifying a crack-tip temperature of T_{CT} = −30°C at x = 0.20 m and a midplate temperature of T_{MP} = 50°C at x = 0.5 m, implying that T_{min} = −83.8°C and T_{max} = 183.3°C. As indicated in Fig. 5.3(*b*), the temperature gradient actually achieved at the time of the run-arrest event deviated somewhat from the proposed profile in the region of $0.2 \leq x < 0.6$. Consequently, the posttest WPSTAT calculations of the static factors K_I^F (a, ΔT) and K_I^{DSP} (a, ΔT) used the actual temperature profile provided in Fig. 5.3(*b*) (i.e., T_{CT} = −33.7°C and T_{mid} = 56°C). For this specified temperature profile, the dependence of the arrested crack length and crack stability on the applied initiation load F_{in} was investigated with WPSTAT, and the results are presented in Fig. 6.1. Figure 6.1 includes the statically calculated final crack length a_{fc}, as well as the instability-limit crack lengths for (1) reinitiation a_{rein} (F_{in}), (2) tensile instability a_{I_1} (F_{in}), and (3) tearing instability a_{I_2} (F_{in}). Because fixed-displacement conditions at the load point are assumed to prevail during the nonarrest event, the calculated parameters in Fig. 6.1 are based on the static factor K_I^{DSP}. The tensile

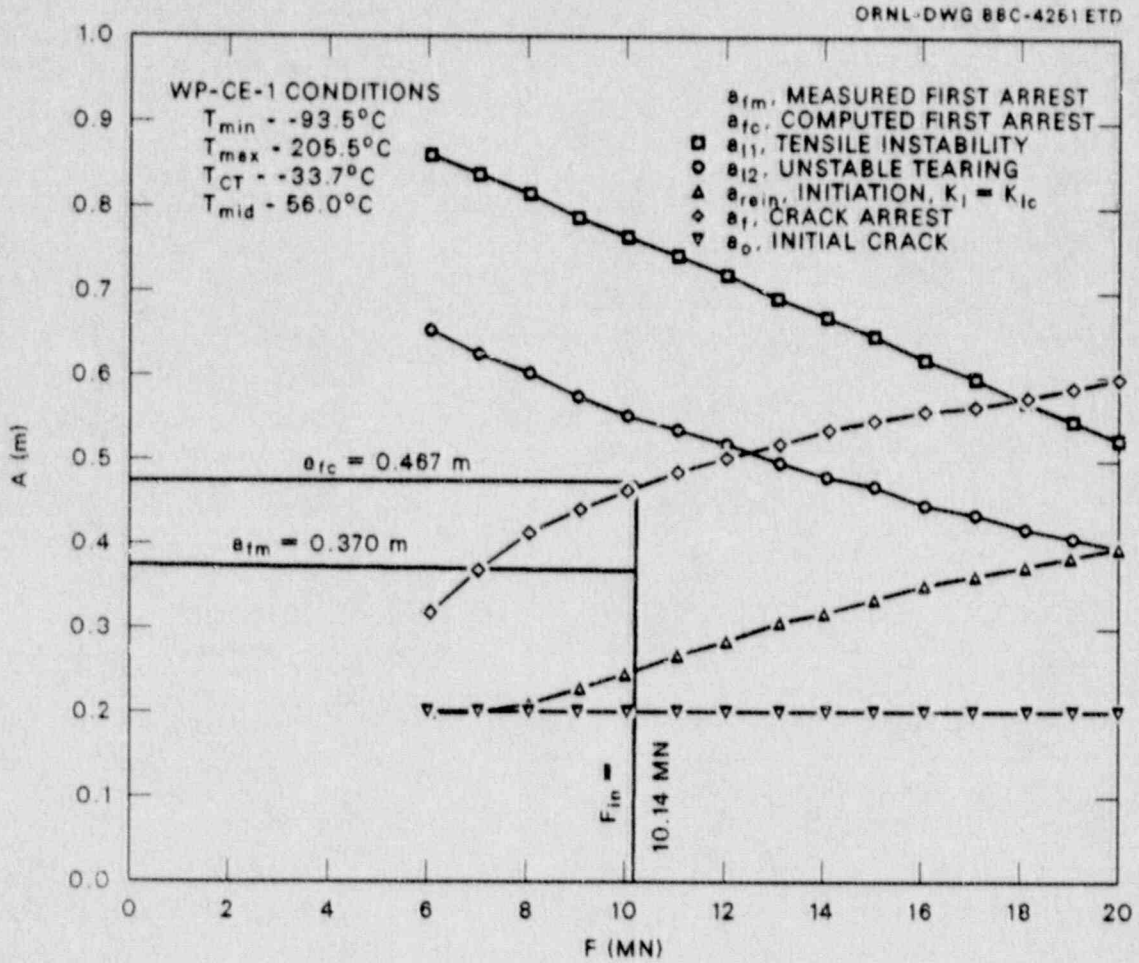

Fig. 6.1. Statically calculated crack lengths: test WP-CE-1.

instability calculation is based on the average stress in the remaining ligament equal to an ultimate stress of σ_u = 550 MPa, which represents the lowest value for the temperature range of interest. For the tearing instability calculation, the material tearing resistance is assumed to be represented by a power-law J-resistance curve $J_R = C(\Delta a)^m$, where C = 0.3539, m = 0.4708, and the units of J_R and Δa are megajoules per square meter and millimeter, respectively. In Fig. 6.1, the statically computed arrest length corresponding to the measured initiation load F_{in} = 10.14 MN is given by a_{fc} = 0.467 m. This computed arrest point is below the tensile instability curve a_{I_1} and the tearing instability curve a_{I_2}, implying a stable condition. The measured initial arrest point a_{fm_1} = 0.370 m is also below the tensile and tearing instability curves. Figure 6.1 indicates that tearing instability is expected when the crack length exceeds ≈0.54 m, which occurs after the first measured arrest position at a_{fm_1} = 0.370 m (see Table 5.2).

In Fig. 6.2, the K_{Ia} function presented in Eq. (3.2) is evaluated on the arrest crack-length curve $a_f(F)$, on the incipient tearing-instability curve $a_{I_2}(F)$, and on the cleavage-reinitiation curve $a_{rein}(F)$. The K_{Ic} function presented in Eq. (3.1) is evaluated on the curve $a_{rein}(F)$. Evaluation of the $K_{Ia}(a_f)$ curve at the initiation load F_{in} = 10.14 MN yields an arrest toughness of K_{Ia} = 229.1 MPa·$\sqrt{m}$ at the computed arrest point of a_{fc} = 0.467 m, where the crack-tip temperature would be T = 47.7°C.

The complete static fracture mechanics and stability analyses are depicted in Fig. 6.3 for initiation load F_{in} = 10.14 MN, for initial crack depth a_o = 0.2 m, and for the temperature gradient presented in Fig. 5.3(*b*). Included in the figure are curves for initiation toughness K_{Ic}, arrest toughness K_{Ia}, displacement-controlled stress-intensity factor K_I^{DSP}, and force-controlled stress-intensity factor K_I^F. The regions

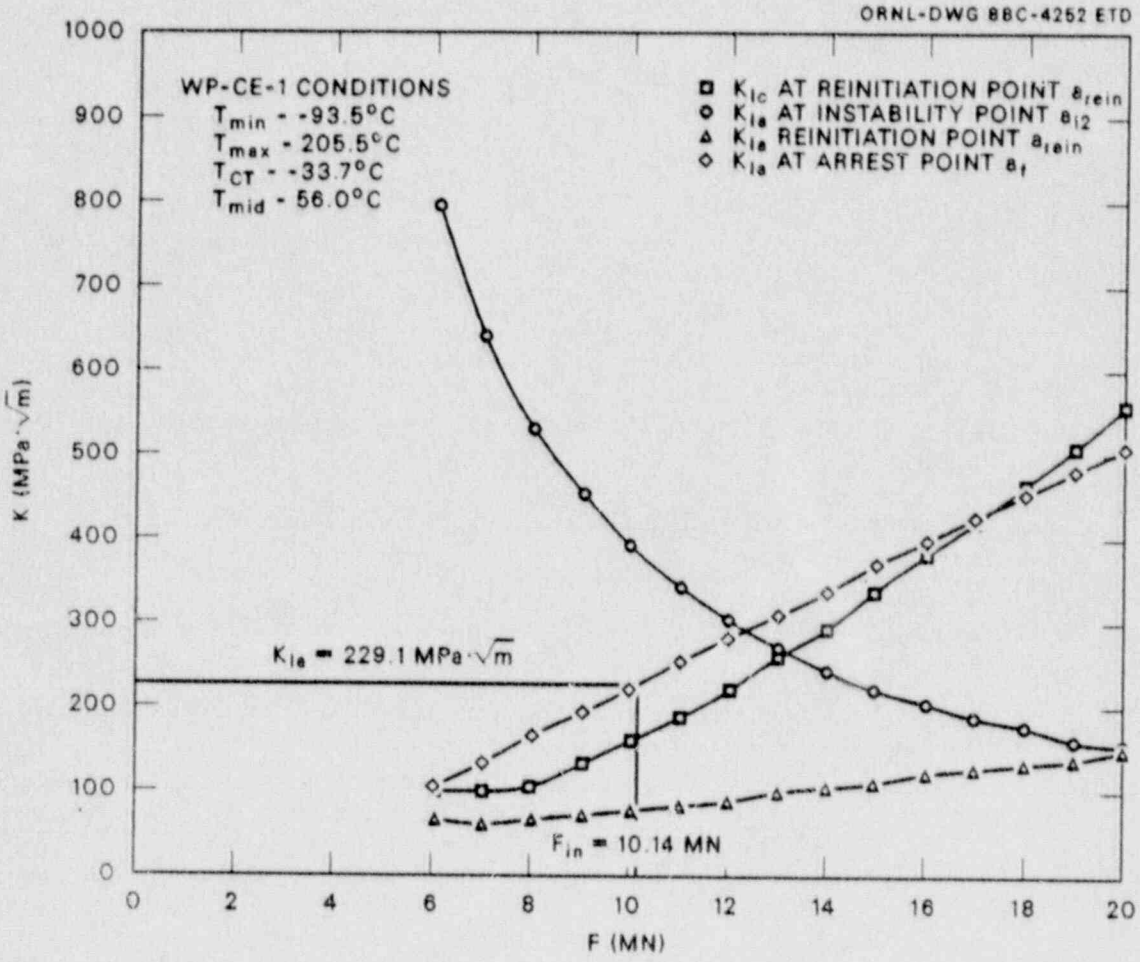

Fig. 6.2. Determination of arrest toughness at initiation load of 10.14 MN: test WP-CE-1.

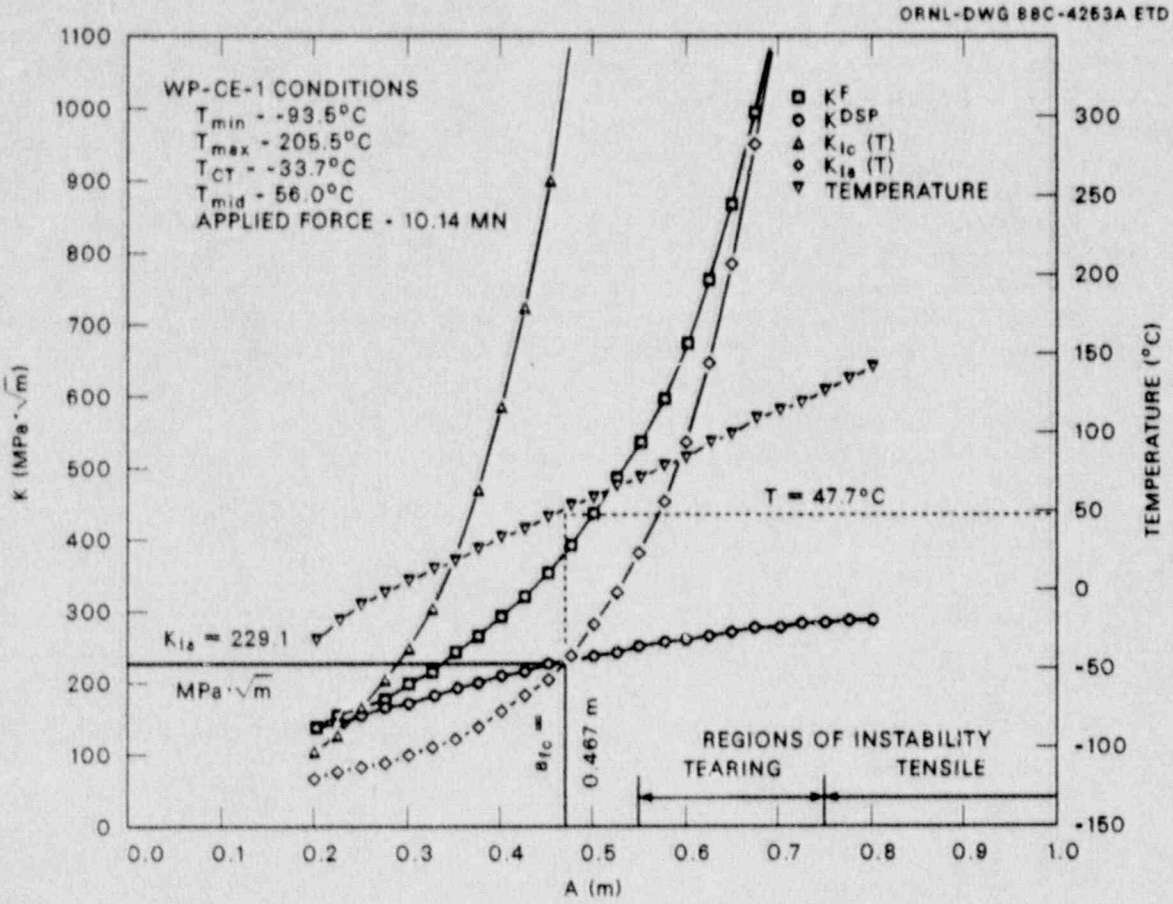

Fig. 6.3. Complete static and stability analyses for initiation load of 10.14 MN: test WP-CE-1.

of tearing and tensile instability and the computed cleavage arrest point a_{fc} are also identified in Fig. 6.3.

6.1.1.3 Application-mode dynamic analysis (fixed-load boundary condition)

Elastodynamic analyses of wide-plate test WP-CE-1 were carried out with the ADINA/VPF dynamic crack-analysis code.[5] The 2-D, plane-stress, finite-element model of the wide-plate configuration used in the analyses consists of 863 nodes and 264 eight-noded isoparametric elements. Side grooves were taken into account by adjusting the resulting stress-intensity factor calculated in each time step of the analysis. The in-plane bending of the plate assembly caused by the thermal gradient across the plate was also incorporated into the analyses.

A posttest application-mode analysis of WP-CE-1 was performed using the material properties given in Chap. 3. Although the steady-state temperature distribution imposed on the plate assembly does not include thermal stresses, the global deformation of the assembly caused by thermal strains must be incorporated into the analyses. For finite-element applications, static thermoelastic analyses were performed with

the ADINA/ADINAT finite-element codes[3] to determine the thermal deformation of the plate assembly. These thermal displacements were added to the nodal point data that defined the finite-element model. The temperature distribution for the analyses was interpolated from the data measured along the crack plane [Fig. 5.3(*b*)] and was used only for determination of dynamic fracture toughness. For the dynamic analysis, the load was fixed at the value of the measured fracture load, 10.14 MN, as a prescribed concentrated load. The time step was set at $\Delta t = 5$ μs.

The calculated crack-depth history from this analysis is presented in Fig. 6.4. Figure 6.5 shows the dynamic stress-intensity factor K_I^{DYN}, the static toughness K_{Ia}, and the crack velocity $\dot{a}$ as a function of instantaneous crack depth. In Fig. 6.5, the crack velocity decreases smoothly and crack propagation continues at small velocities for values of a/w greater than ~0.45. Because it is unlikely that a real crack would propagate at these low velocities for an extended period of time, arrest has been arbitrarily defined to occur when the crack velocity drops below a threshold velocity of 2% of the shear wave velocity (C_S) (i.e., 0.02 C_S = 64 m/s). Based on this assumption, an arrest is predicted at a_{fp} = 0.47 m, where the crack-tip temperature would be T = 48.4°C and the arrest toughness would be K_{Ia} = 236 MPa·$\sqrt{m}$. The predicted arrest point exceeds the measured arrest point, a_{fm} = 0.370 m,

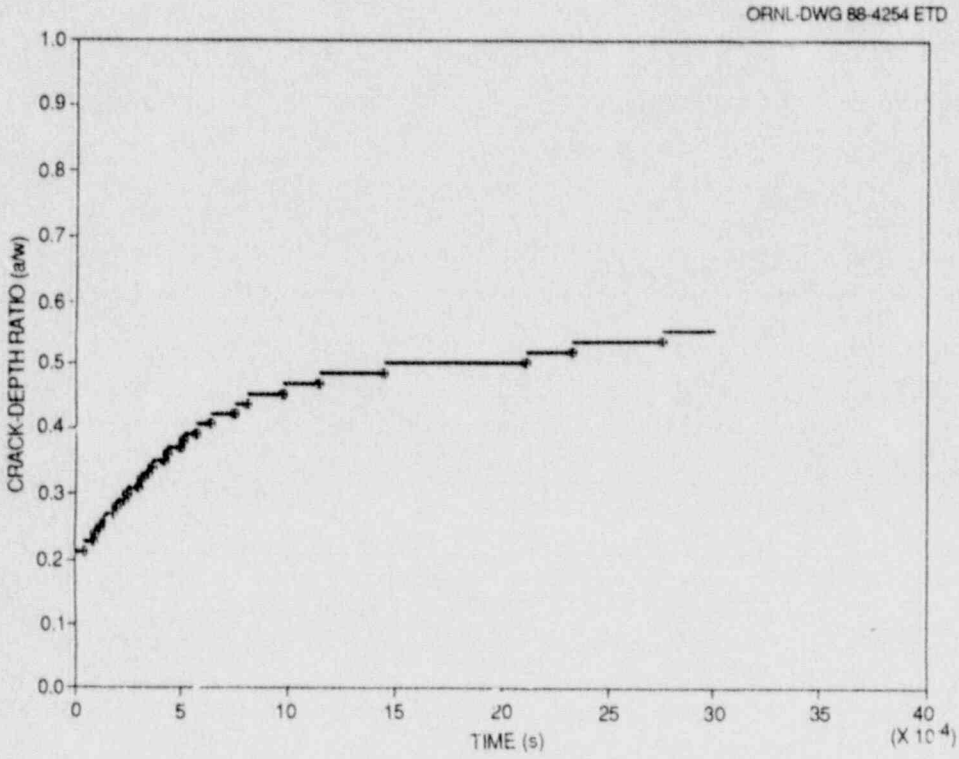

Fig. 6.4. Dynamic-analysis, crack-depth history: test WF-CE-1.

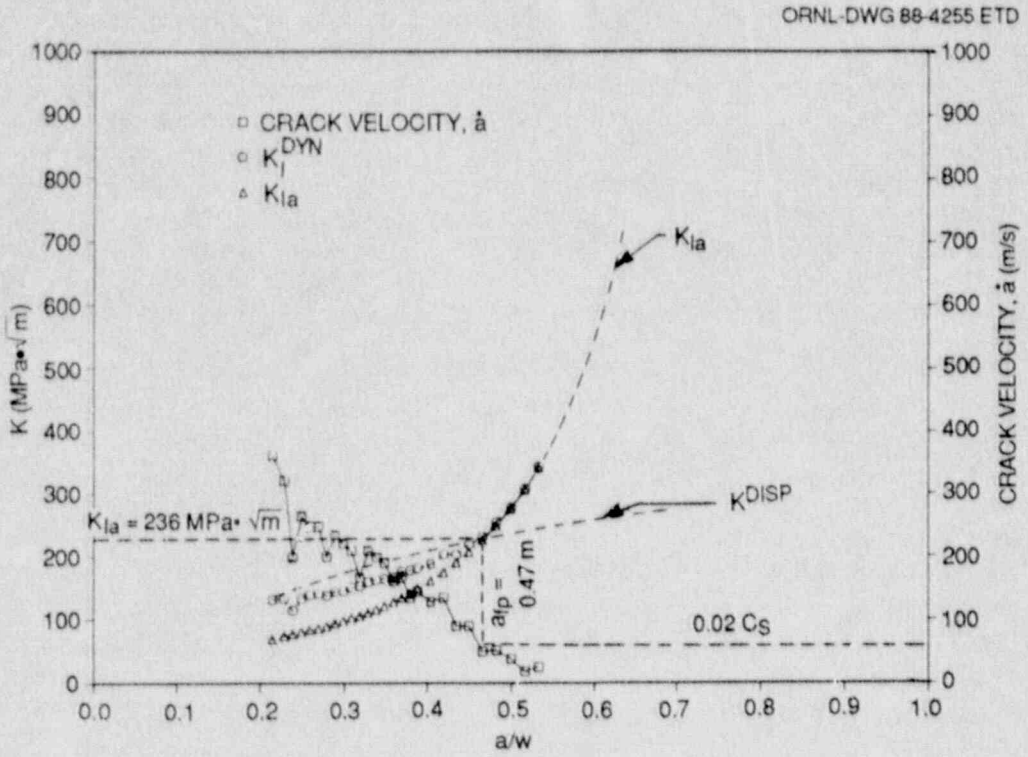

Fig. 6.5. Dynamic factor, static toughness, quasistatic displacement-controlled factor, and crack velocity vs instantaneous crack length: test WP-CE-1.

where T = 23.3°C and K_{Ia} = 135.9 MPa·$\sqrt{m}$. The analyses were terminated at time t = 3 ms.

6.1.1.4 Generation-mode dynamic analysis (fixed load boundary condition)

From the output of the crack-line gages and from an inspection of the fracture surface, estimates of the crack position as a function of time were constructed and listed in Table 5.2 for the plate front and back faces. Figure 6.6 depicts the apparent crack position vs time that was derived from Table 5.2 and used as input for the posttest generation-mode elastodynamic analysis of test WP-CE-1. For these analyses, the load point was fixed at the value of the initiation load, 10.14 MN, as a prescribed concentrated load, and the time step was set at Δt = 5 ms. From these calculations, the stress-intensity factor as a function of time is given in Fig. 6.7. The generation-mode analysis results are presented in Table 6.1.

The computed strain histories from selected points close to crack-line strain gages 1–4, 5 and 13–15, and 16–18 (see Fig. 4.7 for strain-gage locations) are depicted in Figs. 6.8–6.10, respectively, for the generation-mode analysis (fixed load) along with measured data from the

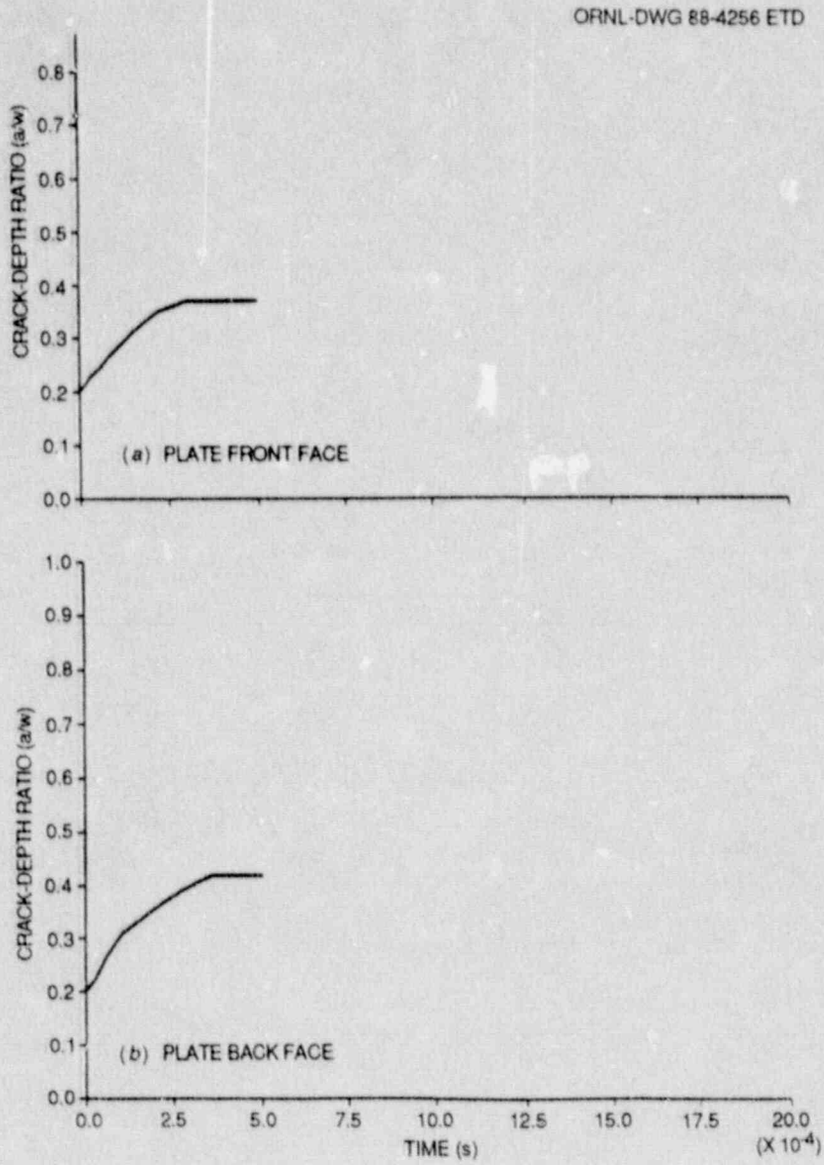

Fig. 6.6. Crack-front position history used as input for generation-mode dynamic analysis: test WP-CE-1.

gages. The sharply defined strain peaks are associated with the fast-running crack passing under a gage point, with the peak being transformed into a more blunted curve as the crack-tip propagation slows down. The comparison of strain histories in these figures indicates generally good agreement between measured and computed times for the occurrence of peak strain values. The transition of strain pulse from a sharp peak for gage 4 (Fig. 6.8) to a blunted curve for gage 5 (Fig. 6.9) reflects occurrence of the arrest event on the plate front face between these gages. The arrest event on the plate back face can

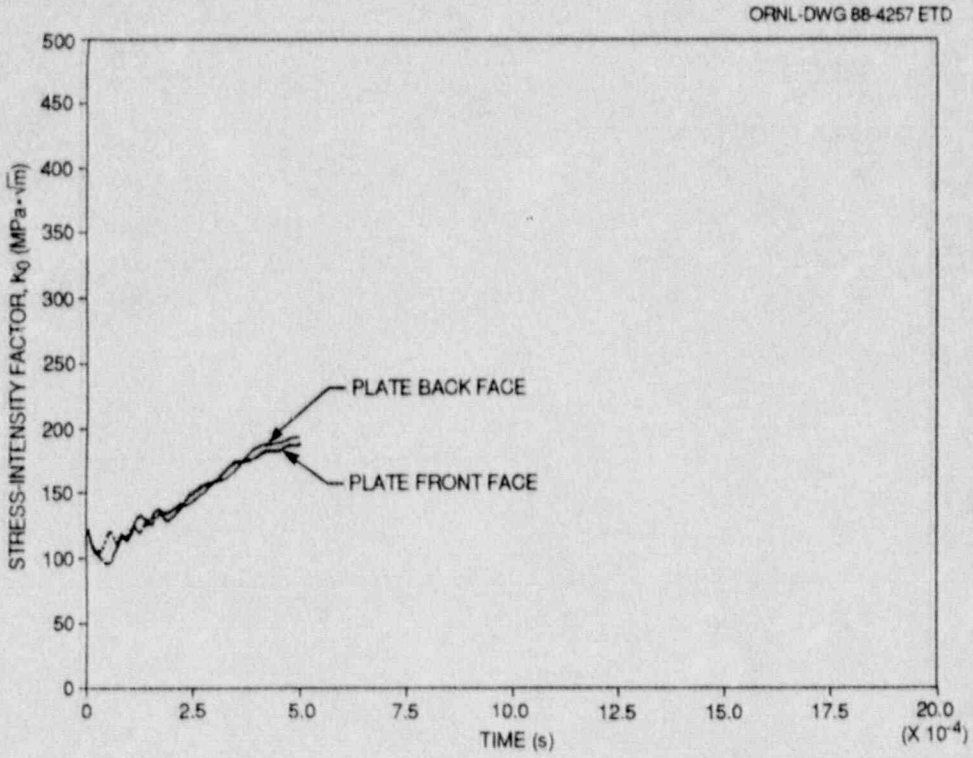

Fig. 6.7. Calculated stress-intensity factor vs time from the generation-mode dynamic analysis (fixed-load case): test WP-CE-1.

Table 6.1 Summary of computed results for test WP-CE-1

Event	Time (ms)	a (m)	K^a (MPa·√m)
Initiation	0.0	0.200	130[b]
Arrest			
Front face	0.308	0.370	159
Back face	0.364	0.420	170

[a]Generation-mode, fixed-load dynamic analysis.

[b]From ADINA static analysis.

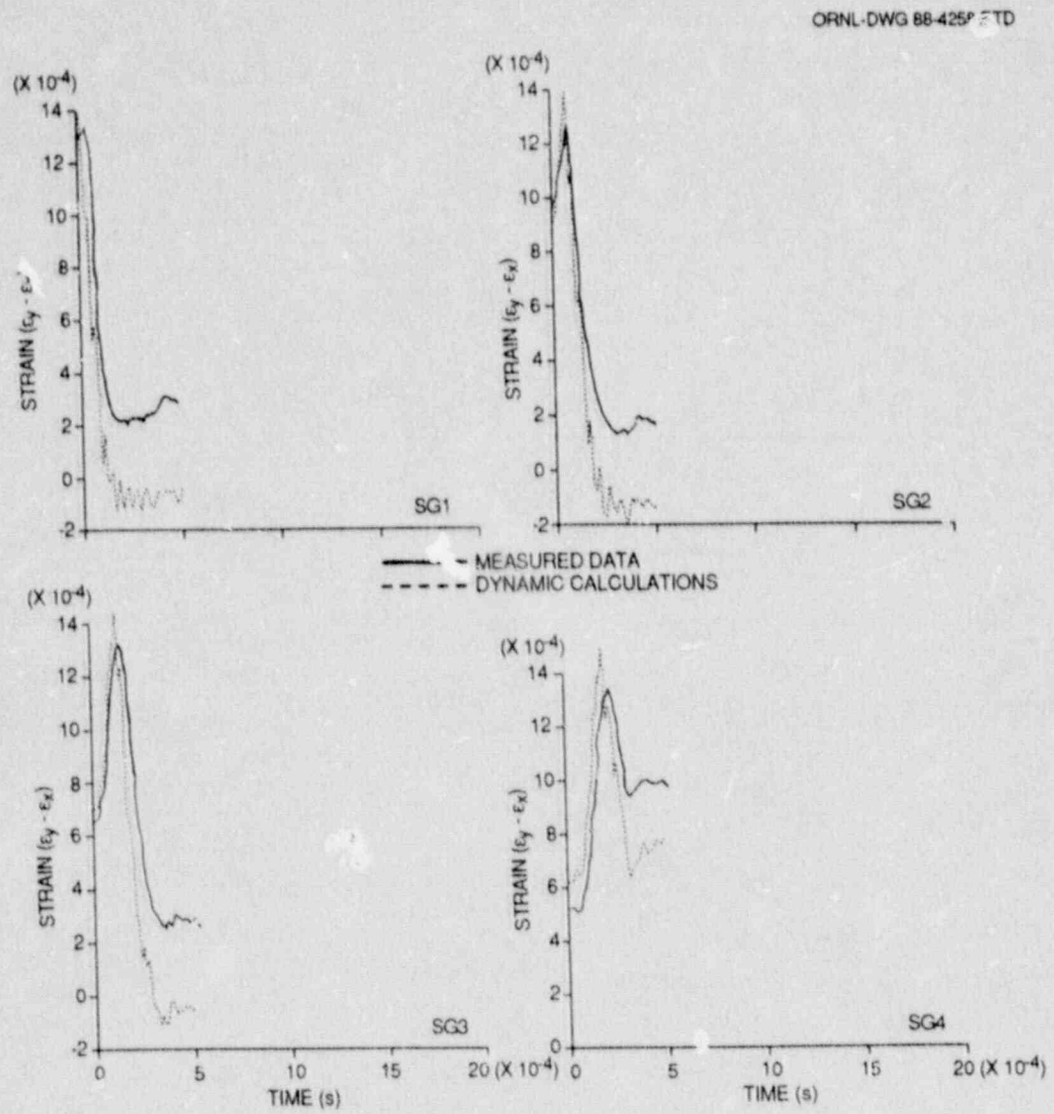

Fig. 6.8. Actual and computed strain histories for front-face crack-line gages: test WP-CE-1 (strain gages 1–4).

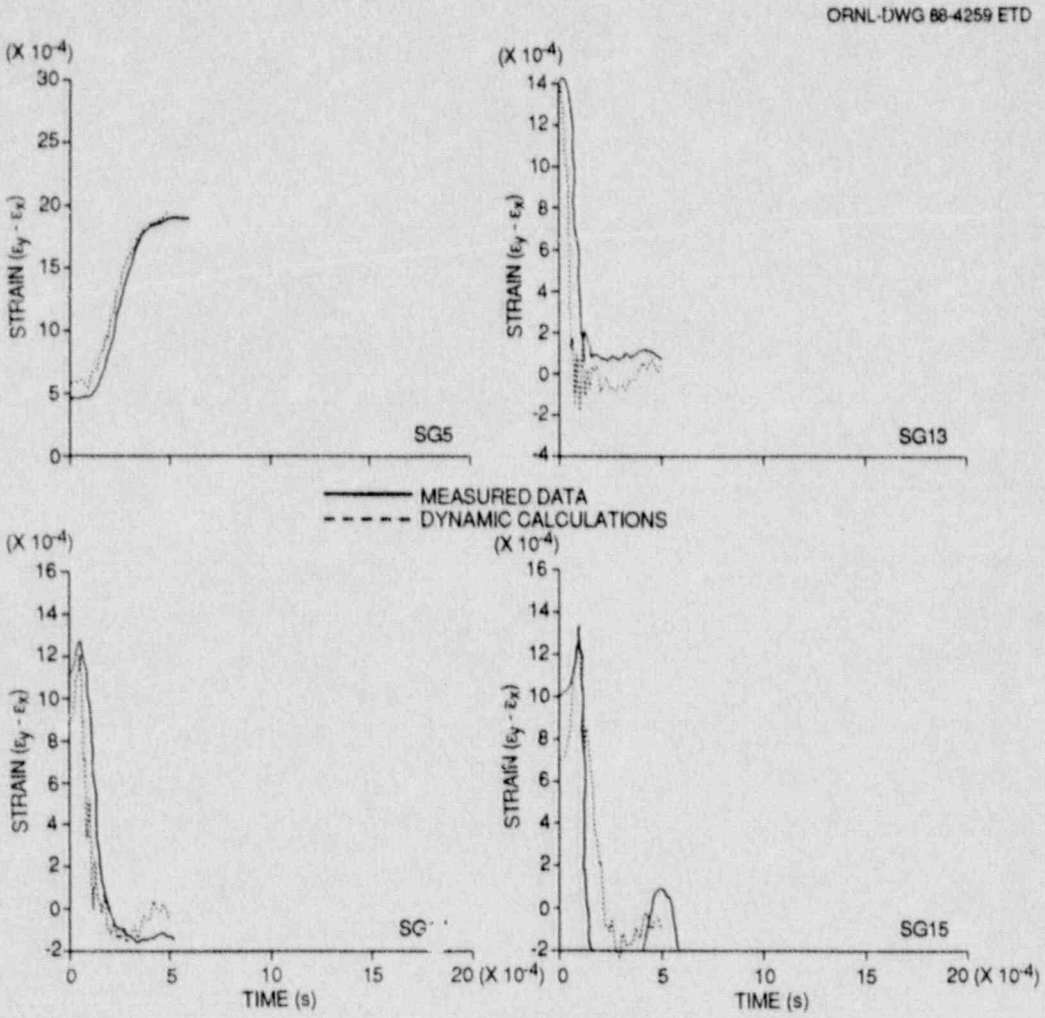

Fig. 6.9. Actual and computed strain histories for crack-line gages: test WP-CE-1 (strain gages 5 and 13-15).

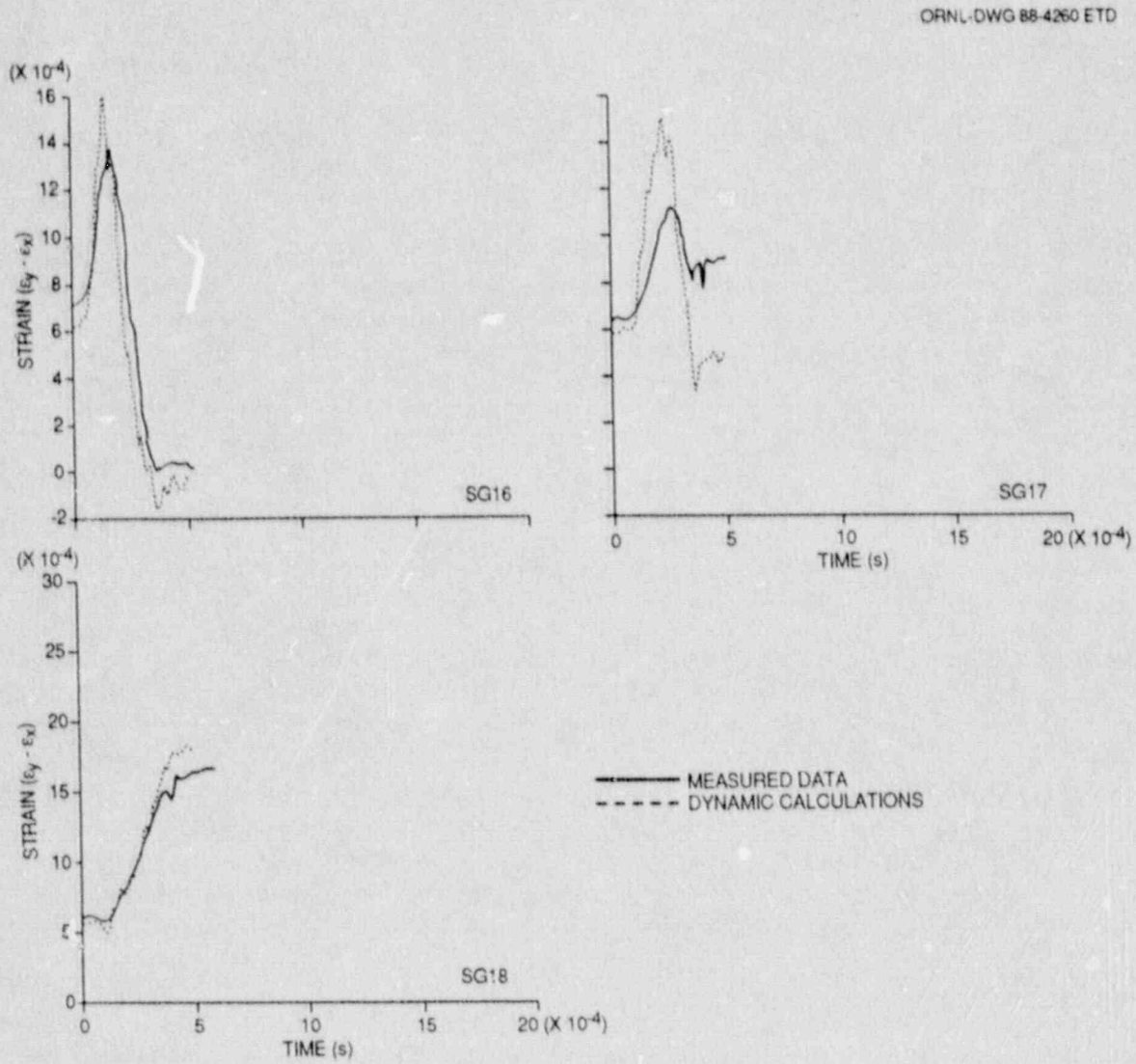

Fig. 6.10. Actual and computed strain histories for back-face crack-line gages: test WP-CE-2 (strain gages 16-18).

be viewed in the same manner by noting transition in the strain pulse between gages 17 and 18 (Fig. 6.10).

6.1.2 Posttest Analyses of Test WP-CE-2

6.1.2.1 Posttest 3-D static analyses

The 3-D finite-element model for test WP-CE-2 incorporated a segment of the plate assembly that was 4.689 m long from the crack plane to the top of the load-pin hole. The crack-tip region of the model included the side grooving and the edge notch, the dimensions of which are shown in Table 4.1. Based on symmetry conditions that neglected out-of-plane eccentricity, one-quarter of the partial pull-plate assembly was modeled using 3751 nodes and 720 20-noded isoparametric elements.

Thermal deformations superimposed on the 3-D finite-element model to account for the in-plane bending effect were computed from a 2-D analysis, which assumed that the heated and cooled edges of the plate were fixed at T_{max} = 205.9°C and T_{min} = −101.9°C, respectively. The in-plane thermal bending produced a load-line (through the top of the load-pin hole) eccentricity of 2.33 cm relative to the geometric center of the plate.

In the 3-D analysis, thermal stress effects were neglected, and a uniform line load statically equivalent to the WP-CE-2 test initiation load of 14.6 MN was applied at the location corresponding to the top of the load-pin hole. This analysis produced a static stress-intensity factor of K_I = 240.6 MPa·$\sqrt{m}$ at the center plane of the plate at the time of the first crack initiation. Comparing this computed K_I value with the static initiation value of K_{Ic} = 93.7 MPa·$\sqrt{m}$ [evaluated from the relationship presented in Eq. (3.1) by using a crack-tip temperature of −40.0°C] yields a ratio of K_I/K_{Ic} = 2.56. Initiation stress-intensity factors obtained from this test, test WP-CE-1, and from previous tests that used A 533 grade B class 1 steel,[6,7] are compared in Table 6.2.

6.1.2.2 Posttest 2-D static analyses

Posttest 2-D analyses for test WP-CE-2 were carried out in the same manner as for test WP-CE-1. A temperature profile defined by specifying a crack-tip temperature of T_{CT} = −40.0°C and a midplate temperature of T_{MP} = 52°C was used with WPSTAT to investigate the dependence of arrested crack length and crack stability on the applied initiation load F_{in} = 14.6 MN; the results are presented in Fig. 6.11. In Fig. 6.11, the statically computed arrest length corresponding to the measured initiation load F_{in} = 14.6 MN is given by a_{fc} = 0.544 m. This computed arrest point is above the tearing instability curve (a_{I_2}), implying an unstable condition. The measured initial arrest a_{fm_1} = 0.456 m (back face) is below both the tensile and tearing instability curves. Figure 6.11 indicates that tearing instability is expected when the crack length exceeds 0.47 m, which occurs after the first arrest on the back face but before all other arrest locations (see Table 5.3).

Table 6.2 Initiation stress-intensity factor comparisons

Test designation	Crack-tip temperature (°C)	Calculated static K_I[a] (MPa•√m)	Property correlation K_{Ic}[b] (MPa•√m)	K_I/K_{Ic}
WP-1.2	−33	251.5	87.5	2.87
WP-1.3	−51	173.5	70.1	2.48
WP-1.4	−62	213.0	63.9	3.33
WP-1.5	−30	179.8	91.6	1.96
WP-1.6	−19	233.8	111.2	2.10
WP-1.7	−22.7	280.6	103.7	2.71
WP-1.8	−47.2	290.0	73.0	3.97
WP-CE-1	−33.7	166.2	104.5	1.59
WP-CE-2[c]	−40.0	240.6	93.7	2.56

[a]Computed from 3-D static analysis using ORMGEN/ADINA/ORVIRT.

[b]Calculated from $K_{Ic} = 51.276 + 51.897e^{0.036(T - RT_{NDT})}$ using crack-tip temperature of initial flaw and material RT_{NDT}.

[c]Specimen was warm prestressed to 14 MN at 25°C.

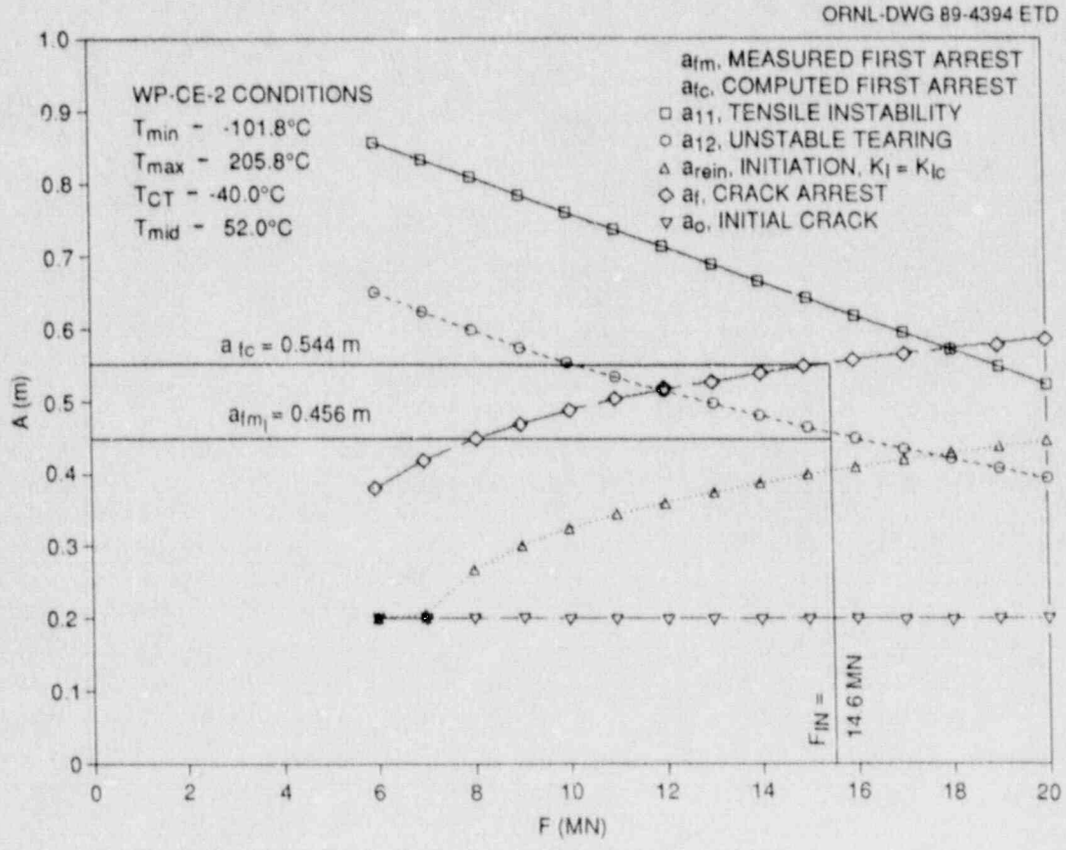

Fig. 6.11. Statically calculated crack lengths: Test WP-CE-2.

Figure 6.12 presents an evaluation of the K_{Ia} function of Eq. (3.2) on the arrest crack-length curve $a_f(F)$, on the incipient tearing-instability curve $a_{I_2}(F)$, and on the reinitiation curve $a_{rein}(F)$. The K_{Ic} function of Eq. (3.1) is also evaluated on the curve $a_{rein}(F)$. Evaluation of the K_{Ia} (a_F) curve at the initiation load F_{in} yields an arrest toughness of K_{Ia} = 359.8 MPa·$\sqrt{m}$ at the computed arrest point a_{fc} = 0.544 m, where the crack-tip temperature would be T = 66.7°C. The complete static-fracture mechanics and stability analyses are depicted in Fig. 6.13.

6.1.2.3 Application-mode dynamic analyses (fixed-load boundary condition)

The 2-D, plane-stress, finite-element model of the wide-plate configuration used in the analyses consisted of 986 nodes and 303 8-noded isoparametric elements. For the dynamic analysis, the load was fixed at the value of the measured fracture load, 14.6 MN, as a prescribed concentrated load. The time step was set at Δt = 5 ms.

Figure 6.14 shows the calculated crack-depth history from this analysis. Figure 6.15 presents the dynamic stress-intensity factor K_I^{DYN}, the static toughness K_{Ia}, and the crack velocity $\dot{a}$ as a function of instantaneous crack depth. The crack propagates into a rising K_I field, and, with the assumption that arrest occurs for crack velocities <0.02 C_S, the predicted arrest is at a_{fp} = 0.53 m where the crack-tip temperature would be T = 61.9°C and the arrest toughness would be K_{Ia} = 325.5 MPa·$\sqrt{m}$. The predicted arrest a_{fp} = 0.53 m exceeds the measured initial arrest a_{fm_1} = 0.46 m.

6.1.2.4 Generation-mode dynamic analysis (fixed-load boundary condition)

Figure 6.16(*a*) and (*b*) depict the apparent crack-position-vs-time curves, developed from the front- and back-face strain gage outputs, respectively, that were used as input for the posttest generation-mode elastodynamic analyses of test WP-CE-2. For these analyses, the load was fixed at the value of the initiation load, 14.6 MN, as a prescribed concentrated load, and the time step was set at Δt = 5 ms. The history of the stress-intensity factor, calculated from the dynamic J-integral and the crack-tip-opening displacement (CTOD), in the generation-mode dynamic analysis for the plate front and back faces, is presented in Fig. 6.17(*a*) and (*b*) respectively. The linear-elastic relationship between K and CTOD is

$$K = \frac{Ey}{4}\sqrt{\frac{2\pi}{r}}, \qquad (6.1)$$

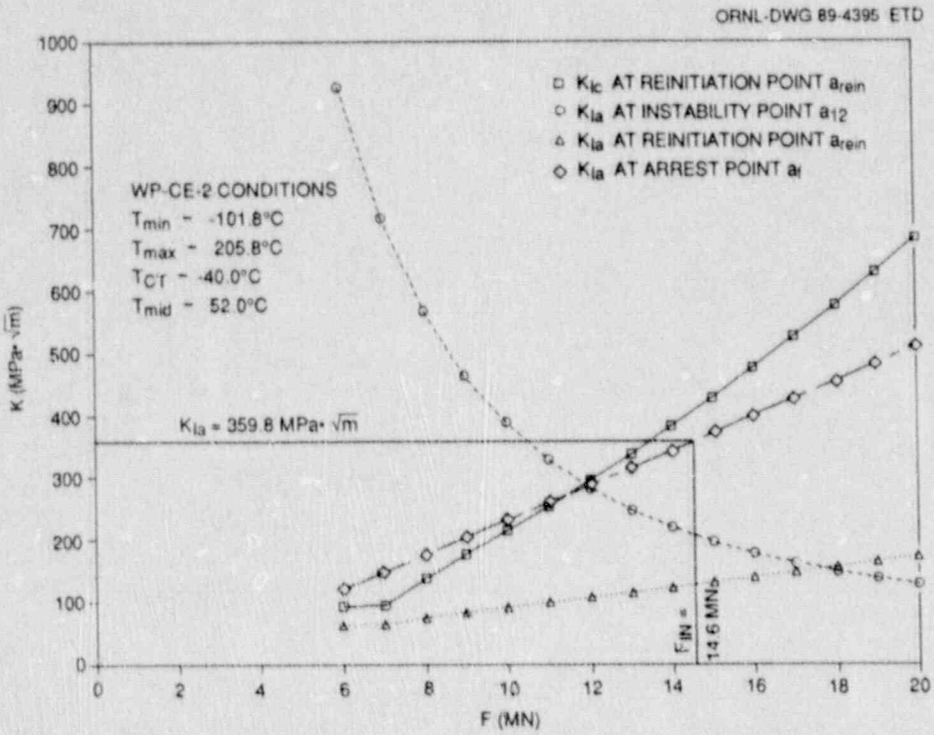

Fig. 6.12. Determination of arrest toughness at initiation load of 14.6 MN: test WP-CE-2.

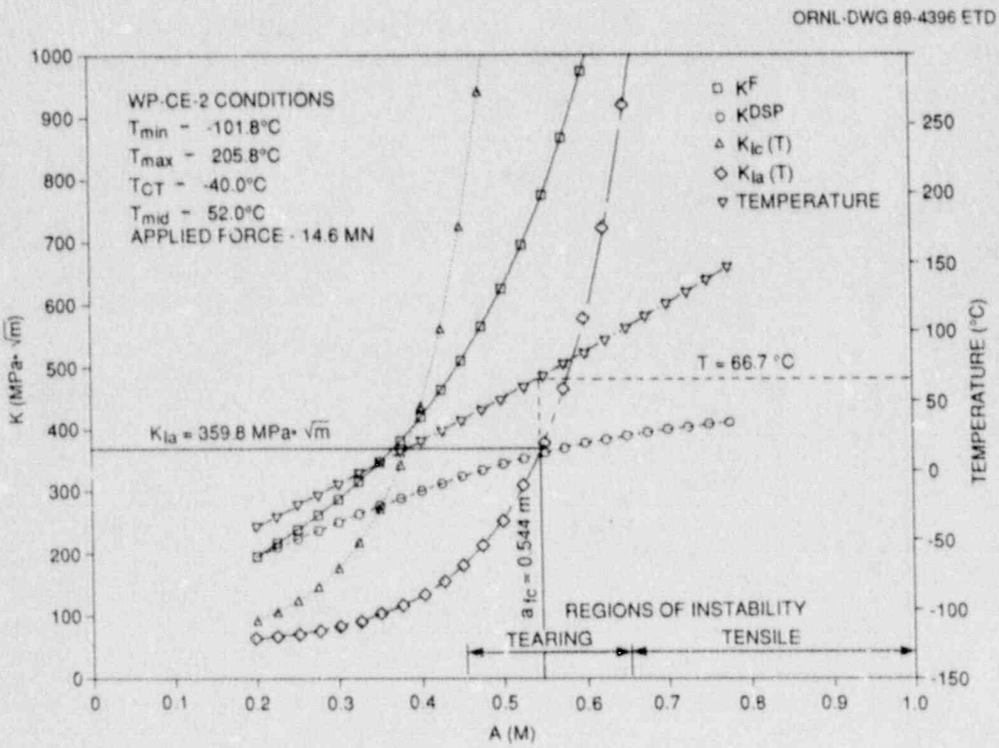

Fig. 6.13. Complete static and stability analyses for initiation load of 14.6 MN: test WP-CE-2.

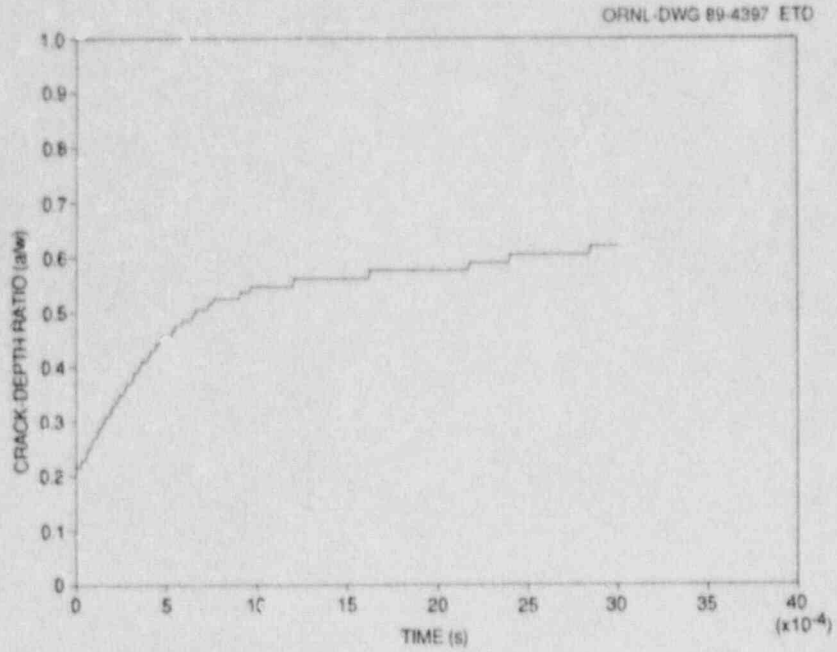

Fig. 6.14. Dynamic analysis, crack-depth history: test WP-CE-2.

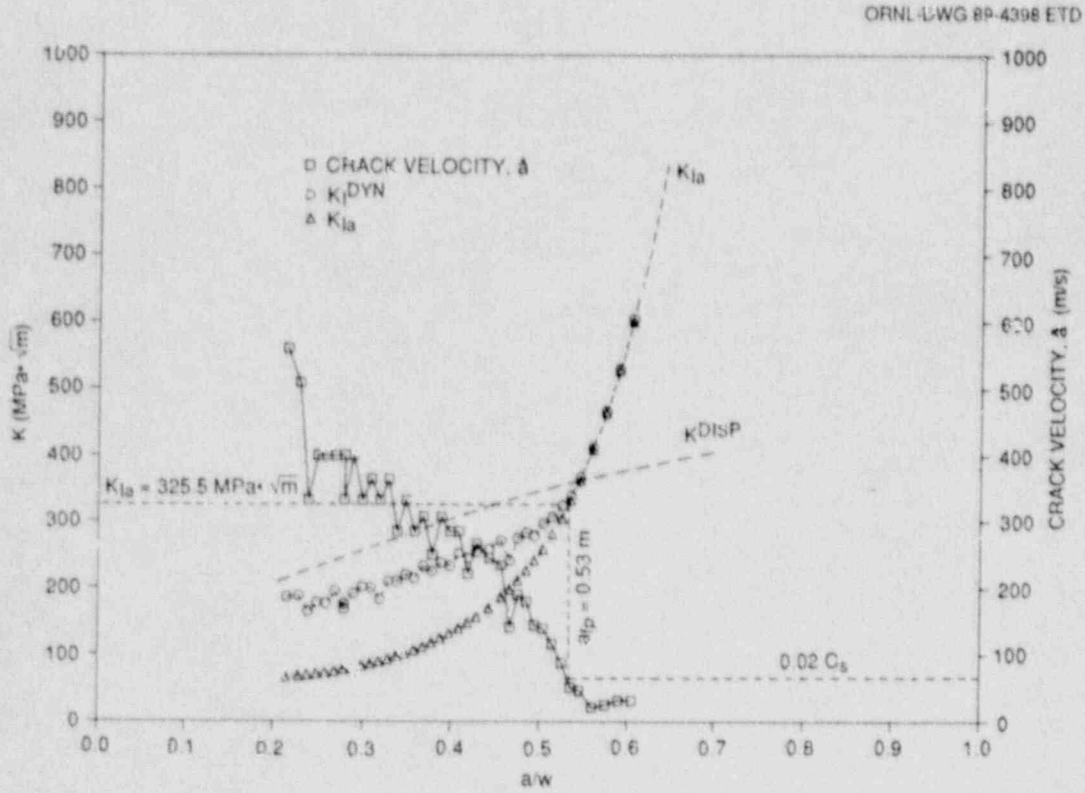

Fig. 6.15. Dynamic factor, static toughness, quasistatic displacement-controlled factor, and crack velocity vs instantaneous crack length: test WP-CE-2.

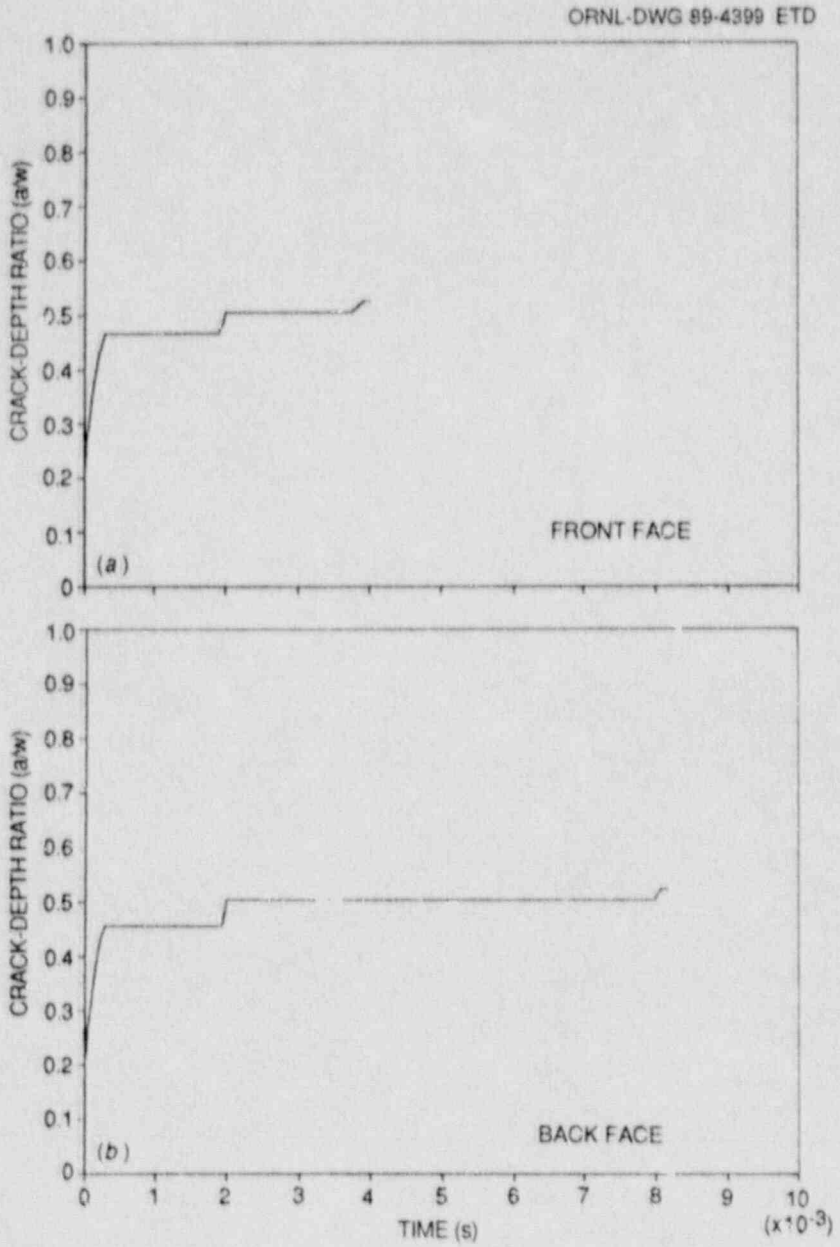

Fig. 6.16. Crack-front position history, derived from (*a*) front-face strain gages, and (*b*) back-face strain gages, that was used as input for generation-mode dynamic analysis: test WT-CE-2.

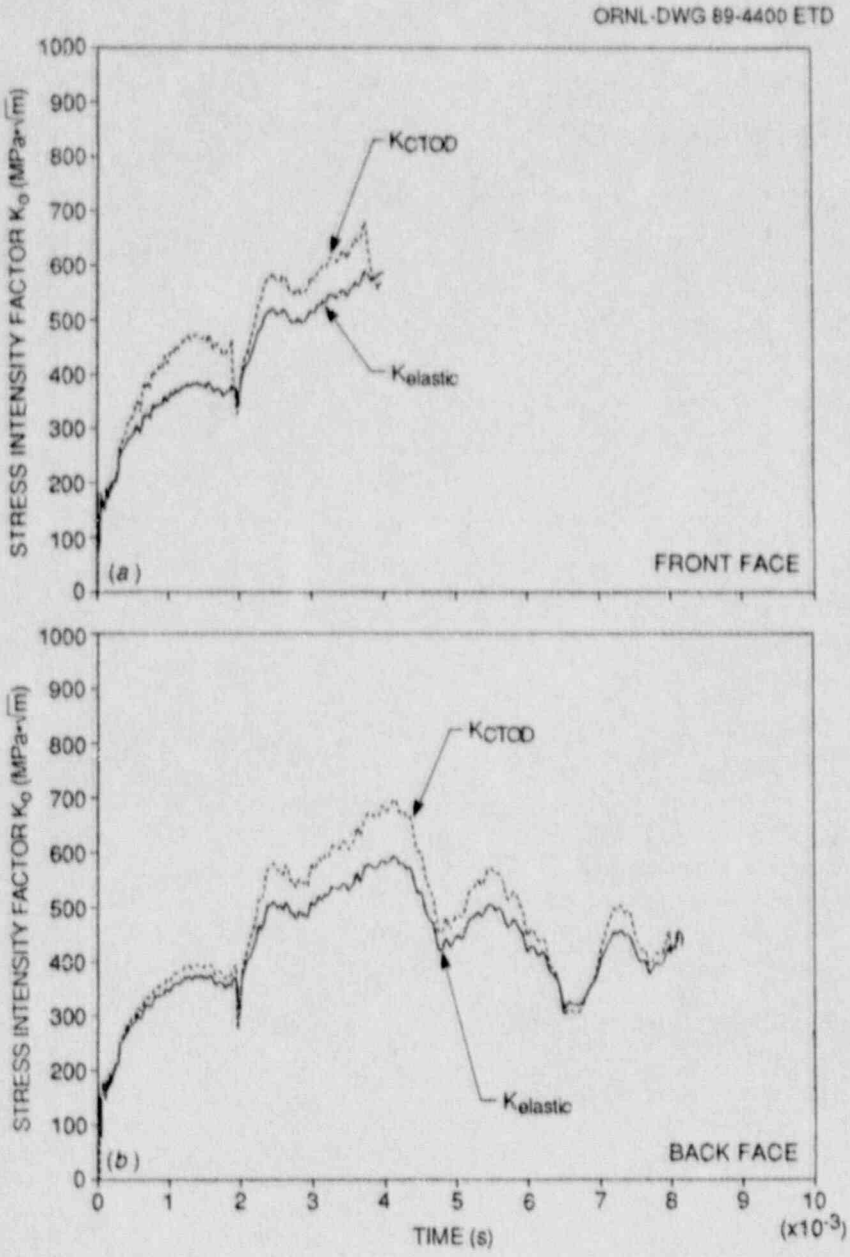

Fig. 6.17. Stress-intensity factor vs time calculated from CTOD history and generation-mode dynamic analysis for (*a*) plate front face and (*b*) plate back face: test WP-CE-2.

where y is the value of the computed displacement (CTOD/2) at a distance r from the crack tip. Table 6.3 summarizes the generation-mode results for the arrest events of test WP-CE-2.

Table 6.3 Summary of computed results for test WP-CE-2

Event	Plate front face			Plate back face		
	Time (ms)	a (m)	K^a (MPa·$\sqrt{m}$)	Time (ms)	a (m)	K^a (MPa·$\sqrt{m}$)
Initiation	0.0	0.201	185.8[b]	0.0	0.201	185.8[b]
Arrest A	0.299	0.466	217.8	0.293	0.456	215.5
Reinitiation	1.899	0.466	379.3	1.927	0.456	372.8
Arrest B	1.995	0.504	354.1	1.995	0.504	330.4
Reinitiation	3.753	0.504	590.4	7.961	0.504	426.3
Arrest C	3.913	0.525	576.3	8.141	0.546	

[a]Generation-mode, fixed-load dynamic analysis, $K_I = \sqrt{E\ J_{dyn}}$.

[b]From ADINA static analysis.

Computed strain histories from selected points close to the crack-line strain gages 1-8 and 13-20 (see Fig. 4.7 for strain-gage locations) are depicted in Figs. 6.18-6.20 for the generation-mode analysis (fixed load) along with measured data from the gages. The comparisons of strain histories in these figures indicate generally good agreement between measured and computed times for occurrence of peak strains. The transition of the strain pulse from a sharp peak for strain gage 6 (Fig. 6.19) to a blunt curve for gage 7 (Fig. 6.20) reflects the first arrest event on the plate front face. The first arrest event on the plate back face can be viewed in the same manner by noting the strain pulse transition between gages 18 (Fig. 6.19) and 19 (Fig. 6.20).

Finally, Fig. 6.21(*a*) and (*b*) compares F-COD and B-COD results, respectively, calculated at a/w = 0.15 with measured data. The calculated COD values compare reasonably well with the measured values.

6.2 CRACK-ARREST TOUGHNESS RESULTS

Crack-arrest toughness values for wide-plate tests WP-CE-1 and -2 have been determined by static and dynamic analyses, as well as by handbook techniques. Some of these values are presented in Table 6.4 (see Table 5.1 for a summary of the general test conditions). Fixed-load generation-mode, crack-arrest toughness values* for tests WP-CE-1 and -2 are plotted in Fig. 6.22 against the arrest toughness temperature

*Reference 9 discusses the importance of the analysis method (static vs dynamic) and boundary conditions (fixed load or fixed load-pin displacement) used to interpret the wide-plate crack-arrest tests.

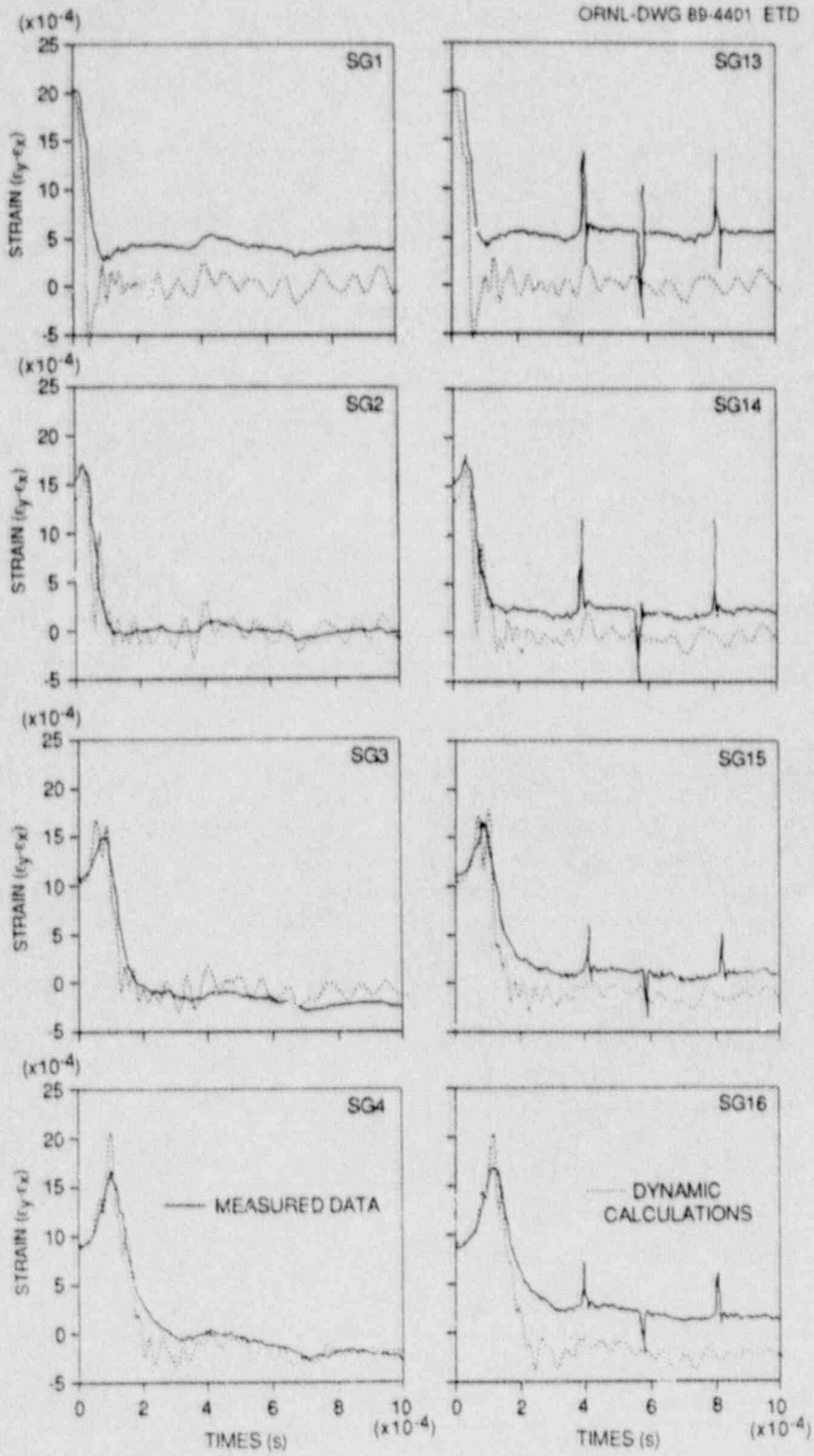

Fig. 6.18. Actual and computed strain histories for companion crack-line gages: test WP-CE-2 (strain gages 1-4 and 13-16).

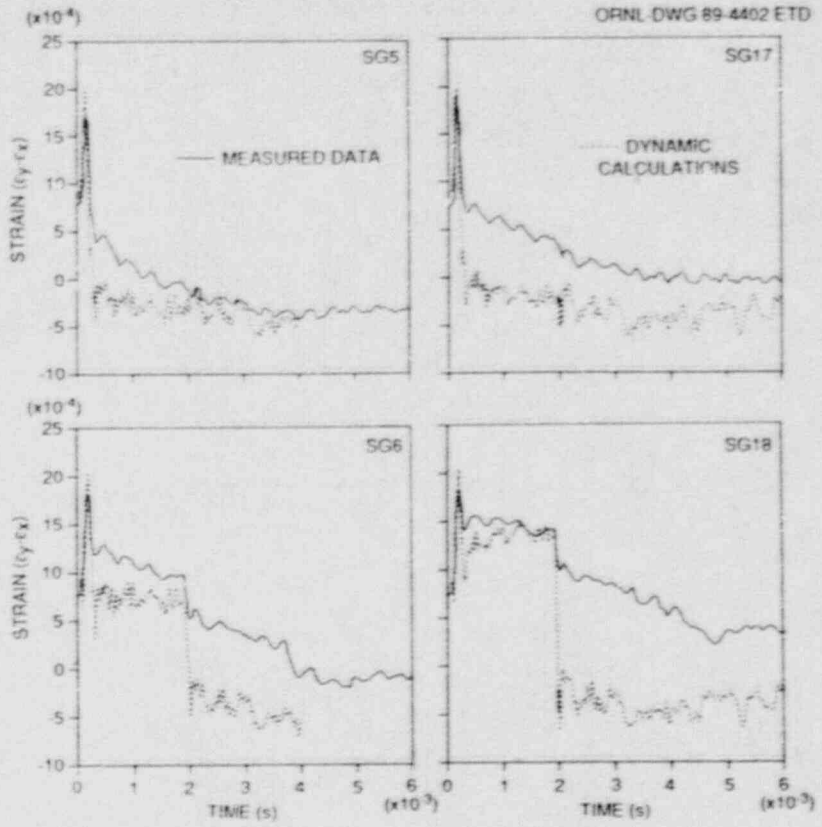

Fig. 6.19. Actual and computed strain histories for companion crack-line gages: test WP-CE-2 (strain gages 5–6 and 17–18).

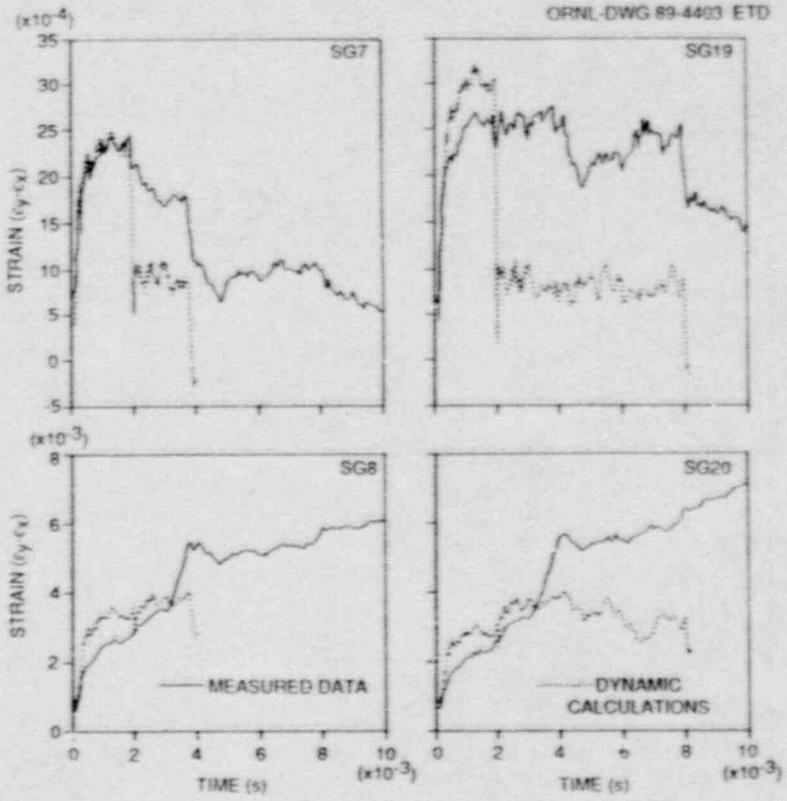

Fig. 6.20. Actual and computed strain histories for companion crack-line gages: test WP-CE-2 (strain gages 7–8 and 19–20).

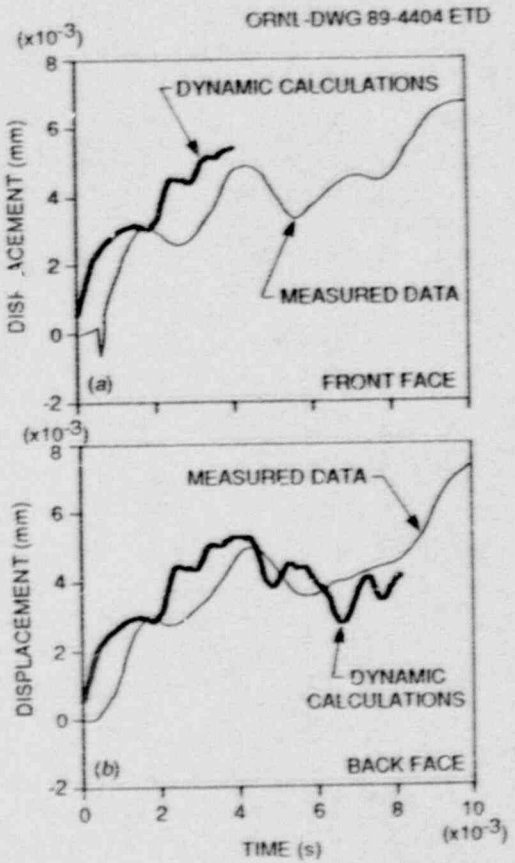

Fig. 6.21. Actual and computed crack-opening displacement at a/w = 0.15 for (a) front-face gage and (b) back-face gage: test WP-CE-2.

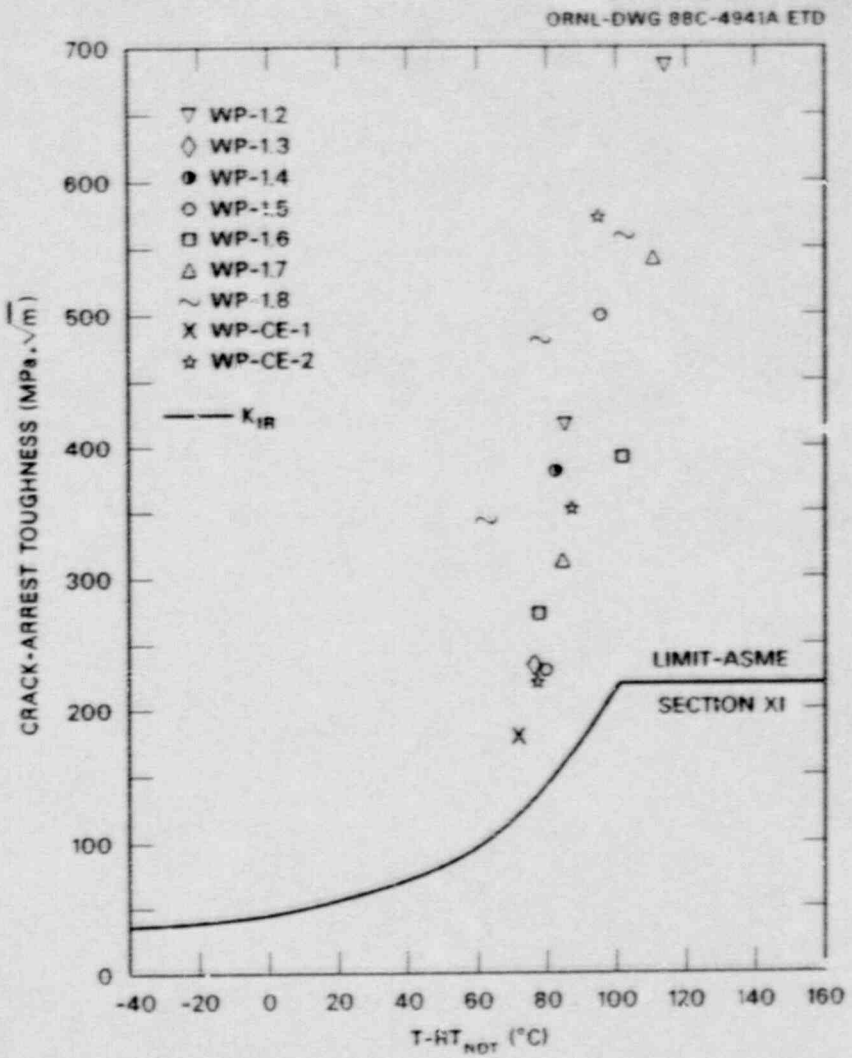

Fig. 6.22. Fixed-load generation-mode dynamic crack-arrest toughness results for HSST wide-plate tests using A 533 grade B class 1 materials.

Table 6.4 Computed crack-arrest toughness values for HSST wide-plate specimens WP-CE-1 and -2

Test No.	Crack-arrest toughness values ($MPa\cdot\sqrt{m}$)			
	Tada static SEN formulas		Fedderson alternate secant formula[c]	Dynamic finite element[d]
	Displacement control[a]	Load control[b]		Generation mode
WP-CE-1	180	293	148	170[e]
WP-CE-2A	274	509	232	218[f]
WP-CE-2B	285	597	249	354[f]
WP-CE-2C	291	653	258	576[f]

[a]From Ref. 8 (pp. 2.10–2.11) while assuming that $a = a_f$ and that no further bending is caused by propagation of the crack.

[b]From Ref. 8 (pp. 2.10–2.11) while assuming that $a = a_f$ and full bending occurs according to the SEN formula when the final crack depth is used. As noted in Ref. 9, these values are considered to provide an upper bound to K_{Ia} determinations for each test.

[c]$K_I = \sigma \left[\pi a \sec\left(\frac{\pi a}{2w}\right)\right]^{1/2}$, where σ = far-field tensile stress, $a = a_f$ = final crack length, and w = full plate width.[10] As noted in Ref. 9, these values are considered to provide a lower bound to K_{Ia} determinations for each test.

[d]Fixed-load conditions. K_{Ia} values are now being reassessed to incorporate tunneling effects. Values should therefore not be considered as final.

[e]Plate back-face arrest location.

[f]Plate front-face arrest locations.

minus RT_{NDT}. (Note, however, that the K_{Ia} results in Fig. 6.22 and Table 6.4 are now being reassessed to incorporate the influence of tunneling, thus possibly resulting in a slight revision of the K_{Ia} values.) Also included in the figure are the results for the previous tests that also used A 533 grade B class 1 material (WP-1 series),[6,7] and the K_{IR} curve from Sect. XI of the *ASME BSPVC*. The crack-arrest toughness values obtained from the WP-1 and WP-CE series tests consistently extend above the reference fracture-toughness curve. At temperatures near and above the onset of Charpy USE ($T - RT_{NDT}$ = 78°C and 85°C

for the WP-1 and WP-CE series materials, respectively), the K_{Ia} values increase with temperature at an accelerating rate. This finding suggests that a temperature limit may exist at or below which a cleavage crack propagation will arrest, no matter how high the driving force. Also, as noted in the figure, crack arrests have occurred at temperatures up to 95°C above the RT_{NDT} (−35°C) and up to 10°C above the temperature corresponding to the onset of Charpy upper-shelf energy ($T - RT_{NDT} = 85$°C) for the WP-CE series material.

6.3 COMPARISON OF WIDE-PLATE CRACK-ARREST TOUGHNESS DATA WITH OTHER LARGE-SCALE TEST RESULTS

The trend for K_{Ia} values to extend above the limit proposed in *ASME B&PVC* Sect. XI, as shown in Fig. 6.22, is further substantiated in Fig. 6.23. Included in the figure are K_{Ia} data from several large-scale tests[11-22] plus the wide-plate results for tests WP-CE-1 and -2, series WP-1 specimens,[6,7] and several series WP-2 specimens.[9] Series WP-2 uses specimens fabricated from a Charpy low-upper-shelf (CVN USE ~65-J)

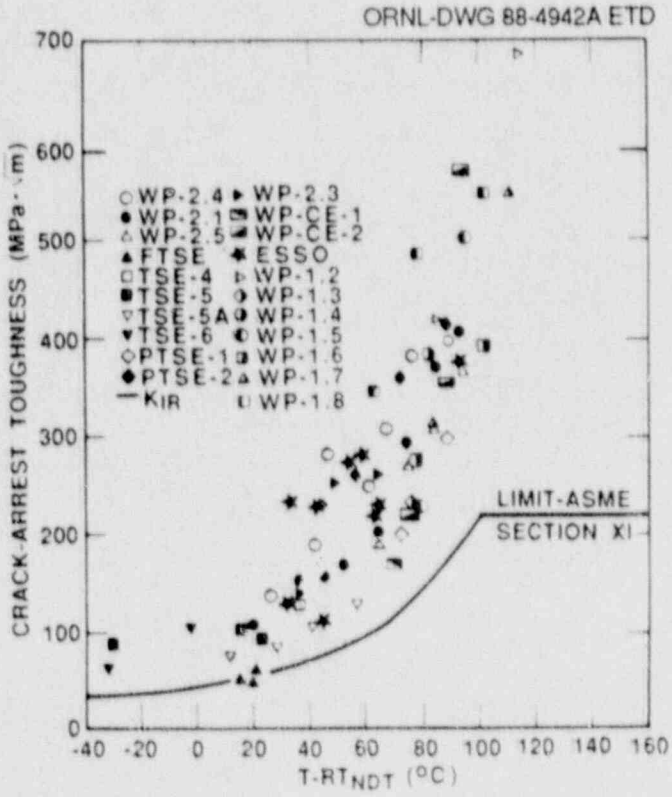

Fig. 6.23. HSST wide-plate crack-arrest data (fixed-load, generation-mode) show trend consistent with data from other large crack-arrest specimen tests.

material. The rate of K_{Ia} increase with temperature obtained in these tests appears to increase significantly at $T - RT_{NDT}$ above ~90°C. All HSST wide-plate tests have demonstrated that arrest occurs before the onset of ductile fracture, even at very high K_{Ia} values and high temperatures. All HSST wide-plate specimens achieved arrest, with the arrest period ranging from a few milliseconds to a completely stable period.

REFERENCES

1. B. R. Bass and J. W. Bryson, Union Carbide Corp. Nuclear Div., Oak Ridge Natl. Lab., *Application of Energy Release Rate Technique to Part-Through Cracks in Plates and Cylinders, Volume 1, ORMGEN-3D: A Finite Element Mesh Generator for 3-Dimensional Crack Geometries*, USNRC Report NUREG/CR-2997,V1 (ORNL/TM-8527/V1), December 1982.*

2. B. R. Bass and J. W. Bryson, Union Carbide Corp. Nuclear Div., Oak Ridge Natl. Lab., *Applications of Energy Release Rate Technique to Part-Through Cracks in Plates and Cylinders, Volume 2, ORVIRT: A Finite Element Program for Energy Release Rate Calculations for 2-D and 3-D Crack Models*, USNRC Report NUREG/CR-2997, V2 (ORNL/TM-8527/V2), February 1983.*

3. K. J. Bathe, *ADINA – A Finite Element Program and Automatic Dynamic Incremental Nonlinear Analysis*, Report A-1, Massachusetts Institute of Technology, Cambridge, 1984.*

4. B. R. Bass, C. E. Pugh, and H. K. Stamm, "Dynamic Analyses of a Crack Run-Arrest Experiment in a Nonisothermal Plate," in *Pressure Vessel Components Design and Analysis*, Vol. 4, ASME Publication PVP, Vol. 98.2, 175–84 (1985).

5. B. R. Bass and J. Keeney-Walker, Martin Marietta Energy Systems, Inc., Oak Ridge Natl. Lab., "Computer Program Development for Dynamic Fracture Analysis," in *Heavy-Section Steel Technology Program Semiann. Prog. Rep. April–September 1985*, USNRC Report NUREG/CR-4219,V2 (ORNL/TM-9593/V2), January 1986.*

6. D. J. Naus et al., Martin Marietta Energy Systems, Inc., Oak Ridge Natl. Lab., *Crack-Arrest Behavior in SEN Wide Plates of Quenched and Tempered A 533 Grade B Steel Tested Under Nonisothermal Conditions*, USNRC Report NUREG/CR-4930 (ORNL-6388), August 1987.*

7. D. J. Naus et al., Martin Marietta Energy Systems, Inc., Oak Ridge Natl. Lab., *High-Temperature Crack-Arrest Behavior in 152-mm-Thick SEN Wide Plates of Quenched and Tempered A 533 Grade B Class 1 Steel*, USNRC Report NUREG/CR-5330 (ORNL/TM-11083), April 1989.*

8. H. Tada, P. C. Paris, and G. R. Irwin, *The Stress Analysis of Cracks Handbook*, Del Research Corp., Hellertown, Pa., 1973.

9. D. J. Naus et al., "Summary of HSST Wide-Plate Crack-Arrest Tests and Analyses," pp. 17–40 in *Proceedings of United States Nuclear Regulatory Commission Fifteenth Water Reactor Safety Information Meeting*, National Bureau of Standards, Gaithersburg, Md., USNRC Conference Proceeding NUREG/CP-0091, Vol. 2, February 1988.*

10. C. F. Fedderson, "Current Status of Plane Strain Crack Toughness Testing of High-Strength Metallic Materials," *Crack Arrest Methodology and Applications*, ASTM STP-410, 77–79 (1967).†

11. R. D. Cheverton et al., Martin Marietta Energy Systems, Inc., Oak Ridge Natl. Lab., *Pressure Vessel Fracture Studies Pertaining to the PWR Thermal-Shock Issue: Experiments TSE-5, TSE-5A, and TSE-6*, USNRC Report NUREG/CR-4249 (ORNL-6163), June 1985.*

12. R. D. Cheverton et al., Martin Marietta Energy Systems, Inc., Oak Ridge Natl. Lab., *Pressure Vessel Fracture Studies Pertaining to the PWR Thermal-Shock Issue: Experiment TSE-7*, USNRC Report NUREG/CR-4304 (ORNL-6177), August 1985.*

13. R. H. Bryan et al., Martin Marietta Energy Systems, Inc., Oak Ridge Natl. Lab., *Pressurized-Thermal-Shock Test of 6-in.-Thick Pressure Vessels. PTSE-1: Investigation of Warm Prestressing and Upper-Shelf Arrest*, USNRC Report NUREG/CR-4106 (ORNL-6135), April 1985.*

14. R. H. Bryan et al., Martin Marietta Energy Systems, Inc., Oak Ridge Natl. Lab., *Pressurized-Thermal-Shock Test of 6-in.-Thick Pressure Vessels. PTSE-2: Investigation of Low Tearing Resistance and Warm Prestressing*, USNRC Report NUREG/CR-4888 (ORNL-6377), December 1987.*

15. Japan Welding Council, *Structural Integrity of Very Thick Steel Plate for Nuclear Reactor Pressure Vessels*, JWES-AE-7806, 1977 (in Japanese).†

16. T. Kanazawa, S. Machida, and T. Teramoto, "Preliminary Approaches to Experimental and Numerical Study of Fast Crack Propagation and Crack Arrest," *Fast Fracture and Crack Arrest*, ASTM STP 627, 39–58 (1977).

17. N. Ohashi et al., "Fracture Toughness of Heavy Section LWR Pressure Vessel Steel Plate Produced by Basic Oxygen Furnace and Ladle Refining Process," pp. 391–96, in *Proceedings of the Fourth International Conference on Pressure Vessel Technology, I. Mech. E.*, Vol. 1, 1980.

18. T. Kanazawa et al., "Study on Fast Fracture and Crack Arrest," *Experimental Mechanics* 21(2), 77–88 (February 1981).

19. S. Machida, Y. Kawaguchi, and M. Tsukamoto, "An Evaluation of the Crack Arrestability of 9% Ni Steel Plate to an Extremely Long Brittle Crack," *Journal of the Society of Naval Architect of Japan* 150, 511–17 (1981), translation ORNL-tr-5052.†

20. T. Kanazawa, S. Machida, and H. Yajima, "Recent Studies on Brittle Crack Propagation and Arrest in Japan," in *Fracture Mechanics Technology Applied to Material and Structure Design*, G. C. Sih, N. E. Ryan, and R. Jones, Eds. (Martinua Nijhoff, The Hague, 1983), pp. 81-100.

21. Y. Nakano, "Stress Intensity Factor During Brittle Crack Propagation and Arrest in ESSO Specimens," pp. 204-9 in *Proceedings of the 18th National Symposium on X-Ray Study on Deformation and Fracture Solids, Society of Materials Science, Japan, July 13-14*, 1981.

22. A. Pellissier-Tanon, P. Sollogoub, and B. Houssin, "Crack Initiation and Arrest in an SA 508 Class-3 Cylinder Under Liquid Nitrogen Thermal-Shock," paper C/F 1/8, Vol. G/H, pp. 137-42 in *Transactions of the 7th International Conference on Structural Mechanics in Reactor Technology, Chicago, August 22-26, 1983*.

---

*Available for purchase from National Technical Information Service, Springfield, Virginia 22161.

†Available in public technical libraries.

7. CONCLUSIONS

The HSST Program has an integrated effort under way to extend the range of applicability of current state-of-the-art crack-arrest practices and to develop alternatives when needed. A consistent trend forms when the crack-arrest data now available from the three types of HSST large-specimen tests are combined on a plot of K_{Ia} vs $T - RT_{NDT}$. Collectively, these data, along with other large-specimen test results, show that arrest can and does occur at temperatures up to and above that which corresponds to the onset of Charpy upper-shelf behavior, and the measured K_{Ia} values extend above the limit included in Sect. XI of the *ASME B&PVC*. Further, the data suggest the existence of a limiting temperature above which a cleavage crack cannot propagate. In summary, the data being obtained under an HSST wide-plate crack-arrest program support (1) the use of fracture-mechanics concepts to analyze cleavage run-arrest events, (2) the treatment of cleavage- and ductile-fracture modes as separate events, and (3) the fact that cleavage arrest can occur at toughness levels well above the ASME limit and at temperatures above that which corresponds to the onset of CVN USE for A 533 grade B class 1 material.

NUREG/CR-5408
ORNL/TM-11269
Dist. Category RF

Internal Distribution

1. D. J. Alexander
2-4. B. R. Bass
5. S. E. Bolt
6. J. W. Bryson
7. R. D. Cheverton
8. J. M. Corum
9-10. W. R. Corwin
11. J. A. Getsi
12. F. M. Haggag
13-14. S. K. Iskander
15. J. E. Jones Jr.
16-18. J. Keeney-Walker
19. A. P. Malinauskas
20. J. G. Merkle
21. R. K. Nanstad
22-24. D. J. Naus
25. C. D. Oland
26. J. S. Parrott
27. W. E. Pennell
28. N. Perrone
29. C. E. Pugh
30. G. C. Robinson
31. J. C. Thesken
32. ORNL Patent Section
33. Central Research Library
34. Document Reference Section
35-36. Laboratory Records Department
37. Laboratory Records (RC)

External Distribution

38. C. Z. Serpan, Division of Engineering, Nuclear Regulatory Commission, Washington, DC 20555
39-40. M. E. Mayfield, Division of Engineering, Nuclear Regulatory Commission, Washington, DC 20555
41. M. Vagins, Division of Engineering, Nuclear Regulatory Commission, Washington, DC 20555
42-43. R. J. Fields, Fracture and Deformation Division, National Institute of Standards and Technology, Gaithersburg, MD 20899
44. G. R. Irwin, Department of Mechanical Engineering, University of Maryland, College Park, MD 20742
45. C. W. Schwartz, Department of Mechanical Engineering, University of Maryland, College Park, MD 20742
46. W. L. Fourney, Department of Mechanical Engineering, University of Maryland, College Park, MD 20742
47. J. W. Hutchinson, Division of Applied Science, Pierce Hall, Harvard University, Cambridge, MA 02138
48. L. B. Freund, Division of Engineering, Brown University, Providence, RI 02912
49. R. J. Dexter, Engineering and Material Science Division, Southwest Research Institute, San Antonio, TX 78284
50. Office of Assistant Manager for Energy Research and Development, Department of Energy, Oak Ridge Operations Office, Oak Ridge, TN 37831
51-52. Office of Scientific and Technical Information, P.O. Box 62, Oak Ridge, TN 37831
53-302. Given distribution as shown in category RF (NTIS-10)

NRC FORM 335 (2-89) NRCM 1102, 3201, 3202

U.S. NUCLEAR REGULATORY COMMISSION

BIBLIOGRAPHIC DATA SHEET

(See instructions on the reverse)

1. REPORT NUMBER (Assigned by NRC, Add Vol., Supp., Rev., and Addendum Numbers, if any.)

NUREG/CR-5408
ORNL/TM-11269

2. TITLE AND SUBTITLE

SEN Wide-Plate Crack-Arrest Tests Using A 533 Grade B Class 1 Material: WP-CE Test Series

3. DATE REPORT PUBLISHED

MONTH: November
YEAR: 1989

4. FIN OR GRANT NUMBER

B0119

5. AUTHOR(S)

D. J. Naus, J. K[illegible]eney-Walker, B. R. Bass, S. K. Iskander, ORNL
R. J. Fields, E. [illegible]eWit, S. R. Low III, NIST

6. TYPE OF REPORT

Topical

7. PERIOD COVERED (Inclusive Dates)

8. PERFORMING ORGANIZATION – NAME AND ADDRESS (If NRC, provide Division, Office or Region, U.S. Nuclear Regulatory Commission, and mailing address; if contractor, provide name and mailing address.)

Oak Ridge National Laboratory
P.O. Box 2008
Oak Ridge, TN 37831

Subcontractor:
National Institute of Standards and Technology
Gaithersburg, MD 20899

9. SPONSORING ORGANIZATION – NAME AND ADDRESS (If NRC, type "Same as above"; if contractor, provide NRC Division, Office or Region, U.S. Nuclear Regulatory Commission, and mailing address.)

Division of Engineering
Office of Nuclear Regulatory Research
U.S. Nuclear Regulatory Commission
Washington, DC 20555

10. SUPPLEMENTARY NOTES

11. ABSTRACT (200 words or less)

Two 102-mm-thick wide-plate crack-arrest tests (WP-CE series) are discussed in this report. Each test used a 1 × 1 × 0.1 m thick single-edge notched specimen (a/w = 0.2) fabricated from A 533 grade B class 1 steel that was subjected to a linear thermal gradient along the plane of crack propagation. The tests were conducted at the National Institute of Standards and Technology and were designed to provide fracture-toughness measurements at temperatures approaching or above the onset of the Charpy upper-shelf regime in a rising toughness region and with an increasing driving force. Results obtained from these tests have produced crack-arrest toughness values well above the limit recognized by the current ASME guidelines (220 MPa·$\sqrt{m}$) with arrests occurring at 58 to 95°C above the material RT_{NDT} (−35°C). The fracture data support (1) the use of fracture mechanics concepts to analyze cleavage run-arrest events, (2) the treatment of cleavage run-arrest and ductile fracture modes as separate events, and (3) the fact that cleavage arrest occurs above the ASME limit.

12. KEY WORDS/DESCRIPTORS (List words or phrases that will assist researchers in locating the report.)

Cleavage Fracture
Crack-Arrest Toughness
Ductile Tearing
Fracture Mechanics
LWR Pressure Vessels
Safety Assessments
Wide-Plate Testing

13. AVAILABILITY STATEMENT

Unlimited

14. SECURITY CLASSIFICATION

(This Page)
Unclassified
(This Report)
Unclassified

15. NUMBER OF PAGES

16. PRICE

NRC FORM 335 (2-89)

*U.S. GOVERNMENT PRINTING OFFICE:1989-262-436:00351

UNITED STATES
NUCLEAR REGULATORY COMMISSION
WASHINGTON, D.C. 20555

120555139531 1 1AN1RF
US NRC-OADM
DIV FOIA & PUBLICATIONS SVCS
TPS PDR-NUREG
P-223
WASHINGTON DC 20555